Development of Modular, Droplet Microfluidic Workflows to Investigate Cellular Heterogeneity

by

Claire D. Cook

A dissertation submitted in partial fulfillment
of the requirements for the degree of
Doctor of Philosophy
(Chemistry)
in the University of Michigan
2023

Doctoral Committee:

Professor Ryan C. Bailey, Chair
Professor Julie S. Biteen
Assistant Professor Kristin S. Koutmou
Associate Professor Sunitha Nagrath

Claire D. Cook

cneice@umich.edu

ORCID iD: 0000-0003-2180-6807

Dedication

To my family, especially Jack and Bebeh Cook.

Lamentations 3:22 – 24, ESV

The steadfast love of the Lord never ceases;

His mercies never come to an end;

They are new every morning;

Great is your faithfulness.

“The Lord is my portion,” says my soul,

“Therefore I will hope in him.”

Acknowledgements

I am incredibly grateful to my committee members for assisting me throughout this journey, supplying detailed experimental suggestions as well as bigger picture advice for graduate school. I would also like to thank the National Science Foundation for supporting me to pursue research through the NSF – Understanding the Rules of Life – Epigenetics Grant No. 1921677. The Rackham Graduate School and the Chemistry Department awarded me multiple travel grants that allowed me to present my research at conferences such as PittCon and the International Symposium of Microscale Separations and Bioanalysis. The Chemistry Department at the University of Michigan also supported me by providing opportunities for me to teach several chemistry lab courses, developing my instructional and mentorship skills.

Professor Ryan C. Bailey, thank you for inspiring me to join your research group. It is where I discovered a passion for developing technologies that improve accessibility of scientific tests and knowledge, and I admire your zeal in pursuing these kinds of research gaps. Your mentorship challenged me to move beyond my comfort zone as a scientist and develop the critical thinking skills I needed to finish this PhD. Thank you for also being an incredibly understanding and empathetic PI throughout all the peaks and valleys of grad school.

I am also grateful to my other committee members, Professor Julie S. Biteen, Assistant Professor Kristin Koutmou, and Professor Sunitha Nagrath, as well as my previous cognate member, Assistant Professor Kaushik Ragunathan. Dr. Biteen, Dr.

Koutmou, and Dr. Ragunathan, you provided me with thoughtful feedback, expertise, and guidance throughout the various phases of my projects to help me to continue making progress with my projects. Dr. Ragunathan especially helped deepen my understanding of epigenetics so I could design wiser experiments for my FADS-MNase project. Dr. Nagrath, I am grateful I got the opportunity to collaborate with members of your lab for the CellMag-CARWash project and for your guidance through the manuscript production process. Thank you for being willing to join my committee for this last leg.

Both of my projects were incredibly collaborative, and I would not have been able to complete the work I accomplished without several outstanding scientists. I would like to highlight Brittany T. Rupp, who I have worked closely with for the entirety of my graduate school experience to develop, optimize, characterize, and apply the CellMag-CARWash workflow. I have always admired your intellect and diligence, and I am excited that our work together is reaching the publication stage! Emma A. Purcell also worked with us to establish the foundations for the workflow, and I am grateful for the example you set for me during my early years of grad school. For the FADS work, I had the pleasure of working with J. Damon Hoff in the Single Molecule Analysis in Real-Time (SMART) Center at the University of Michigan. Your expertise and insight were incredibly valuable as I learned how to operate the system and made changes to improve its capabilities. Thank you for all your advice and troubleshooting help for that project.

I'd also like to mention Kathleen Nolta and Alexander Poniatowski, who mentored me throughout my many years of teaching during graduate school. You both

demonstrated excellent examples to me on how to instruct chemistry to students in an engaging way, and I am hopeful that one day I'll be able to have my own classroom and use the tools I learned from you. To Kathleen specifically, thank you for allowing me to try my hand at curriculum development through the FF-GSI program and letting me stop by to chat whenever I passed by your office to go into the Bailey Lab cleanroom.

My labmates, past and present, also deserve a shoutout for their aid in shaping me as a scientist. I would like to thank Steven R. Doonan and Vishal Sahore for teaching me the basics of microfluidics and the finer details involved in the projects I inherited and advanced throughout graduate school. Thank you to Sara Medfisch for encouraging me and chatting with me during our early mornings in lab as I was just setting out on my PhD voyage. To the #currentcrew, thank you for fostering such a good lab culture. I admire you all so much as scientists! Nick, I'm grateful for your positive attitude and flexibility. Nico, thank you for being the best officemate ever, always game to chat about life or dig deep into research challenges I was facing. Marina, thank you for picking me as your board game teammate during our first year! I am grateful for all the brainstorming conversations we had as I tried to decipher my science, and I'm glad we got to enjoy double dates with Josh and Jack. I'm hopeful we can make it to Indianapolis for future IndyCar races! Krista, thank you for being a fabulous carpool buddy while we lived in Howell! I enjoyed all our podcasts and crazy weather commutes. I am glad we got to work together in several teaching and mentoring events, and I'm grateful you read the entirety of my intro chapter! I'm rooting for you as you head into your final year and wrap up your PhD. Gloria, I'm so thankful for your mentorship and friendship throughout the years—you helped me push through so many

obstacles in my projects. I am proud of our scientific discussions in the conference room, brainstorming ideas that advanced both of our projects. Your positivity and encouragement meant so much to me when I was feeling disheartened. Even more so, I'm thankful for fun wine, board game, and plant memories together!

My friends from UM have also played a big role in keeping me sane throughout this grad school experience. To Ashley and Anna, thank you for being my best friends from Day 1! I treasure the memories of our many board game nights, D&D one-shots, Bagel Wednesdays, apple picking excursions, and my baby shower. I admire your scientific instincts and I'm so proud of all the work we've done. I can't wait for future reunions as we all move onto new, exciting adventures. To Alondra, I'm so thankful we met during that jargon exercise during RELATE. And even more thankful we got to bond as RELATE Coordinators and LegalBytes fans during pop culture legal drama. Thank you for your enthusiasm and support through my last year of grad school. And lastly, Jen, you've been the best mentee-turned-friend ever! I have enjoyed giving you advice about life and science and SciComm! I'm so grateful that you were happy to support me with desk dates at Sweetwaters and a listening ear when I needed to brainstorm.

To my family, thank you for your support from afar! I have enjoyed getting to experience life with you through 3 weddings, many Christmas holidays, and the elusive mid-year visits. Phone calls to check in with you were so encouraging to me, getting to hear about life in your corner of the world and remember that grad school is only a season. Mom and Dad, thank you for believing in me and challenging me to persevere or take chances when I was disheartened. Your insights helped me to push through challenges at work and make memories during the chaos. I'd also like to mention my

cat, Nova, who was my dissertation writing buddy, distracting me and giving me reasons to smile when I needed to take a break.

Most of all, I'm grateful to my husband, Jack, who always supported and encouraged me. If it weren't for you, I don't think I would have finished this degree. Thank you for always cheering me on, pushing me to persevere, and praying for me. I am so thrilled to step into whatever this next phase of life brings to us as young professionals and new parents.

Table of Contents

Dedication ii

Acknowledgements iii

List of Tables xii

List of Figures xiii

List of Videos xix

List of Equations xxi

List of Appendices xxii

Abstract xxiii

Chapter 1 Investigating Innate Cellular Heterogeneity Through the Use of Customizable Microfluidic Platforms for Single-Cell and Low-Cell Input Studies 1

1.1 Cellular heterogeneity 1

1.1.1 Techniques to study cellular heterogeneity: cellular isolation 3

1.1.2 Techniques to study cellular heterogeneity: single-cell analysis 8

1.1.3 The need for high throughput, accessible technologies for cellular isolation . 10

1.2 Microfluidics 10

1.2.1 Microfluidic devices for cellular isolation 11

1.3 Applications 20

1.3.1 Extracellular vesicle (EV) dynamics 20

1.3.2 Epigenetic regulation 25

1.4 Dissertation Overview 37

Chapter 2 CellMag-CARWash: A Droplet Microfluidic Workflow for Isolation of Single Cells from Complex Mixtures for Use in Downstream Processing and Analysis 39

2.1 Introduction 39
2.2 Materials and Methods 43
2.2.1 Cell culture 43
2.2.2 Magnetic bead preparation and attachment to cells 44
2.2.3 Microfluidic device fabrication 44
2.2.4 Microfluidic device set-up 45
2.2.5 Single-cell droplet generation 46
2.2.6 CellMag-CARWash processing 47
2.2.7 Magnetic droplet splitter processing 48
2.2.8 Droplet manipulation and analysis coalescence 48
2.2.9 Live/dead analysis 49
2.2.10 Bulk EV quantification using nanoparticle tracking analysis (NTA) 49
2.2.11 Single-cell secreted EV droplet analysis 50
2.3 Results 51
2.3.1 Attachment of magnetic beads to cells using target specific antibodies 52
2.3.2 CAR-Wash design adjustments for expansion to cell isolation 55
2.3.3 CellMag-CARWash processing of cell mixtures 57
2.3.4 Optimizing a magnetic droplet splitter device to collect EVs from cell-containing droplets 61
2.3.5 Single-cell EV quantification in droplets 64
2.4 Discussion 68
2.5 Conclusions 72
2.6 Acknowledgements 73
2.7 Attribution Information 73
Chapter 3 Development and Characterization of the FADS-MNase, Droplet Microfluidic Workflow to Enrich and Epigenetically Profile *S. Pombe*-Containing Droplets 74

3.1 Introduction: 74
3.2 Materials and Methods: 79
3.2.1 Buffer, media, and oil phase formulations 79
3.2.2 Cell Culture 80
3.2.3 Microfluidic device fabrication 81
3.2.4 Microfluidic device operation 82
3.2.5 Droplet generation 82
3.2.6 Fluorescence Activated Droplet Sorting 83
3.2.7 qPCR sample and data processing 84
3.2.8 Nucleosome positioning device 84
3.3 Results and Discussion: 85
3.3.1 FADS validation 86
3.3.2 qPCR analysis of FADS processed S. pombe mixtures 94
3.3.3 MNase module application to yeast cells and pairing with FADS 98
3.4 Conclusion: 103
3.5 Acknowledgements: 105
3.6 Attribution Information 106
Chapter 4 Modular Droplet Microfluidic Workflows for Isolation and Analysis of Limited Cell Samples 107
4.1 Dissertation Motivation 107
4.2 CellMag-CARWash workflow for cellular isolation and EV studies 109
4.2.1 Future directions for CellMag-CARWash 111
4.3 FADS-MNase workflow development and characterization 115
4.3.1 Future Directions for FADS-MNase 118
4.4 Broader impacts of the dissertation 119
Appendices 123

Bibliography 130

List of Tables

Table 3.1. Percent production of mono-nucleosome DNA fragments for microfluidic versus bulk processing. The number of replicates per sample type is indicated. 102

Table 3.2. Percent production of mono-nucleosome DNA fragments for FADS versus bulk processed samples. The number of replicates per sample type is indicated. 103

Appendix Table C.1. Averaged Percentage of Reads Aligned to S. pombe genome for various sample types. No Cell controls consistently exhibit <0.2% reads aligned to the genome, indicating the majority of DNA present in these samples is a contaminant. Since it is not changed with fresh buffers, the initial buffers are assumed to not be the source of contamination. Interestingly, the droplet processed samples exhibit a higher percentage of aligned reads for the 10 min incubation time than bulk, indicating improved reaction efficiency in the droplet processing context. 127

Appendix Table C.2. Averaged GC content for various sample types. All cell-containing samples exhibit two peaks of GC content prevalence, one around 40% and one around 62%. The latter matches the prominent peak present within all No Cell controls. 128

List of Figures

Figure 1.1. Important cases of heterogeneity. (A) Originally homogeneous assumption of genetically identical populations. (B) Seemingly stochastic changes in cell states can have wider reaching impacts. (C) Population averages (blue) can hide the presence of important but rare subpopulations (yellow). (D) The presence of equal yet distinct subpopulations (shown in yellow and blue) can lead to a biologically irrelevant population average (green). 3

Figure 1.2. Commonly used cellular isolation and analysis tools for single-cell studies. Isolation tools include serial dilution (A), micromanipulation (B), LCM (C), FACS (D), and MACS (E). Microarrays (F) and NGS (G) technologies have paved the way for analyzing single-cell samples. Figure produced using BioRender 7

Figure 1.3. Common microfluidic cellular isolation principles and examples from literature. Cells can be separated hydrodynamically using pillar arrays[42] (A) or differences in inertial flow[44] (B), via immobilization with capture agents[50] (C), or by dielectrophoretic manipulation[53] (D). Multilayer devices[55] can be used to capture cells in individual compartments (E). Magnetic tags can enable MACS separation[29] (F) and droplets[67] can be used to isolate cells into individual, mobile aqueous compartments (G). Figures have been reproduced with permission. 19

Figure 1.4. Illustration of cellular communication facilitated by extracellular vesicles (EVs). EVs are composed of the membrane materials and contents of their origin cells. Nucleic acids, proteins, and small molecules make up the possible cargoes for EVs to ferry between cells. 21

Figure 1.5. Bulk versus single-cell methods for isolating and studying extracellular vesicles. Commonly used bulk isolation techniques include ultracentrifugation[81] (A), ultrafiltration[81] (B), and immunochemical capture using capture agent coated surfaces[82] (C) or magnetic beads. Single-cell methods include SRM techniques such as STORM[74] (D), microfluidic capture in wells[73] (E) and droplets[72] (F). Figures were reproduced with permission. 25

Figure 1.6. Common mechanisms of epigenetic regulation employed in the cell to balance DNA compaction and accessibility. Figure produced using BioRender. 27

Figure 1.7. Comparison of common protocols for profiling chromatin accessibility and nucleosome positioning assays. Figure produced using BioRender. 32

Figure 2.1. Process Overview. A) Development of the CellMag-CARWash device for single-cell isolation. Cells are incubated with 2.8 μm Dynabeads coated with cell type specific antibodies. After incubation with the cells, Dynabeads attach to the desired cell population. The cell mixture is then emulsified into droplets, which are inputted into the CARWash to separate cells attached to Dynabeads into droplets containing a single cell. New media and other cell culture reagents can be used as a wash buffer and added to the newly resegmented droplets. B) Examining single-cell EV secretion profiles in droplets using fluorescent imaging. Cells in droplets are incubated to allow for single-cell EV secretion. After short-term culture, droplets are inputted into a Droplet Splitter device to divide each droplet into two smaller droplets, one containing the cell and another containing EVs. Droplets containing EVs are placed into a 50 μm tall chamber and imaged. Fluorescence intensity of the droplets is recorded and used to determine relative EV concentration inside the droplets..... 52

Figure 2.2. Attachment of 2.8 μm Dynabeads to a desired cell population within a mixed population. A) Anti-CD56 coated Dynabeads attached to NK92mi cells in a mixture of NK cells and T-cells. i) Images of Dynabeads attached to NK cells (red). T cells are shown in blue. Scale bar 20 μm. ii) Percentage of NK cells with various amounts of anti-CD56 Dynabeads. N=3 iii) Percentage of T-cells with various amounts of anti-CD56 coated Dynabeads. N=3 B) Anti-EpCAM/ anti-EGFR/ anti-CD133 coated Dynabeads attached to MCF7 GFP cells in a mixture of MCF7 GFP cells and NK cells. i) Images of Dynabeads attached to MCF7 GFP cells (green). Scale bar 20 μm. ii) Percentage of MCF7 GFP cell population with various amounts of anti-EpCAM/ anti-EGFR/ anti-CD133 coated Dynabeads. N=4 iii) Percentage of NK cell population with various amounts of anti-EpCAM/ anti-EGFR/ anti-CD133 coated Dynabeads. N=4..... 54

Figure 2.3. CellMag-CARWash cell recovery. A) Diagram of the CellMag-CARWash with labeled inlet and outlet streams. Blue box shows premade droplets containing cells coalescing with the wash buffer upon entering the device. Cells with beads will be attracted to the magnet and resegmentation of droplets containing media (yellow box bottom right). Cells without beads and other waste components will exit into the waste stream (yellow box top right). MCF7 GFP cells (target cells) are circled in green. NK cells (contaminating cells) are circled in red. Side panel of (A) shows an image of CellMag-CARWash with channels filled with dyes. Blue food coloring fills the fluid handling channels; yellow food coloring fills the electrode channel. Droplet input and output are labeled. B) The percentage of each cell type in the solution, with anti-CD56 beads, inputted into the CellMag-CARWash and recovered from the CellMag-CARWash in the product stream. N=4 D) The percentage of NK cells resegmented and recovered from the CellMag-CARWash based on the number of anti-CD56 beads attached to cells. N=5 E) The percentage of each cell type in the solution, with anti-EpCAM/anti-CD133/anti-EGFR, inputted into the CellMag-CARWash and recovered from the CellMag-CARWash in the product stream. N=6 F) The percentage of MCF7 GFP cells resegmented and recovered from the CellMag-CARWash based on the number of anti-EpCAM/anti-CD133/anti-EGFR Dynabeads attached to cells. N=6. 58

Figure 2.4. Measured size of desired cell populations. Brightfield images of cells were taken after beads were attached and Nikon Elements software was used to measure the size of each cell population. 61

Figure 2.5. Droplet splitter recovery. A) Diagram of the droplet splitter device. Box shows the junction of the device where droplets are divided into two smaller droplets, with the cell being recovered in the magnetic output. Scale bar indicates100 μm. Side panel of (A) shows an image of the droplet splitter device. Channels are filled with green food coloring, and droplet input, EV output, and magnetic output ports are labeled. B) Recovery of beaded MCF7 GFP cells in the magnetic output based on droplet velocity in the device and the type of oil used. Either fluoroinert FC-40 (FC-40) or 2% F008 in Novec 7500 oil (N-7500) was used. N=3. The red bar indicates the condition that was used for future experiments..... 63

Figure 2.6. Comparison of extracellular vesicle size and concentration from bulk NK cells cultured with and without anti-CD56 beads attached. NK cells were cultured in bulk and the supernatant ultracentrifuged to obtain EVs. EV concentration and size was determined using NTA analysis via the NanoSight. N=5..... 65

Figure 2.7. Comparison of extracellular vesicle size and concentration from NK cells cultured with and without supplemental β-Estradiol. The experiment was performed in triplicate across different days, with each run corresponding to one graph. For each run, NK cells were cultured in bulk with or without supplemental β-Estradiol for the same period of time. After culturing, the supernatant ultracentrifuged to obtain EVs. EV concentration and size was determined using NTA analysis via the Zetaview..... 66

Figure 2.8. Full system runs of MCF7 GFP purified and isolated into single-cell droplets using the CellMag-CARWash system before short term incubation with or without supplemental β-Estradiol. After incubation, cells were removed using the droplet splitter device and the fluorescent intensity of the remaining EVs was analyzed. A) Image of droplet with fluorescent EVs taken at 60X magnification. Dotted line indicates droplet border. Scale bar 20 μm. B, C, and D show the distribution of fluorescent intensities of droplets containing EVs secreted by single cells obtained using the workflow on different days. B) P-value <0.0001. C) P-value =0.003. D) P-value <0.0001. 67

Figure 2.9. MCF7 GFP EV secretion with various concentrations of β-Estradiol. A) Relative EV concentration obtained from the supernatant of bulk MCF7 GFP cells cultured with various concentrations of β-Estradiol. N=3 B) Relative EV concentration of EVs secreted by single cells based on the mean fluorescent intensity of the droplets post droplet splitter, compared to the background fluorescent intensity. N=3 68

Figure 3.1. Diagram for the FADS-MNase, droplet microfluidic workflow. Following culture, cells are encapsulated into droplets (Device 1) which are sorted via FADS (Device 2). Fluorescent cell-containing droplets are enriched in the “Sort” output, while empty and low fluorescent droplets are collected into the “Waste” output. The output droplets from FADS can then be processed through the MNase digestion device (Device 3) to perform simultaneous cell wall digestion, cell lysis, and DNA fragmentation

before the MNase enzyme is quenched through the injection of EDTA at the end of the device. DNA is subsequently purified and amplified prior to analysis of DNA fragments. 86

Figure 3.2. Diagrams of optical and electrical components used for FADS sorting. (A) Excitation light is directed from the LED source to the microscope stage using filters and mirrors. The excitation path is filtered to narrow the wavelength range that reaches the microfluidic device. Brightfield light is filtered to facilitate imaging of the device during operation with a high-speed camera without impacting the excitation and emission of fluorescent droplets. A dichroic beamsplitter is used to filter out excitation and brightfield light from droplet fluorescence emission that travels to an avalanche photodiode detector (APD). (B) Fluorescence emission is detected by the APD whose signal outputs to a Teensy Arduino running the FADS sorting script. A threshold for sorting can be set on the script; above this threshold, a signal is sent to the function generator to trigger an AC pulse, which is amplified and delivered onto the microfluidic device via solid-metal electrodes. The AC burst from the function generator and amplifier can be visualized on an oscilloscope. Application of the AC field on device results in diversion of oil away from the electrodes, which displaces droplets passing through the device towards the electrodes and into the Sort output. 88

Figure 3.3. Validation of the FADS device. (A) FADS device diagram with inputs and outputs labeled. Fluorescent signal from fluorescein-optiPBS droplets (B) and a 1:10 mixture of fluorescein-optiPBS and optiPBS droplets (C). APD signal is shown for a subset of the collection time (18.1 – 19.5 s and 3.8 – 5.6 s, respectively). The time windows correspond to synchronized videos collected of droplets passing through the device. Droplet occurrence in the device is indicated with peaks in the graphs above the fluorescent signal traces. Fluorescent peaks above the set thresholds (red lines) correspond to fluorescein droplets passing through the detection point. 90

Figure 3.4. Fluorescent signal and corresponding snapshots of video imaging for FADS processing of yeast cell-containing droplets. (A) Fluorescent signal of yeast cell-containing droplets during FADS processing for a subset of the APD collection time (53.9 – 56.7 s). The time window corresponds to a synchronized video collected of droplets passing through the device. Droplet occurrence in the device is depicted as peaks in the graph above the fluorescence trace. Fluorescent peaks above the threshold (red line) correspond to droplets containing yeast cells. (B) Snapshots a yeast-cell-containing droplet being diverted into the Sort output. The cell is circled in the middle frame. This droplet corresponds to the peak present at 55.07 highlighted in the fluorescence trace. 93

Figure 3.5. Quantitative PCR analysis of bulk (A) versus FADS-processing (B, C) of synthetic cell mixtures. The fold enrichment of the FADS-processed samples is split with respect to samples obtained from the Sort (B) and Waste outputs (C). 97

Figure 3.6. Possible causes for non-fluorescent cells entering the Sort output. (A) The expected distribution of cells in droplets based on calculated Poisson statistics from 6 million cells/mL sample segmented into 200 pL droplets. Only 36% of droplets are

expected to contain a single cell, with 30% of droplets being empty and 34% of droplets containing 2 or more cells. (B) Merged droplets observed in tubing headed into the FADS device. Droplets are delivered onto the FADS device as soon as 1 hour following generation. However, processing of samples takes 1.5 – 2 hours, so droplets could be sitting in the reinjection container for up to 3 hours or more for subsequent samples... 98

Figure 3.7. Expansion of the MNase droplet device to process cell-wall containing cells. (A) The adapted design features an adjustment of the inputs to facilitate processing of pre-made droplet samples with a droplet input, oil spacer, and picoinjector for adding digestion and lysis components (outlined in yellow). Following the digestion injection, droplets are mixed through a serpentine channel, incubated through delay channels, and injected with quenching buffer. Digestion profiles from bioanalyzer analysis are shown for droplet versus bulk processing (B) and droplet processing versus No Cell controls (C). The location of mono-nucleosome-length DNA fragments (200 – 350 bp) is highlighted in yellow. Some fluorescence intensity for primer dimers at < 100 bp is cut off. 720,000 S. pombe cells emulsified for data shown. 101

Figure 3.8. Digestion profiles from bioanalyzer analysis are shown for the full FADS-MNase droplet processing versus bulk processing. (A) and versus No Cell controls (B). The location of mono-nucleosome-length DNA fragments (200 – 350 bp) is highlighted in yellow. 180,000 S. pombe cells emulsified for experiment. 103

Figure 4.1. Proposed design for a multi-output CellMag-CARWash device. Extra outputs along the magnet-facing wall have been incorporated to collect cells with different numbers of beads attached. To maintain the oil barrier that prevents sample from sticking to the PDMS wall, extra oil coflow inputs have also been incorporated between each output. 113

Figure 4.2. Initial device design for an array to study cell-cell communication between droplets using droplet crosstalk. (A) The overall device design features two inlets to feed in the two droplet types (green = origin cell droplets; orange = recipient cell droplets), an oil inlet, and two flow outputs. Droplets will be immobilized in the chambers over time. Oil flows from the top of the device to the bottom to induce droplet crosstalk. (B) A zoomed in image of individual chambers. Oil flows from the origin cell droplet (light green) to the recipient cell droplet (orange). Secreted molecules from the origin cell (dark green dots) are encapsulated in shear-created micelles due to oil flow and merge with the recipient cell droplet. Responses from the recipient cell could then be observed through imaging. 115

Appendix Figure A.1 Schematics for droplet generator devices used in these projects. The top device was used to generate droplets for the CellMag-CARWash project, and the bottom device was used to produce droplets for the FADS-MNase project. Cell input, oil input, and droplet outputs are labeled with colored dots. 123

Appendix Figure B.1. Schematics for previous iterations of the CellMag-CARWash device. (A) Initial extension of the washing chamber to accommodate smaller magnetic bead sizes. This design was created by Dr. S.R. Doonan, a previous member of the Bailey Lab to wash Dynabeads. (B) Same as A, but the magnet is placed 1 mm farther from the washing channel. The distanced magnet position was incorporated to enable potential interactions with the washing buffer. (C) Same as B, but the washing chamber was extended 1.5X. The distanced magnet position still offers potential for interactions with the washing buffer, but the longer channel accounts for the longer time needed to divert cells across the streamlines due to their increased size. C was initially observed to recover high numbers of cells through video imaging, but offline measurements of cell recovery later revealed poor reproducibility. Thus, the magnet was moved back closer to the washing channel (as in A) to increase the magnetic force experienced by cells and improve recovery. This final design was used for the experiments in Chapter 2. The various inputs are labeled with colored dots shown in the table. 124

Appendix Figure B.2. Percentage of cells recovered from processing with the chosen CellMag-CARWash design (Figure B.1C) as a function of the number of beads attached per cell. (A) shows an initial sample result, indicating promising levels of recovery. However, subsequent processing of two additional samples (B) revealed poor reproducibility in recovering cells. Thus, the decision was made to bring the magnet closer to the washing channel in the final design used in Chapter 2. 125

Appendix Figure B.3. Representative schematics of major feature changes in previous iterations of the magnetic splitter device. (A) The initial design featured a channel expansion after the droplet spacer and serpentine outputs that were useful for mixing droplet contents to ensure equal distribution. (B) The channel expansion was removed, since it did not add to the function of the device. (C) The serpentine outputs were removed to improve device robustness in processing fibers that entered samples. Each design iteration featured designs with different channel widths to facilitate processing of different droplet volumes, and the final design used in Chapter 2 possessed wider channels compared to (C) due to its appropriateness for processing the ~200 pL droplets from CellMag-CARWash while minimizing blockage by fibers at the splitting junction. Various inputs and outputs are indicated with colored dots. 126

Appendix Figure C.1. Representative graphs showing mean GC content of sequenced samples. Peak locations are indicated with black lines and labels. Cell containing samples exhibited 2 peaks of GC content prevalence, indicating multiple species of DNA present. The higher GC containing shoulder peaks aligned well with the location of the No Cell control peaks. The prevalence of the shoulder peak decreases with incubation time and microfluidic processing. Note that the # of reads axes do not match – data was considered qualitatively for the prominent peak GC contents. 129

List of Videos

Video 2.1. Droplet Coalescence: Mixed cell populations with magnetic beads attached were placed into droplets and inputted into the CellMag-CARWash system. Upon entering the wash chamber, droplets were coalescence with a wash buffer due to the application of an electric field via a ground electrode channel filled with 3 M sodium chloride and a positive electrode from a platinum wire inserted into the wash buffer solution. Cells then moved through the wash chamber due to magnetic force from the attached magnet and/or force from the moving wash buffer. Scale bar depicts 100 μm. 59

Video 2.2. Droplet Resegmentation: At the end of the wash chamber, cells would either exit through the waste stream, top right or product stream, bottom right, where they would be resegmented into droplets. Due to laminar flow within the device and the placement of the cell input, cells without attached magnetic beads remained in the top portion of the chamber and were carried into the waste stream. Cells with magnetic beads attached were attracted to the product stream where they could be collected and resegmented into single-cell droplets. Scale bar depicts 100 μm..... 59

Video 2.3. Magnetic Droplet Splitter: After short-term incubation to allow for cells to secrete extracellular vesicles, droplets were inputted into the splitter device which contains two output streams, the EV output (first output) and Magnetic output (second output). Cells, which have magnetic beads attached, will be attracted to the magnet in the device and move to the bottom of a droplet, thereby forcing cells to exit into the magnet output when the droplet reaches the junction. Free floating EVs, which have no magnetic beads attached will remain suspended in the droplet solution and exit the device in the EV output droplet. Scale bar depicts 100 μm. 64

Video 3.1. Video imaging of FADS processing of a pure sample of 10 nM fluorescein-optiPBS droplets. Droplets consistently diverted into the Sort output channel. A shadow appears across the channel which results from the edge of a filter passing through the camera's field of view – this shadow has no effect on the excitation light path or sorting of droplets. 91

Video 3.2. Synchronized imaging of FADS processing of a 1:10 mixture of 10 nM fluorescein-optiPBS and optiPBS droplets. Individual droplets were observed diverting into the Sort output channel. A shadow appears across the channel which results from the edge of a filter passing through the camera's field of view – this shadow has no effect on the excitation light path or sorting of droplets. 91

Video 3.3. Synchronized video imaging for FADS processing of yeast cell containing droplets. Droplets were generated at a concentration of 7 million cells per mL and sorted on the same day. Individual droplets containing a yeast cell were observed entering the Sort output between adjacent empty droplets. However, several droplets containing yeast cells were not diverted. It was determined that the fluorescence emission from these cells was not high enough to trigger a sorting event..... 94

List of Equations

Equation 1.1 4

Equation 1.2 4

Equation 2.1 56

Equation 2.2 56

Equation 2.3 60

Equation 3.1 95

Equation 3.2 95

Equation 3.3 95

List of Appendices

Appendix A: Droplet Generator Device Schematics 123

Appendix B: Device Schematics Involved in Optimization of the CellMag-CARWash Droplet Microfluidic Workflow 124

Appendix C: No Cell Control Troubleshooting Data 127

Abstract

Cells exist in unique contexts within a population, but miniscule differences in their environment, epigenome, and cell cycle produce an assortment of observable characteristics in cells. Conventional cellular analysis tools routinely combine millions of cells within samples to ascertain “averaged” cellular states. Many methods have been developed to isolate, process, and analyze small and even single-cell samples, but they require long experiments, large reagent volumes, and expensive equipment. Microfluidic technologies have been developed as cheaper, automated, high-throughput routes to study cells in a miniaturized context. Droplet microfluidic platforms encapsulate individual cells in sub-microliter droplets for isolated processing. However, most of these devices adapt singular steps from benchtop protocols, requiring pre-purification of cells or post-processing to generate results. This dissertation describes the development of multi-device, droplet microfluidic workflows as wholistic, automated alternatives for single-cell assays.

Chapter 2 introduces CellMag-CARWash–a workflow that combines positive, magnetic selection with droplet microfluidic devices to isolate desired cells from a mixture and incorporate specific biochemical cues within individual droplets. We demonstrate CellMag-CARWash’s abilities by isolating single cells from multi-cell mixtures with two different cell types from equal prevalence to >93% purity. Cells require a minimum of 4 – 5 beads to be recaptured, depending on size, which prevents

non-specific, bead-bound contaminating cells from entering the product stream. Molecular treatments can be delivered to cells at the single-cell level through CellMag-CARWash's washing buffer. We leveraged this feature to study heterogeneity in extracellular (EV) secretion dynamics from MCF7 cells. A magnetic droplet splitter enabled isolation and analysis of secreted EVs from single cells within droplets, revealing the underlying distribution of secretion rates. This chapter reports the first measurement of β-estradiol's effect on EV secretion from single MCF7 cells.

Chapter 3 combines two previously isolated droplet microfluidic devices into a cohesive workflow to study nucleosomal organization within cellular subpopulations. Nucleosome positioning throughout chromatin controls DNA accessibility so cells can respond to environmental cues. Our workflow employs fluorescence activated droplet sorting (FADS) and a micrococcal nuclease (MNase) digestion device to gently enrich cells within droplet populations and produce mononucleosomal DNA fragments. Diversion of droplets via FADS is demonstrated for pure and mixed samples containing fluorescent solutions and cells. Successful enrichment of fluorescent cells is demonstrated for multiple cell mixture compositions. Simultaneous cell wall digestion, lysis, and DNA fragmentation occur via the MNase digestion device, generating ~70% mononucleosome-length fragments and demonstrating improved reaction efficiencies relative to benchtop controls. The full FADS-MNase workflow is applied to generate mononucleosomal DNA fragments from enriched droplet samples produced by both FADS outputs.

The final chapter summarizes major findings for each workflow, proposes technical improvements and interesting new concepts to explore, and places them into

the broader context of tools enabling study of cellular heterogeneity. These technologies automate multiple portions of cellular protocols, and all devices are input independent, making implementation easier, faster, and more flexible for the user. Further work to integrate them with next generation sequencing analysis would produce all-in-one, high-throughput technologies for studying heterogeneity in cell samples. Scaling to larger numbers of cells is as simple as increasing the number of droplets generated, which positions these workflows for rapid deployment into clinical spheres and patient sample analysis. Overall, this dissertation demonstrates the capability and potential of modular, droplet microfluidic workflows to revolutionize cellular heterogeneity studies.

Chapter 1 Investigating Innate Cellular Heterogeneity Through the Use of Customizable Microfluidic Platforms for Single-Cell and Low-Cell Input Studies

1.1 Cellular heterogeneity

Cells within a genetically identical population exhibit heterogeneity in their observable characteristics. Walter Elsasser first proposed this theory of cellular heterogeneity in 1984[1] to comment on Harry Rubin's results demonstrating morphological heterogeneity observed in cells derived from the same tumor.[2] This theory has since been supported in various ways with heterogeneity observed in routine biological processes,[3–5] responses to environment changes,[6] and disease progression.[2,7–9] Common cellular analysis tools typically combine molecules and features of interest contained within many cells, resulting in a population-averaged picture with the assumption that all cells present are homogeneous (Fig. 1.1A). This "bulk" measurement helps define the prevailing cellular response to a stimulus, with any variations considered to be biological "noise." However, this assumption does not always hold true.[10,11]

Firstly, if we consider "biological noise" more closely, some cells will naturally exhibit traits different from the observed average. These differences can be random, but in some cases, they reflect fundamental differences in cell function (Fig. 1.1B). As an example, Lai *et al.* found that differences in deoxyribonucleic acid (DNA) packaging in

mouse embryonic stem cells resulted in heterogeneous priming for differentiation.[4] Secondly, rare subpopulations may be present in a cell sample, but the bulk measurement can mask their presence (Fig. 1.1C). Such is the case for some small subsets of tumor cells that can prove resistant to therapeutics,[12] allowing them to survive and causing cancer recurrence. Lastly, it is possible for the population average to reflect a cell that does not naturally exist. This occurs when two or more important, but distinct, subpopulations are present (Fig. 1.1D). The average of the subpopulations will reflect a cell that is biologically meaningless. This was observed in *Xenopus* oocytes by Ferrell and Machleder, where the population average missed an “all-or-nothing” cell maturation response following progesterone treatment.[13] These cases of biologically and clinically relevant heterogeneous cells necessitate the development of novel technologies capable of isolating and analyzing fewer numbers of cells and further down to single-cell levels.

Isolation and analysis tools have been developed and applied to study cellular populations at reduced and individual scales. Cellular isolation is a vital step in assay protocols to ensure purity of cell samples (i.e., separation of different cell types) and collection of individual cells. Current methods include serial dilution, micromanipulation, laser capture microdissection (LCM), fluorescence activated cell sorting (FACS), and magnetic activated cell sorting (MACS). Of these, FACS is by far the most widely used approach. Following isolation and sample processing, single-cell samples are commonly analyzed via DNA microarrays or next generation sequencing (NGS), although the latter has emerged as the analytical route of choice.

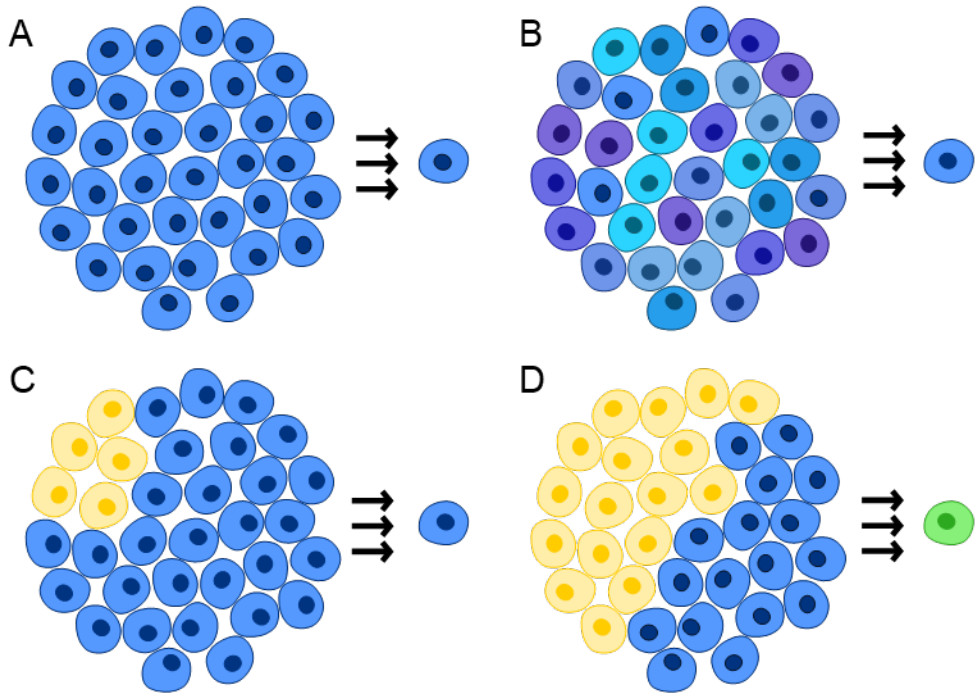

Figure 1.1. Important cases of heterogeneity. (A) Originally homogeneous assumption of genetically identical populations. (B) Seemingly stochastic changes in cell states can have wider reaching impacts. (C) Population averages (blue) can hide the presence of important but rare subpopulations (yellow). (D) The presence of equal yet distinct subpopulations (shown in yellow and blue) can lead to a biologically irrelevant population average (green).

1.1.1 Techniques to study cellular heterogeneity: cellular isolation

1.1.1.1 Serial Dilution

In serial dilution, cell suspensions are iteratively diluted to achieve low cell concentrations (Fig. 1.2A). These concentrations are based on Poisson statistics (Eqn. 1.1), where the probability, P(x), that a certain number of cells, x, occupies a volume, depends on the solution concentration and the volume. These parameters determine the average number of cells expected to occupy each aliquot, λ (Eqn. 1.2). It can be universally assumed that about a third of aliquots will contain single cells with a concentration of 0.5 cells per aliquot.[14] This method is straightforward and inexpensive to implement, but, due to the statistical reliance, it lacks efficiency and throughput.[14,15]

$$P(x) = \frac{e^{-\lambda}\lambda^{x}}{x!} \quad \text{(Equation 1.1)}$$

$$\lambda = cell\ concentration * \ aliquot\ volume \quad \text{(Equation 1.2)}$$

1.1.1.2 Micromanipulation

Micromanipulation has existed since the 1960's.[16,17] In this technique, cell populations are observed through a microscope, and a micromanipulator machine is used to mechanically relocate cells to the chosen reaction container (Fig. 1.2B; typically a well plate or small tube). This technique is beneficial since the tools required are often already available in most lab spaces, making it generally accessible.[17] In addition, users may visually inspect and choose cells of interest to isolate. However, visual inspection inherently reduces the throughput of the technique, and the manipulation can cause mechanical stress on cells.[15]

1.1.1.3 Laser Capture Microdissection (LCM)

LCM enables the isolation of cells from tissue samples (Fig. 1.2C). [15,18] This facilitates comparison of distinct cell populations from heterogeneous tissue, for example normal cells vs diseased cells. In LCM, tissue samples are observed through microscopy, irradiated with a laser, and dissected into desired cell samples. Like micromanipulation, LCM allows the user to visually inspect and choose cells of interest for analysis. However, this reliance on human observation lowers throughput since imprecision in dissection can lead to shearing of cells and loss of material of interest.[19] The requirement of a laser to perform dissections also limits LCM's accessibility.

1.1.1.4 Fluorescence Activated Cell Sorting (FACS)

FACS was developed in 1969 by the Herzenberg group[20] and has become the most widely used cell isolation method to enable single-cell studies (Fig. 1.2D). A low concentration solution of cells passes in front of an excitation laser, and the presence of a desired fluorophore within the cell is interrogated. The cell of interest and its surrounding solution are aerosolized and electrostatically diverted into a separate outlet in response to fluorescence intensities above a set threshold. Individual cells can be isolated by diverting them into different wells on a well plate to be ready for downstream analysis. Subsequent iterations have elevated the complexity of sorting parameters to search for up to 12 different fluorophores and two scattering parameters with throughputs up to 50,000 Hz.[21] The incorporation of imaging software has expanded possible investigation to isolation based on cell size and shape,[22–24] which is beneficial, as it reduces reliance on fluorescent labeling or modification of cells. FACS requires extensive training to operate efficiently, and the mechanism of sorting often impedes cell viability and homeostasis, an obstacle for studying cellular processes.[25] Additionally, FACS commonly relies on cellular expression of a fluorophore that remains contained inside the cell membrane, not being secreted into the extracellular solution.[26] This limits the types of cells that can be isolated via FACS and raises concerns that *in vivo* processes will be altered.

1.1.1.5 Magnetic Activated Cell Sorting (MACS)

Miltenyi *et al* developed MACS in 1990 to rapidly isolate cells using differential magnetic activity.[27] Figure 1.2E shows the MACS process where a dilute cell solution flows through a chamber surrounded by a magnet to detain cells responsive to

magnetic fields. Non-magnetic cells elute immediately, while magnetically active cells only elute following the removal of the magnet. Multiplexed magnetic sorting has also been developed to isolate cells in up to 25 different outputs, utilizing differently sized magnetic beads and diversion trajectories.[28,29] A major drawback of MACS is that it requires cells to be magnetically active, either through natural magnetic properties—of the cells or a surrounding fluid—or through tagging with magnetic beads. This is commonly accomplished by functionalizing magnetic beads with antibodies specific to surface markers on the desired cell type's surface, although expression of surface markers can be a heterogeneous feature of cell types.[30,31]

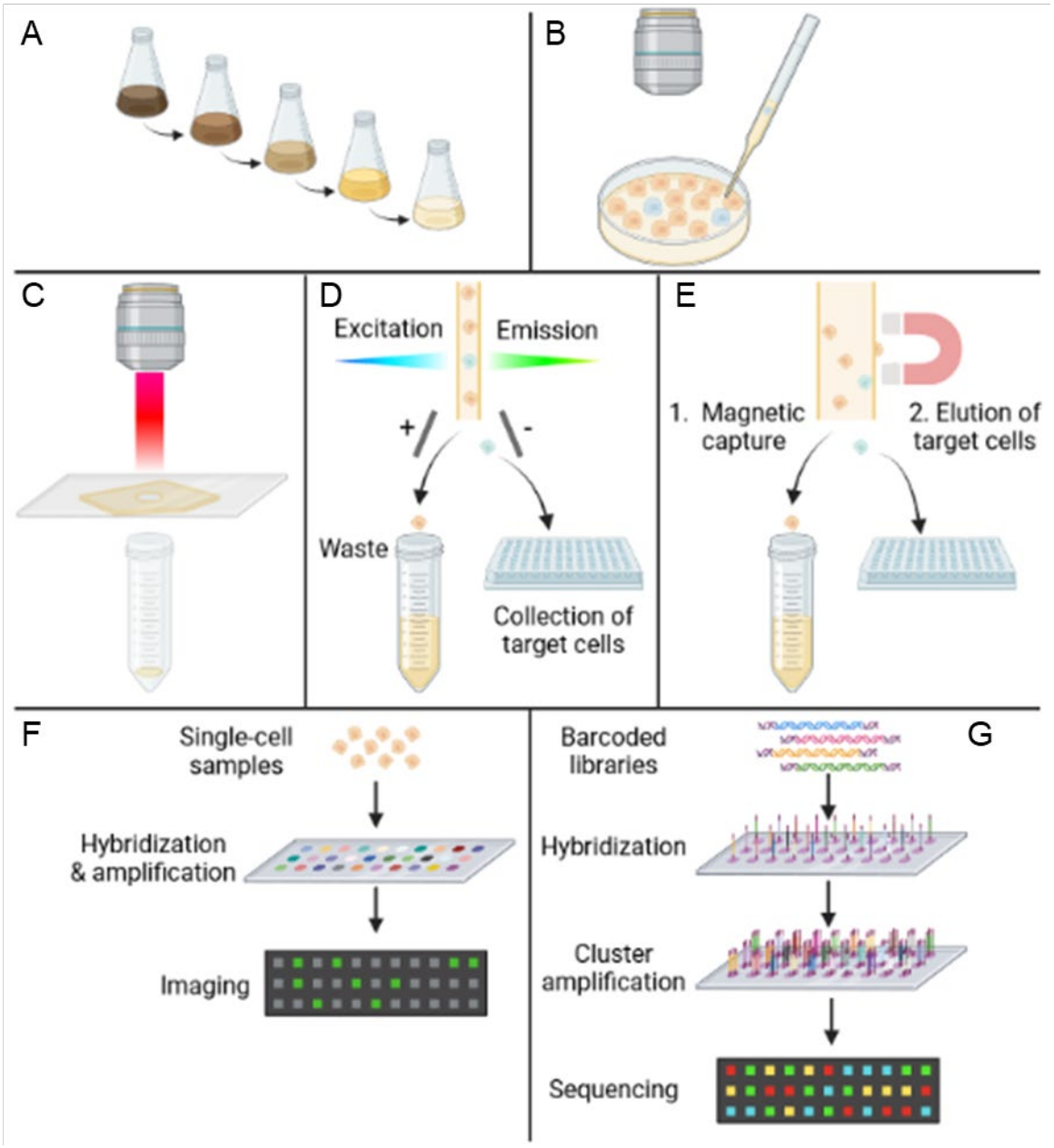

Figure 1.2. Commonly used cellular isolation and analysis tools for single-cell studies. Isolation tools include serial dilution (A), micromanipulation (B), LCM (C), FACS (D), and MACS (E). Microarrays (F) and NGS (G) technologies have paved the way for analyzing single-cell samples. Figure produced using BioRender

1.1.2 Techniques to study cellular heterogeneity: single-cell analysis

1.1.2.1 Microarray technologies

Microarrays consist of small glass slides, or "chips," that are patterned with known DNA fragments in such a way that tens of thousands of probe sequences are deposited per chip (shown in Fig. 1.2F). The transcriptome of a single cell or group of cells can be assessed by converting messenger ribonucleic acid (mRNA) molecules into complementary DNA (cDNA), fragmenting and fluorescently labeling the resulting cDNA, and injecting them on chip. The fragments hybridize with anchored DNA probes, and fluorescent emission occurs at specific locations, allowing the original mRNA to be identified. DNA microarrays can also be used to study genomic content within cells, with DNA molecules added directly into fragmentation and labeling steps. Integration with computer software enables rapid imaging and analysis, while the patterned nature of the chip allows for many sequences to be analyzed at once. This makes microarrays an attractive tool for high throughput, single-cell analyses. However, DNA microarray analysis requires previous knowledge about genomic features so that appropriate probes can be designed and incorporated for detection.[32] These probes are limited to sequences that will not cross-hybridize and lead to errors in identification. The genetic material requirement is also large, typically requiring 1 – 10 million cells per analysis, so single-cell studies must pre-amplify the nucleic acid content from single cells prior to the chip.[33,34] PCR amplification is known to biasedly amplify AT-rich sequences over GC-rich sequences, which will affect the analysis of sequences assessed on microarrays.[34,35] Additionally, the technique requires access to the precisely patterned

microarrays and sensitive imaging capabilities, leading to an expensive investment that limits its application.

1.1.2.2 Next generation sequencing (NGS)

NGS technologies became available at the beginning of the 21st century as an alternative to Sanger sequencing for identifying genome sequences.[36–38] Sanger sequencing is a gel-based method that identifies DNA sequences by performing base-specified digestion steps and separating fragments by size. Gel separation and analysis are time consuming and typically performed with large numbers of cells. NGS performs automated sequence identification of DNA molecules. As shown in Figure 1.2G, "libraries" of fragmented DNA or cDNA samples of interest must be prepared by attaching universal adapters that enable hybridization with DNA probes patterned onto a glass slide, similar to microarrays. Fluorescently tagged nucleotides are added one by one to the hybridized DNA fragments, and the chip is imaged after subsequent additions to determine the sequence. Contrary to microarrays, patterned DNA probes bind to universal adapter sequences attached to DNA fragments, rather than the DNA itself. This means NGS does not require the user to design DNA probes to investigate genomic loci of interest, which allows for unbiased sequence identification.[32] NGS technologies achieve high levels of sensitivity and produce large amounts of data, with human genomes now able to be sequenced in a day.[34,36] With the large production of data, bioinformatic pipelines have been developed to assist in the analysis. These investments in sequencing instruments and bioinformatic analyses make NGS a relatively expensive analysis technique.[34] And, like microarrays, samples need to be

pre-amplified to produce enough sample from single cells to be detected and can be victim to PCR amplification biases.

1.1.3 The need for high throughput, accessible technologies for cellular isolation

Taken together, the current methods for cellular isolation and analysis have enabled promising advances in uncovering heterogeneity within cell samples. However, there remains a lack of accessible, high-throughput isolation methods that produce outputs amenable to the discussed analysis techniques. Microfluidics is a recently developed field focused on developing miniaturized devices that automate sample processing for high-throughput applications. These technologies are a promising step towards this goal.

1.2 Microfluidics

Microfluidic technologies have found a unique niche in the study of biological phenomena, since their small dimensions transfer well to the isolation, culture, manipulation, and analysis of cells. Culturally known as lab-on-a-chip (LOC) systems, these devices use channels for fluid handling with dimensions on the micrometer (μm) scale, leading to reaction volumes ranging from pico- to attoliters. These smaller volumes enhance reaction efficiencies, reduce sample and reagent requirements, shorten reaction times, and improve detection sensitivities.[39] Many microfluidic geometries have been designed throughout the years to perform various sample manipulations. Combination of these geometries in series automates multi-step sample processing workflows, reducing sample losses that compound from repetitive pipetting steps and decreasing user variability originating.

The customizability of microfluidics makes it an attractive platform for improved isolation and analysis tools for studying rare and single cells. Isolation strategies have been developed to separate cells based on size, morphology, surface marker expression, fluorescent marker presence, and magnetic activity.[40,41] These cell isolations can be performed passively, through diversion of the cell of interest to a unique outlet or capture within the device, or actively, where cells are manipulated to collection locations following their identification. Various methodologies for cellular isolations are described below.

1.2.1 Microfluidic devices for cellular isolation

1.2.1.1 Hydrodynamic sorting

Hydrodynamic sorting devices leverage variations in the physical properties of cells to isolate them into pure populations.[41] These properties include characteristics such as size, deformability, density, and morphology. Hydrodynamic sorting incorporates microfluidic features and/or geometries that divert cells into individual outlets. The designs and delivery of cell solutions on device are relatively simple and straightforward to use, leading to the ability to separate multiple cell types at the same time in a high throughput and label-free manner. Because of that simplicity, however, hydrodynamic sorting devices are sometimes unable to resolve different cells that have overlapping ranges of features due to natural heterogeneity or disease. The main categories of hydrodynamic sorting devices include filtration, deterministic lateral displacement (DLD), and inertial flow.

1.2.1.1.1 Filtration

Microfluidic filtration devices pattern an array of posts into a large chamber that cell solutions are passed through. Filtration devices require cells to fit between closely placed posts as shown in Figure 1.3A; thus, cells are separated based on their size and deformability.[42] Intuitively, larger, more stiff cells are unable to pass through the array, allowing smaller, more deformable cells to travel the entire length of the device. The arrays can be comprised of increasingly smaller posts and gaps to allow for successive separation of different cell populations. The main challenges of filtration devices include clogging of devices and physical stress imposed on cells as they deform to fit through the gaps between posts.

1.2.1.1.2 Deterministic lateral displacement (DLD)

Similar to microfluidic filtration, DLD devices use an array of posts for cell solutions to pass through. However, DLD separates cells based on their hydrodynamic radii.[43,44] Fluid flow through the chamber leads to the formation of fluid streamlines that mold around the posts. Cells with smaller hydrodynamic radii will be swept away by thinner streamlines positioned closer to the posts, whereas the center of mass of larger cells will be positioned more centrally in the gaps between the posts. These different behaviors will lead to different trajectories through the device and an ability to separate different cell types. Unfortunately, the occurrence of fibers within DLD arrays can block the passage of cells through the device and diminish the discretion ability of the device.[44]

1.2.1.1.3 Inertial flow isolations

In inertial flow-based devices, curved channels are used to apply inertial and drag forces on cells passing through. As fluids pass through a curved channel, their inertia causes them to travel towards the outer curve of the channel, but, when reaching the channel wall, boundary effects recycle the fluid around the outer edges and back towards the center of the curve.[45] Differences in cell size, density, and buoyancy lead to different magnitudes of displacement that result from the boundary effects and cells being focused into distinct equilibrium trajectories (Fig. 1.3B). This allows users to use serpentine,[46] spiral,[44] or maze-like channels[47] that can separate multiple cell types into different outputs. The main downside of inertial flow devices is that they sometimes lack selectivity when separating cell types, given that different cell types can have overlapping sizes and buoyant properties.

1.2.1.2 Immunochemical

Immunochemical devices rely on interactions between cells in solution and the solid surfaces present within the chambers. Microfluidic channels have relatively large surface areas that cells can interact with at multiple points throughout their journey. The cell-surface interactions fall under one of two categories: transient, low affinity interactions that alter cell elution time, and immobilizations that use capture agents with high affinities for specific cell types to bind them within the device.

Because immunochemical isolation methods rely on cell–surface interactions, they need cells to express desired surface proteins or features relatively consistently, which can differ due to natural heterogeneity or heterogeneity resulting from disease. This can reduce the efficacy and recovery of these devices when isolating certain cell

types of interest. Additionally, the performance of immunochemical devices is highly dependent on the flow rate, with higher flow rates leading to improved sample purity since non-specific interactions with non-target cells are minimized, but lower flow rates improving cell recovery due to stronger interactions taking place with device surfaces.

1.2.1.2.1 Transient interactions

Microfluidic devices are often treated with various solutions to alter the interaction of fluids, biological molecules, particles, or cells with the device surfaces. These treatments can be tuned to alter the adhesive interactions between cells and device surfaces to change cell trajectories or elution times inside the device. One example is deterministic cell rolling,[48] that coats the device surface to increase the adhesion of a target cell line to channel walls, leading to their travel through grooves that slowly divert them to a different output. Non-target cells simply float along fluid streamlines and are relatively nondiverted. These kinds of channels can be easily parallelized and scaled up to improve the throughput of sorting.[48]

1.2.1.2.2 Immobilizations

Capture agents like antibodies[49,50] or aptamers[51] have been applied in microfluidic devices to immobilize cell types of interest inside the device. An example of an immobilization device using antibodies to capture circulating tumor cells is shown in Figure 1.3C. These capture agents enable highly specific isolation of individual cells which is desirable for producing cell samples of high purity. However, it can be difficult to release captured cells in a manner that is gentle and does not alter their expressed phenotype. Some options that have been applied include applying higher flow rates,

treating with an enzyme or chemical to break the interactions, or incorporating thermally responsive materials.[41]

1.2.1.3 Dielectrophoresis (DEP)

DEP diversion of cells results from the application of a non-uniform electrical field; this can be achieved by applying an alternating current (AC) field.[40,41] Cells and other materials that are polarizable will take on a dipole moment which leads to movement towards or away from the applying electrodes, rather than the usual fluid flow patterns. Varying the electric field magnitude and frequency of the AC enables isolation of multiple cell types into individual compartments or "cages".[52] DEP-based capture of individual cells has been commercialized in the DEPArray,[53] which integrates automated imaging with DEP manipulation to visually identify cells of interest and usher them towards holding cells for later analysis (Fig. 1.3D). Small electrodes are patterned throughout the DEPArray, and intricate application of electric fields leads to single cells immobilized on DEP "cushions". Occupation of each DEP cage is dependent on Poisson statistics, so despite some arrays possessing many thousands of possible cell holding sites, the number that actually contain single cells will be limited.[53] Additionally, since selection of cells depends on imaging data, throughput will either be limited (by user) or dependent on access to expensive software (by computer).

1.2.1.4 Integrated fluid circuits (IFC)

The Quake group has been the main driver in development of IFC devices made from soft elastomers, such as PDMS.[40] Multiple layers of PDMS are stacked with thin, floor- or ceiling-like layers interspersed. These multilayer devices incorporate flow channels (for conventional liquid handling) with valve channels that can be variably

pressurized to block fluid movement into specific regions of the device. This ability to open and close fluid channels during operation enables precise control over the mixing of different fluids and adjustment of reaction volume, allowing users to subsequently perform multiple reaction steps in the same chamber.[54] Multilayer devices can be used to manipulate, isolate, and hold individual cells in vast array patterns and subsequently perform multi-step reactions and analyses on them, since they are contained in a restricted volume (Fig. 1.3E).[55] The technology has since been commercialized by Standard BioTools, formerly Fluidigm, with products such as the C1 Auto Prep Chip. However, isolation of single cells is limited depending on the size of the array, and fabrication and operation of novel multilayer devices can be challenging for inexperienced users to accomplish.

1.2.1.5 Magnetic sorting

It bears mentioning that MACS techniques were readily adapted into microfluidic formats and have helped facilitate many of the advances for the original technique. The main principles involved are the same as the original MACS technique, but oftentimes, microfluidic, magnetic sorting devices incorporate a permanent magnet positioned outside the main channel or ferromagnetic materials patterned into the device design (the latter is shown in Fig. 1.3F).[29,56] Rather than containing all magnetic cells within the chamber, microfluidic devices often magnetically alter the cellular trajectories within a channel, leading to isolation of pure cell types from different outlets.[29] The main drawback also remains the same, that magnetic sorting requires cells to possess magnetic activity, either naturally or through labeling with magnetic beads.

1.2.1.6 Droplet microfluidics

Droplet microfluidics constitutes a sub-field of microfluidic devices that exist for biological assays. A second, immiscible phase, known as the carrier phase and often made up of fluorinated oils, is employed to segment aqueous sample into droplets. Droplets can be generated rapidly, with rates reaching over 10 kHz.[57] This segmentation compartmentalizes sample into even smaller reaction volumes, with each individual droplet acting as a separate replicate for the experiment. As droplets pass through microfluidic channels, fluid vortices naturally form within the droplet, leading to enhanced mixing of samples[58,59]. The small volume of droplets makes them excellent vehicles for single-cell analyses, and while the number of cells occupying each droplet will depend on Poisson statistics, droplet analyses are easily scalable. The number of cells analyzed can be modulated by adjusting the number of droplets generated. This contrasts with continuous microfluidic devices, where reaction scaling requires a new design with altered dimensions.

Various geometries have been developed to enable droplet-specific fluid manipulations, including reagent addition,[60,61] sample washing,[62] and droplet sorting.[63,64] 10X Genomics has developed a commercial, droplet generator device that pairs single cells with barcoded beads inside droplets with reaction components to accomplish single-cell RNA sequencing (scRNA-seq).[65] This device has been able to perform other single-cell variations on conventional epigenomic techniques,[66] and the principle of incorporating barcoded beads into droplets has been employed for other techniques such as Drop-seq[67] (Fig. 1.3G). Due to the large number of empty droplets that result from the Poisson distribution of cells, many barcoded beads are needed to

ensure no cell is alone in a droplet without a barcode. Alternatively, single cells and beads could be synchronized to enter droplets together, but that is a non-trivial task.

To circumvent the many empty droplets that result during droplet generation, Baret *et al.* invented fluorescence activated droplet sorting (FADS).[63] This technique is comparable to FACS, but droplet contents are now investigated by the laser, and the diversion of droplets relies on differences in polarizability between the droplet and carrier phase. This shift to droplets has two major benefits for single-cell studies. First, laser irradiation and electric field application are distributed over the droplet volume instead of single cells, which helps reduce harmful effects that are characteristic of FACS. Secondly, as mentioned previously, droplets introduce compartmentalization into microfluidic assays, meaning that any components of interest secreted from cells are maintained within the droplet volume This expands the possible molecules that a fluorescent, sorting signal can be derived from. Mazutis *et al*. used this to their advantage to enrich droplet samples for cell- and bead-containing based on the secretion of an antibody from cells.[26]

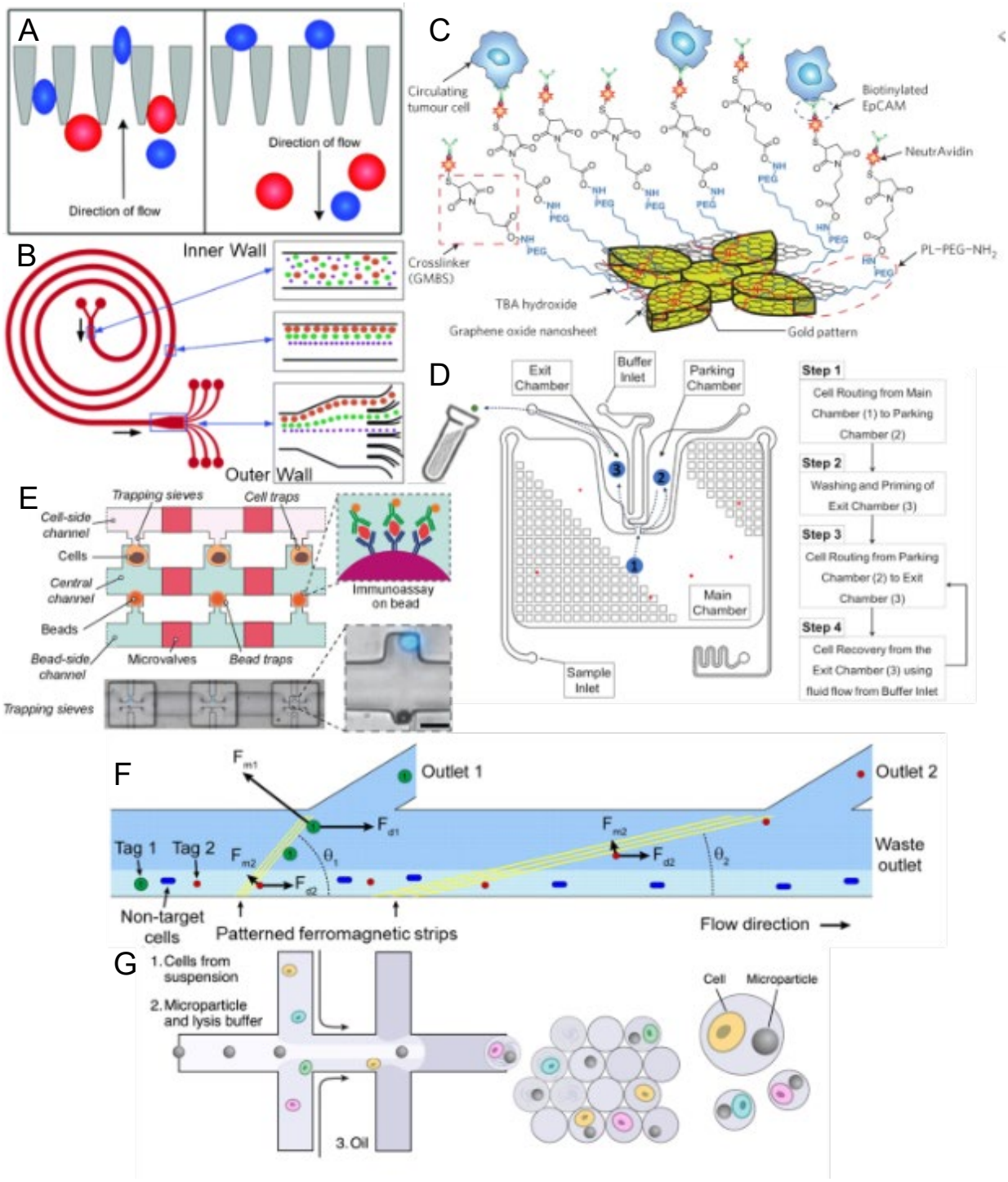

Figure 1.3. Common microfluidic cellular isolation principles and examples from literature. Cells can be separated hydrodynamically using pillar arrays[42] (A) or differences in inertial flow[44] (B), via immobilization with capture agents[50] (C), or by dielectrophoretic manipulation[53] (D). Multilayer devices[55] can be used to capture cells in individual compartments (E). Magnetic tags can enable MACS separation[29] (F) and droplets[67] can be used to isolate cells into individual, mobile aqueous compartments (G). Figures have been reproduced with permission.

1.3 Applications

For the purpose of this thesis, we will focus on two biological applications of cellular heterogeneity: heterogeneity of extracellular vesicles (EVs) and heterogeneity in epigenetic regulation.

1.3.1 Extracellular vesicle (EV) dynamics

Cell-to-cell signaling is vital for the survival of an organism. Different cell types must communicate and cooperate to perform routine biological processes, progress through development, respond to external stimuli, and eliminate unhealthy cells.[68,69] Cells typically communicate by secreting biological materials into the extracellular space. These materials, which include ions and metabolites, proteins, ligands, and EVs,[69] can be bound by receptor proteins on receiver cells. Figure 1.4 depicts cellular communication occurring via EV secretion and uptake. Binding by receptors triggers an internal cascade of protein conformation changes and component binding which culminates in corresponding alterations to gene expression patterns.

EVs are lipid bilayer wrapped vehicles that transport cellular contents and can vary in size (30 – 1000 nm),[70] cargo (nucleic acids or proteins), and composition (lipids and membrane proteins). They participate in waste management and cellular communication through the exchange of materials between cells[70,71] Clinical interest in EVs results from their roles in disease progression and the possibility that their secretion could be used as a biomarker or modulated as a therapeutic route.[72,73] However, they exhibit many facets of heterogeneity, which makes them difficult to study with the commonly applied bulk techniques. These methods lack the required resolution to discover heterogeneity in EV secretion dynamics or EV characteristics,

themselves.[72,74] Thus, single-cell methodologies have been developed to deepen our understanding of heterogeneity in EVs.

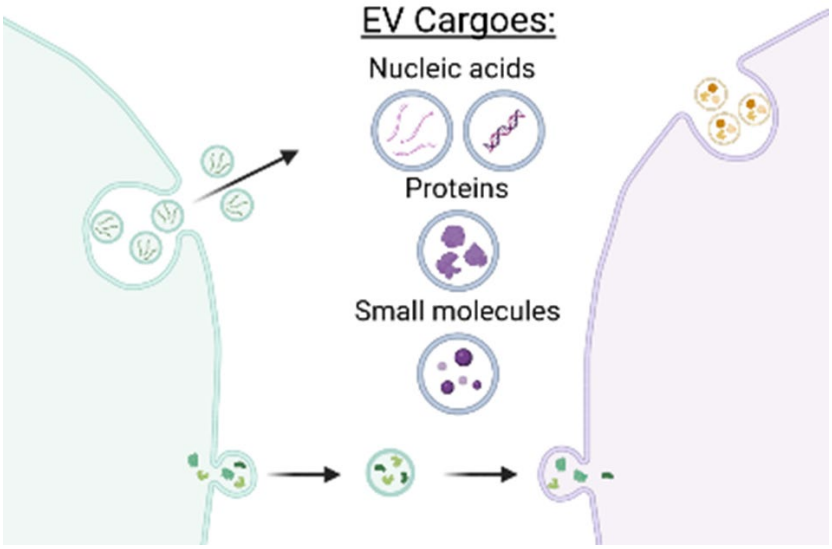

Figure 1.4. Illustration of cellular communication facilitated by extracellular vesicles (EVs). EVs are composed of the membrane materials and contents of their origin cells. Nucleic acids, proteins, and small molecules make up the possible cargoes for EVs to ferry between cells.

1.3.1.1 Bulk EV techniques:

1.3.1.1.1 Ultracentrifugation (UC)

By far, the gold standard for bulk EV studies is ultracentrifugation (Fig. 1.5A).[71,75,76] UC relies on differences in size, density, and shape of biological components to isolate EVs for analysis. Cultured cell solutions are centrifuged to remove cells and cellular debris in the extracellular matrix. An EV pellet results from centrifugation of the supernatant which can be resuspended to analyze the EVs as desired. Incorporation of a density gradient medium can help refine the separation of EVs from other particles present in the supernatant. However, UC techniques suffer from low yields relative to the sample input and lengthened procedures can mechanically damage the collected EVs.

1.3.1.1.2 Ultrafiltration

EVs can also be isolated by size through ultrafiltration—iterative filtration steps that progressively decrease pore size to obtain EVs of a specific size range (Fig. 1.5B).[71,75] Ultrafiltration methods rely on more accessible technology than ultracentrifugation and can be completed in shorter times. Resulting EV populations are highly pure, which can benefit analysis downstream. However, filters easily clog and trap EVs of interest, leading to lower yields in resulting samples.

1.3.1.1.3 Immunochemical techniques

Immunochemical techniques rely on the presence of cell surface markers on EV membranes to isolate EVs of interest.[71] Antibodies are functionalized to a surface, EV-containing sample is applied and washed away, and bound EVs are analyzed. Figure 1.5C shows capture of EVs from a cell mixture through capture by antibodies for cell surface markers on the EVs. Due to the use of antibodies, immunochemical isolation techniques produce highly pure samples of EVs. However, antibody-capture of surface markers also assumes consistent presence on EV membranes. This can lead to loss of EVs of interest that do not possess the cell surface marker in high quantities. Enzyme-linked immunosorbent assays (ELISA) have been applied to isolate and analyze EVs, however, samples often need pre-enrichment steps, limiting their use in clinical settings. Magnetic bead-based techniques have also been employed. Antibody-functionalized beads possess higher surface areas to bind EVs compared to the well plates used in ELISAs. Additionally, the technique is gentler than the gold standard technique, preserving the biological activity of EV components.

1.3.1.2 Single-cell EV tools

While bulk techniques are useful for predicting generalized secretion responses to stimuli and collecting EVs from biological fluids for diagnostics, heterogeneity in EV secretion, makeup, and processing is not accounted for. Thus, tools are needed to visualize EVs at the single-cell level to establish all possible routes of processing, secretion responses, EV compositions.

1.3.1.2.1 Super-resolution microscopy (SRM)

SRM techniques utilize photo-activatable fluorescent tags to investigate subsets of molecules of interest at a time.[74,77,78] Once activated, fluorescently tagged molecules can be imaged to determine their location and preferred binding partners. An example of SRM imaging of EVs is shown in Figure 1.5D, where EVs present in a cell are observed using stochastic optical reconstruction microscopy (STORM). SRM techniques are powerful for studying EVs *in vivo* with precise spatial resolution, and they have been used to study EV secretion, EV-mediated cellular communication, EV uptake, and EV fates inside of cells. However, the equipment required for SRM is expensive, which limits its wider application. Additionally, proteins or lipids on the surface of EVs must be tagged with a photo-activatable fluorophore, which can alter their biological utility.

1.3.1.2.2 Microfluidic, single-cell EV devices

Microfluidic devices provide a customizable format to isolate and analyze single-cell derived EVs, thus there is no standardized design for studying EVs. However, some common features do arise. Mainly, cells are typically encapsulated within an individual compartment, whether it is a patterned array, well feature, or a droplet (Fig. 1.1E,

F).[72,73,79,80] As has been discussed above, the number of cells occupying each compartment will follow a Poisson distribution dependent on cell solution concentration and compartment volume. Following compartmentalization of cells and incubation to allow for EV secretion, microfluidic techniques can leverage concepts from bulk techniques to study secreted EVs, including immunochemical-mediated capture[73,79,80] and fluorescence imaging.[72,79] Microfluidic devices are accessible and flexible, offer multiplexing and parallel processing capabilities, and enable high-throughput analysis the type and amount of EVs secreted by single-cell. However, microfluidic devices employed to study EVs commonly focus on singular assay steps, either isolation of cells only or analysis following pre-purification from complex mixtures. There is a gap in the microfluidic technologies available to perform the entire protocol, encompassing isolation, sample processing, and analysis steps.

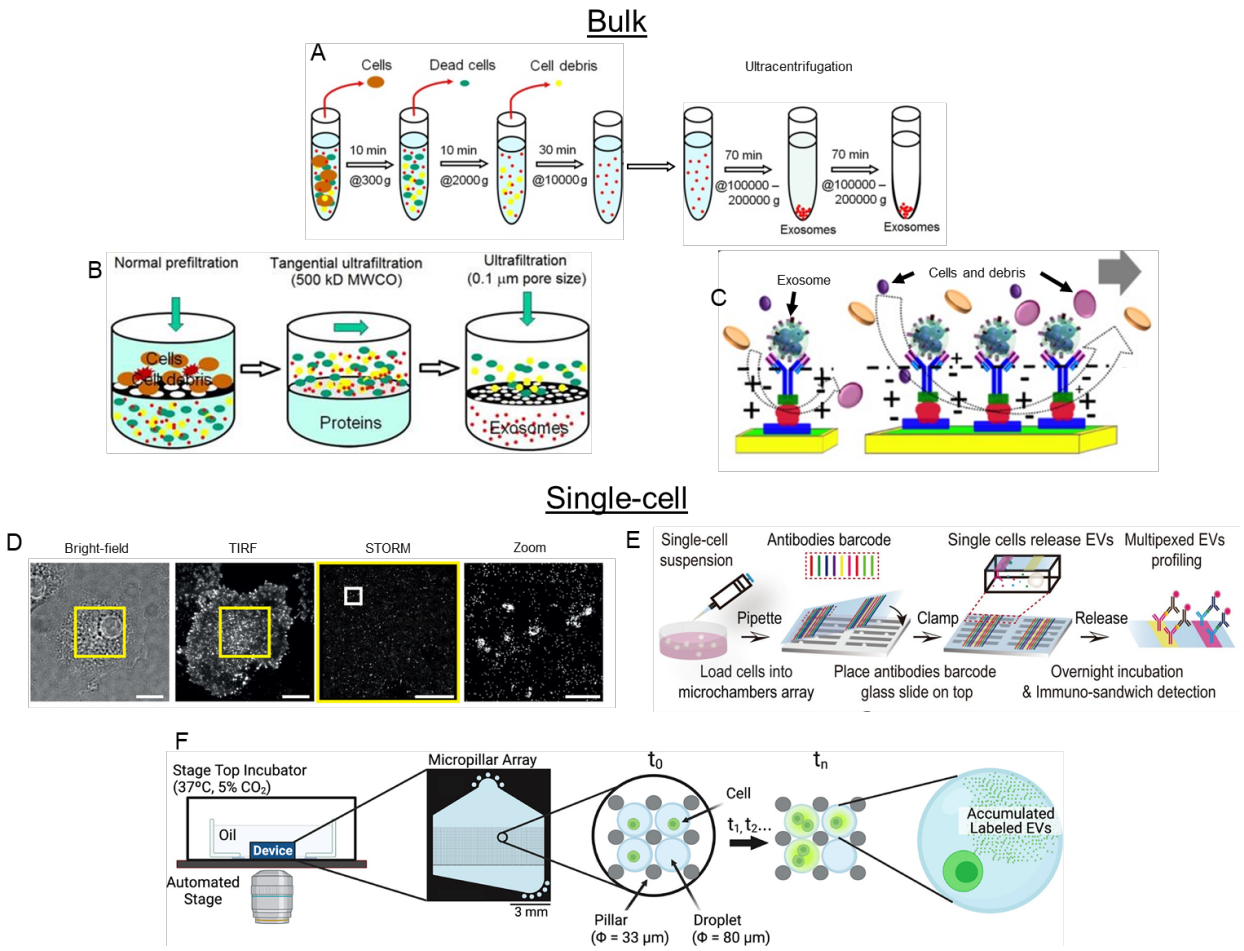

Figure 1.5. Bulk versus single-cell methods for isolating and studying extracellular vesicles. Commonly used bulk isolation techniques include ultracentrifugation[81] (A), ultrafiltration[81] (B), and immunochemical capture using capture agent coated surfaces[82] (C) or magnetic beads. Single-cell methods include SRM techniques such as STORM[74] (D), microfluidic capture in wells[73] (E) and droplets[72] (F). Figures were reproduced with permission.

1.3.2 Epigenetic regulation

The second biological application focused on in this thesis is cellular heterogeneity within epigenetic regulation. Deoxyribonucleic acid (DNA) is the molecule responsible for preserving the information needed for cells to build the molecules and proteins needed for survival and vital functions. Considering that each human DNA molecule is 6 feet in length[83,84] while cells and their nuclei measure ~30- and 10-µm in diameter, respectively, cells must employ various compaction strategies to fit the entire

DNA molecule within each cellular nucleus. Roughly 146 base pairs (bp) of DNA wrap around an octamer of histone proteins to form the nucleosome—the fundamental unit of chromatin. Adjacent nucleosomes then fold around each other in conjunction with the histone protein H1 to form the 30-nm coil, and these structures continue wrapping around themselves to form further condensed chromatin structures until they form the most compact form of chromatin: the chromosome.[85,86]

While the chromosome provides an ideal vehicle to maintain compaction during latent periods, the DNA is not accessible for transcription machinery to bind and construct ribonucleic acids (RNAs) and consequently the proteins needed to respond to stimuli. Thus, cells must balance DNA compaction with the need for DNA accessibility. They accomplish this through epigenetics—the regulation of accessible DNA regions in response to environmental cues. Epigenetic regulation involves chemical modifications to DNA and histone peptide tails, binding to chromatin-associated proteins, binding of RNA molecules, and the three-dimensional architecture of chromatin itself[87]. This regulation leads to the observation of differing phenotypes for cells that possess identical DNA. This is the case for differentiated cell types within an organism as well as phenotypically distinct sets of identical twins. Some common mechanisms of epigenetic regulation are explained in Section 1.3.2.1. Chromatin accessibility and nucleosome positioning are of particular interest in this thesis, so discussion on epigenetic profiling techniques will be limited to those features, some of which are highlighted in Figure 1.6.

The dysregulation of epigenetic mechanisms has been associated with the development of conditions such as cancer,[88–90] cardiovascular disease,[91] Alzheimer's disease, [89,92] Parkinson's disease,[89,92] and autoimmune disorders.[89,93] Thus, there has

been recent interest in investigating the prevalence, location, and distribution of epigenetic mechanisms throughout the genome to identify potential biomarkers for disease diagnosis and progression. Since lifestyle choices can impact an individual's epigenome, epigenetic biomarkers pose an attractive target to link the genome and environment. Additionally, they could contribute to the development of personalized therapies.[92,94–96] The advent of technologies like next generation sequencing (NGS) facilitated the development of a diverse toolbox of epigenetic profiling techniques.[94,97] These techniques advance our understanding of the complex relationships that exist between epigenetic mechanisms, environmental cues, and disease progression.

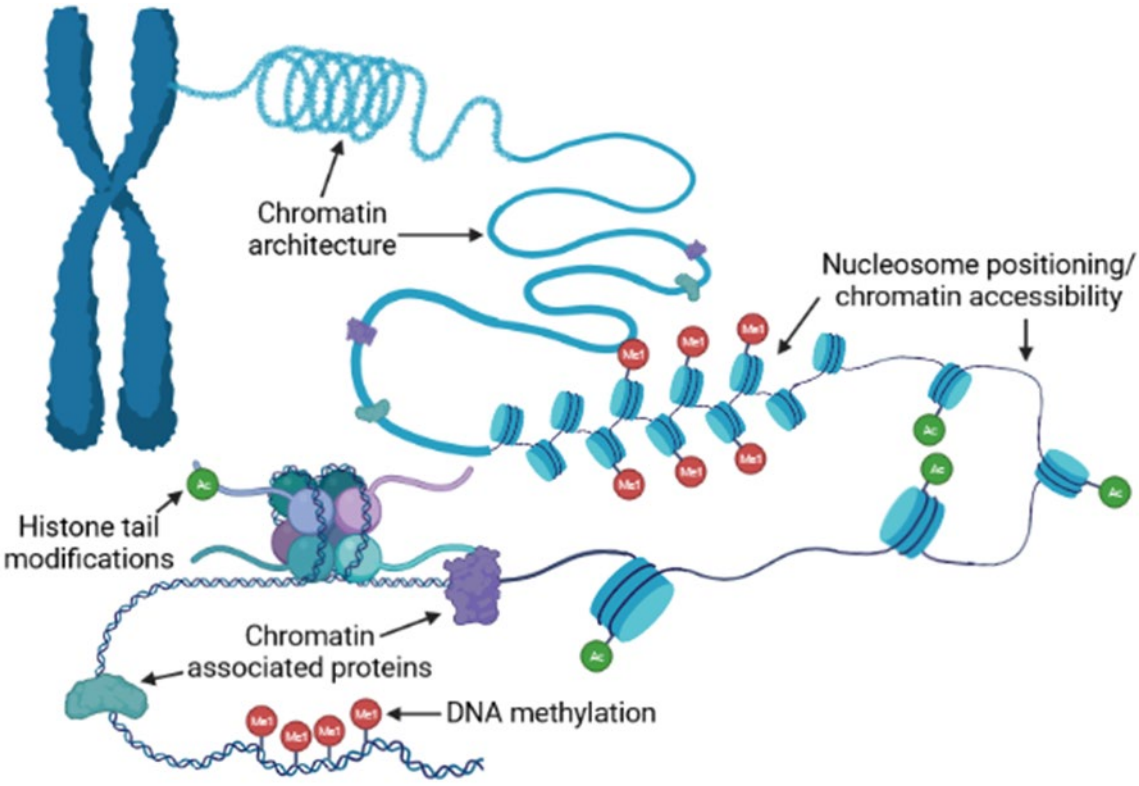

Figure 1.6. Common mechanisms of epigenetic regulation employed in the cell to balance DNA compaction and accessibility. Figure produced using BioRender.

1.3.2.1 Common epigenetic regulation mechanisms

1.3.2.1.1 DNA methylation

DNA is a polymer composed of four nucleotide subunits: adenine, thymine, cytosine, and guanine (A, T, G, C, respectively). These four nucleotides combine in varying sequences to communicate genetic information. DNA methylation occurs when a methyl group is attached to a cytosine nucleotide to form 5'-methylcytosine.[98] Often, this occurs when cytosine is followed by a guanine nucleotide (CpG site). DNA methylation has been shown as an effective gene regulation tool, leading to stable silencing of sections of DNA. It plays a vital role in cellular differentiation, X chromosome inactivation, and embryonic development.[98–101]

1.3.2.1.2 Histone tail modifications, chromatin associated proteins, and transcription factors

The modification of amino acid residues along the peptide "tails" of histone proteins making up the nucleosome alters gene expression patterns.[102,103] These modifications often alter the charge associated with the histone tail which modulates the electrostatic interactions between the nucleosome and DNA molecule, which naturally possesses a negative dipole moment. Modifications that effectively increase the positivity of the histone tails (negative to neutral or neutral to positive) strengthen the electrostatic attraction between DNA and the histone tail. This stronger attraction elicits tighter interactions between the two, decreasing nucleosome mobility along the DNA molecule and the accessibility of the underlying DNA. Conversely, effective decreases in charge (positive to neutral or neutral to negative) weaken the electrostatic interactions between DNA and the histone tails, allowing the DNA to be associated more flexibly

which increases accessibility of the DNA. Commonly studied modifications include methylation, acetylation, phosphorylation, and ubiquitination.[86,90,104]

Histone tail modifications also affect chromatin structure by recruiting remodeling enzymes and other chromatin associated proteins (CAPs) that affect the organization or usage of DNA.[104] CAPs interact with DNA to alter the expression of different genes during development, regular maintenance of homeostasis, and in disease.[105] Transcription factors (TFs) constitute one CAP class that bind DNA and regulate the transcription process.[105–107] Understanding what sequences TFs tend to bind expands our understanding of their biological roles and facilitates prediction of other potential DNA binding sites in the genome.

1.3.2.1.3 Chromatin architecture

Chromatin adopts higher order structures to maintain DNA compaction, but these structures can also have a regulative effect on different gene regions. Outside of mitosis or meiosis, the chromatin of distinct chromosomes occupies different spaces within the nucleus, known as chromatin territories.[108,109] These allow distal regions of DNA on the same chromosome to cluster together and interact in different ways. One example is the promoter/enhancer chromatin loop, where an enhancer DNA sequence contained up- or downstream of a gene promoter sequence is brought into close proximity to the latter, improving transcription dynamics.[110]

1.3.2.1.4 Chromatin accessibility and nucleosome positioning

Transcription of genes begins with binding of proteins to form complexes that recruit TFs and then RNA polymerase II.[107,111] Binding occurs at specific DNA sequences and requires chromatin to be in its extended conformation, known as

euchromatin.[4,112–114] Euchromatin is characterized by looser spacing of nucleosomes over DNA but conserved nucleosome positions relative to the underlying DNA sequence. On the other hand, heterochromatin is more compacted, with nucleosomes evenly spaced but positioned at various locations relative to underlying DNA sequence. Thus, the position of nucleosomes throughout the genome has been investigated to gain insights into epigenetic regulation.

1.3.2.2 Techniques for profiling chromatin accessibility and nucleosome positioning

Profiling the locations of nucleosomes and accessible chromatin throughout the genome is of particular importance in the work of this thesis, so we will specifically highlight the gold standard profiling techniques used to study them. Protocol steps are described following cell and nuclear membrane lysis or extraction of nuclei. Figure 1.7 highlights major protocol steps involved with the three main nucleosome positioning and chromatin accessibility profiling techniques.

1.3.2.2.1 Micrococcal nuclease digestion paired with sequencing (MNase-seq)

MNase-seq utilizes the endo-exonuclease micrococcal nuclease to digest DNA to mono-nucleosome-length DNA fragments.[114–116] The digestion activity of MNase was initially leveraged in 1974[117] by Markus Noll to support the theory that nucleosomes are the fundamental packaging unit of chromatin. The emergence of NGS technologies expanded the usefulness of MNase digestions to generate maps of nucleosome locations throughout the genome in a high-throughput manner.[36] Cells are lysed, which exposes chromatin so that MNase can fragment the DNA. The digestion is quenched by adding EDTA to chelate calcium ions required for enzyme activity. DNA fragments bound to proteins are subsequently released and sequenced. Linker DNA between

nucleosomes and in open regions of chromatin is especially susceptible to MNase digestion, while DNA bound within nucleosomes or to CAPs is blocked and remains intact. Thus, MNase-seq is commonly used to reveal genome-wide locations of nucleosomes and CAPs.

1.3.2.2.2 MNase accessibility of chromatin (MACC-seq)

MACC-seq was developed to maximize epigenomic information derived from MNase-treated cells. [118] The technique applies several concentration levels of MNase to different cell samples to directly map active regions of chromatin in addition to nucleosome positions. Lower concentrations of MNase allow longer higher-order fragments to remain intact while higher concentrations produce mononucleosome-length fragments almost exclusively, allowing researchers to expand their understanding of various levels of nucleosome-mediated organization.

1.3.2.2.3 DNase I hypersensitive sites sequencing (DNase-seq)

Deoxyribonuclease I (DNase I) is another enzyme commonly used to digest chromatin. DNase I cleaves DNA molecules via endonuclease activity at DNase hypersensitive (HS) sites,[119] which occur within nucleosome-free regions of chromatin. Due to their genomic context, DNase HS sites tend to occur near DNA sequences that are actively being transcribed. While DNase I cleaves DNA in open regions, it does not have significant exonuclease activity, meaning it does not continue to digest DNA molecules following cleavage.[120] This contrasts MNase, which fully digests exposed DNA segments. Thus, DNase I digestion produces DNA fragments within open chromatin regions that can be sequenced to map accessible gene regions present throughout the genome.[119]

1.3.2.2.4 Assay for transposase-accessible chromatin (ATAC-seq)

ATAC-seq also identifies accessible chromatin regions within cells.[83,121] The assay employs Tn5, a transposase enzyme that natively catalyzes the transposition, or "jumping", of genes between different chromosomal locations. Tn5 works by cleaving chromatin then tagging on a replacement DNA sequence to the resulting strands, a process known as "tagmentation".[122] This cleavage event occurs preferentially within nucleosome-free regions since they are readily accessible to interact with proteins. Because of this preference, ATAC-seq generated maps of released DNA fragments will cover similar gene regions to DNase-seq. The replacement sequence tagmented onto genomic DNA can be chosen to apply primers and sequencing indices, which streamlines later library preparation steps and helps reduce the number of cells needed to generate usable results. Thus, the standard ATAC-seq sample size is 50,000 cells, and it has been shown to generate sequencing data from as few as 500 cells.[123]

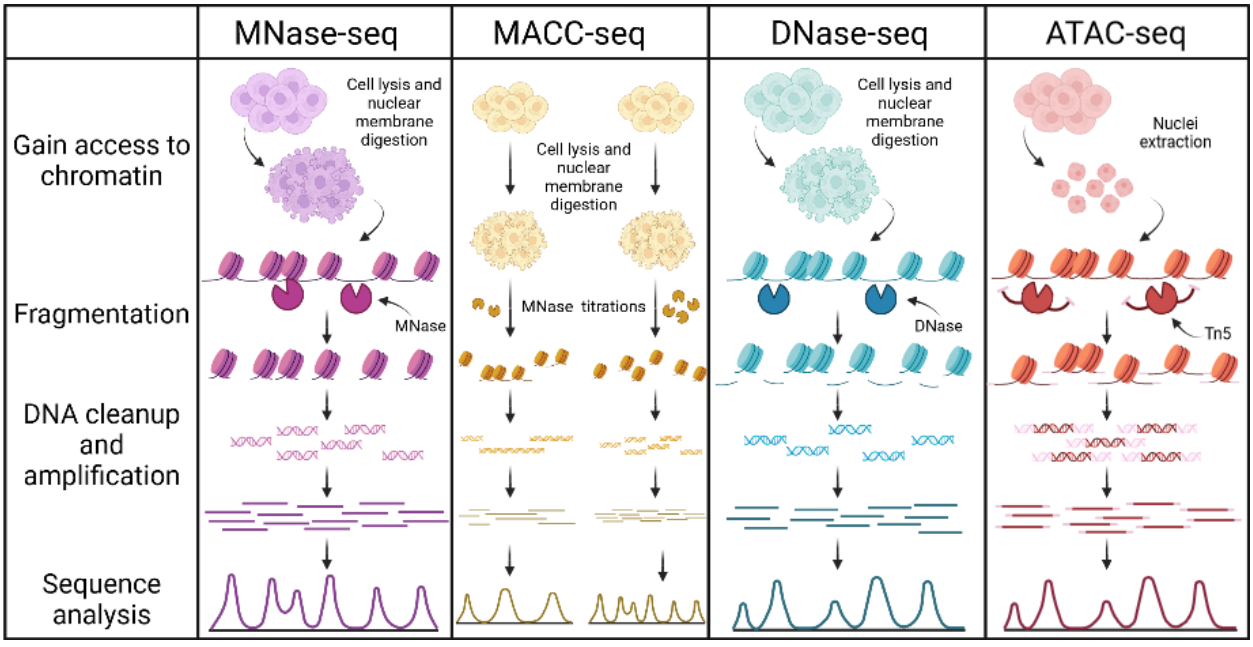

Figure 1.7. Comparison of common protocols for profiling chromatin accessibility and nucleosome positioning assays. Figure produced using BioRender.

1.3.2.3 Low-input techniques for studying chromatin accessibility and nucleosome positioning

The conventional techniques developed to study different epigenetic mechanisms require millions of cells to generate high signal to noise ratios.[115,124,125] This large sample requirement results from routine sample losses through many pipetting steps and poor reaction efficiencies with enzymes and antibodies.[126,127] However, epigenetic regulation is not immune to variations from cellular heterogeneity.[11] Thus, bulk, population-level techniques blur the contributions of individual cells and subpopulations that could be biologically relevant. It also limits the possible application of these methods to studies on rare or limited cell samples, such as those obtained from biopsies (typically only ~1000 cells).[127,128]

Epigenetic profiling techniques have been developed to address this limitation and have profiled the epigenome of limited cell numbers.[121,129,130] Some researchers have turned to using microfluidic methods of analysis due to their miniaturized volume, automated reagent manipulations, and improved reaction efficiencies. Additionally, several techniques have been converted to single-cell formats to expand our understanding of cell-cell variations in the epigenome, some of which incorporate microfluidic technologies.[4,131,132]

1.3.2.3.1 Single-cell MNase-seq (scMNase-seq)

Lai *et al.* adapted MNase-seq to investigate the heterogeneity of nucleosome positioning patterns in single cells.[4] They utilized FACS to obtain single cells in individual PCR tubes, then performed MNase digestions at a volume two orders of magnitude lower than bulk MNase experiments.[116] Libraries were prepared for DNA

fragments derived from individual cells then sequenced. Application of the technique to three mouse cell lines led to the observation that nucleosome spacing was tightly controlled along inactive gene regions, while the positions of nucleosomes within active chromatin was conserved more strictly. Variation in specific spacing or nucleosome positions was apparent between individual cells, so these organizational principles were unclear in bulk MNase-seq processing. Single-cell MNase-seq would still benefit from further volume reductions to improve the MNase reaction efficiency and reduce reagent usage. Additionally, single-cell isolation via methods other than FACS would be desirable to minimize adverse effects on cellular homeostasis.

1.3.2.3.2 Low-input MNase accessibility of chromatin (low-input MACC-seq)

Low-input MACC-seq reduced the volumes of reagents used per titration while scaling the units of MNase applied to the number of cells included.[128,133] This facilitated production of MACC-seq libraries from as few as 50 cells per titration. The reliance of this technique on several MNase titrations requires that different cell samples are used for analysis of each nucleosome-organization level. This means that unique features of organization could be missed, and the total number of cells required will scale with the number of titration steps included. Additionally, low-input MACC-seq relies on FACS to obtain cellular populations which could alter cellular mechanisms of epigenomic organization.

1.3.2.3.3 Droplet microfluidic platform for MNase-seq

The Bailey Lab developed a droplet microfluidic module for performing simultaneous steps of the MNase-seq procedure.[134] Whole cells are injected into droplets along with lytic components and MNase to perform simultaneous cell lysis and

DNA fragmentation. The reaction is quenched by injecting EDTA into droplets at the end of the device, and DNA fragments can be purified and analyzed in bulk. The incorporation of ~150 pL droplets improves reaction efficiencies, allowing the process to be performed at room temperature whereas other techniques require incubation with MNase at 37 °C.[4,115,133] MNase-seq libraries were produced from as few as 2500 cells. This technique would benefit from adaptation to include wider varieties of cell types, including those possessing cell walls.

1.3.2.3.4 Single-cell DNase-seq (scDNase-seq)

Similar to scMNase-seq, scDNase-seq isolates single cells into individual tubes following FACS treatment, then conventional lysis and DNase digestion occur in reduced volumes.[132] Libraries are prepared from released DNase HS fragments. To prevent significant losses of the small amounts of DNA fragments obtained from single cells, circular DNA plasmids are added as carrier DNA to be sacrificed in sample losses that occur during processing. These circular plasmids are incompatible with adapter ligation and will not amplify. Application of scDNase-seq reaffirmed that DHS occurrence in single cells is a strong predictor of gene expression. Consolidation and automation of these processing steps would be desirable to reduce sample losses incurred during multiple pipetting steps.

1.3.2.3.5 Single-cell ATAC-seq (scATAC-seq)

Single-cell ATAC-seq has been accomplished through multiple strategies. The first report of scATAC-seq relied on combinatorial indexing of nuclei to distinguish accessible chromatin regions in single cells while avoiding exclusive processing of individual cells.[135] In combinatorial indexing, nuclei are extracted and distributed into

wells for Tn5 digestion and tagmentation of cells. Nuclei are subsequently pooled before being evenly distributed via FACS into new wells, where DNA fragments are uniquely barcoded a second time during DNA amplification. This technique relies on the assumption that it is unlikely for two single cells to follow the same indexing path, the likelihood of which can be tuned by modulating the number of nuclei present in the second well. However, balancing the desire to minimize single cells with the same combinatorial path impedes the throughput of the method due to the large number of wells needed to facilitate low numbers of nuclei within the second well.

Buenrostoro *et al*. incorporated a commercialized, programmable IFC (Standard BioTools's C1 Single-Cell Auto Prep System) to capture single cells in individual compartments and perform ATAC-seq.[131] Following Tn5-mediated barcoding of DNA fragments, single-cell libraries were pooled, amplified, and sequenced. Buenrostoro *et al*. were the first researchers to accomplish truly single-cell ATAC-seq processing, and they identified specific DNA regulatory elements associated with modulation of chromatin accessibility variance. However, their technique maintains the conventional drawbacks of IFCs, namely that isolation of individual cells on the device is low throughput due to the need to manually identify individual cells for isolation and limited space on each chip.

Subsequent scATAC-seq efforts have turned to droplets as the platform to isolate and process individual cells.[66,136] Tn5 treatment is performed in bulk, single-nuclei suspensions with the assumption that chromatin is contained within intact nuclei. Nuclei are then distributed into droplets with components for barcoding and DNA amplification via commercial droplet generator technologies (BioRad ddSEQ Single-Cell Isolator and

10X Genomics Chromium platform). Via these techniques, Lareau *et al*. were able to unbiasedly identify cell types from tissue samples and observe cell-type-specific changes in chromatin accessibility following stimulation,[66] while Satpathy *et al.* investigated the activity of regulatory elements in cellular differentiation and tumor landscapes.[136] These techniques are inherently scalable, but isolation of single-nuclei into droplets with individual barcoding beads relies on Poisson statistics: multiply-barcoded DNA fragments from individual cells need to be deconvoluted, while some barcode beads will be unused in empty droplets.

1.4 Dissertation Overview

The following dissertation describes work in developing modular, droplet microfluidic workflows to isolate single-cells and cell subpopulations to perform single-cell or low-input biological assays. Chapter 2 focuses on the expansion of a Bailey Lab, droplet washing technology [62] to isolate single cells into droplets through the new CellMag-CARWash workflow. Two different cell types were successfully isolated with high purity in product droplets. CellMag-CARWash was subsequently applied to incorporate a single-cell level molecular treatment to study the response in EV secretion dynamics from single cells. A second device incorporated after droplet incubation removed cells from droplets to facilitate fluorescence imaging of EVs for analysis. CellMag-CARWash processing revealed heterogeneity in EV secretion for treated and non-treated cells. Chapter 3 characterizes the use of FADS to separate fluorescent cell subpopulations from cell mixtures and provide enriched, cell-containing droplet populations for downstream droplet processing. Specifically, a droplet microfluidic, nucleosome positioning device [134] was used to generate mono-nucleosome length DNA

fragments from cell wall-possessing cells. Modifications to the overall setups, device designs, and operation parameters facilitated cohesive use of the devices in series and demonstrated potential for their application to study epigenetic differences between cell subpopulations. Finally, Chapter 4 describes the anticipated application of the FADS-nucleosome positioning workflow, intriguing future work for both device workflows, and comments on the challenges and benefits of modular droplet microfluidic workflows for studying single- and low-input cell samples.

Chapter 2 CellMag-CARWash: A Droplet Microfluidic Workflow for Isolation of Single Cells from Complex Mixtures for Use in Downstream Processing and Analysis

Claire D. Cook, Brittany T. Rupp, Emma A. Purcell, Matei Pop, Abigail E. Radomski, Nicolas Mesyngier, Ryan C. Bailey, Sunitha Nagrath**

The following chapter was adapted from a manuscript currently in preparation.

2.1 Introduction

It has been established that within any population of seemingly identical cells some cell-to-cell differences exist.[1] Traditional bulk analyses of a cell population often results in an average signal of the population being reported, ignoring rare cell populations and heterogeneity within samples. Therefore, single-cell studies have gained momentum over the past ten years as researchers have begun to recognize the value of being able to observe heterogeneity within cell populations.[2–5] Nature has recognized both single-cell sequencing and single-cell multimodal omics as methods of the year in 2013[6] and 2019,[7] respectively. Along these lines, single-cell functional studies are also evolving. Studies examining cellular heterogeneity in diseases such as cancer show how cellular differences can affect everything from immune response to drug resistance.[8–10] Cells also demonstrate heterogeneity in their ability to signal and

communicate with other cells, through either direct interactions or from secreting signaling molecules like cytokines and extracellular vesicles (EVs).[11–14] Cell communication can affect multiple important processes including development, cell growth, differentiation, migration, and apoptosis.[15–17] However, to further examine heterogeneity and how it relates to cellular behavior and function, it is necessary to first isolate and maintain viable single cells in an easy to use and manipulatable format for further analysis.

The most common single-cell isolation techniques are fluorescence activated cell sorting (FACS), magnetic activated cell sorting (MACS), manual cell picking, and microfluidics.[18,19] FACS, MACS, and manual cell picking offer the ability to isolate single cells, but require large sample volumes, can be expensive, non-specific, and/or require specialized training and high skill to perform. Alternatively, microfluidic technologies for single-cell isolation are becoming increasingly common. The small scale of microfluidic devices allows researchers to manipulate fluids on a pico- and micro- scale, allowing them to minimize assay volumes. Commercial single-cell microfluidic technologies are available, including the DEPArray,[20] which manipulates single cells in a chamber using dielectrophoresis (DEP), and integrated fluidic circuits (IFC)[21] that move single cells into chambers using a system of pressure controlled microfluidic valves. Both technologies have been applied in multiple studies to obtain single-cell data,[22,23] but they suffer from limitations, such as lengthy processing time, unvalidated for use in live cells (DEPArray), and limited ability to collect significant numbers of cells (IFC).[24,25]

Droplet-based microfluidics, a sub-type of microfluidic devices, are technologies that enable compartmentalization and analysis of analytes in a high throughput

fashion.[2–5,26] These droplets can isolate single cells into aqueous droplets surrounded by an oil phase. This creates a small reaction chamber for each individual cell that can be characterized or assayed using low volumes. Additionally, droplet microfluidic technologies are scalable, allowing users to adjust the number of cells analyzed per experiment by modulating the volume emulsified.[27,28] One successful, commercially available, single-cell droplet microfluidic technology, the 10X Genomics Chromium system, has been used across multiple studies to examine chromatin accessibility, gene expression and protein expression.[29,30] However, for samples with contaminating cell populations, the Chromium system provides no pre-sorting of the sample to remove unwanted cells, necessitating either incorporation of an additional isolation step using techniques such as FACS or elimination of undesired cell profiles during data analysis. Hence, there is a highly significant, unmet need for easy to use, streamlined strategies that can separate target cells from heterogeneous, complex samples then interrogate them individually at the single-cell level.

Here, we describe the adaptation and expansion of the droplet microfluidic CAR-Wash system to isolate single target cells from a bulk cell mixture. The CAR-Wash system was originally developed to enrich small molecules attached to magnetic beads, such as proteins or DNA fragments, by pulling beads to the edge of the device using a magnet then resegmenting them into product droplets. In this study, we show that a target cell population can be specifically tagged with magnetic beads using custom antibody panels while contaminating cells have minimal bead attachment. When a tagged mixture is inputted into the new CellMag-CARWash system, the target cell population is separated, and single cells are isolated into droplets for further analysis.

The efficiency and purity of this system was quantified on two different mixed populations of cells with different target antigens.

While single-cell droplet suspensions could be used for a variety of applications, such as single-cell sequencing, we chose to use them to study a relatively new field: single-cell EV secretions. EVs are nanovesicles that contain limited genetic material and therefore are typically pooled together from multiple cells for analysis. There is little known about the differences in EV secretion between cells, if certain subsets of cell populations are high or low EV secreting cells, and if a difference in secretion can reveal clinically important biological insights. Single-cell cytokine studies performed using technology such as the Isoplexis system have shown differences in single immune cell cytokine secretion profiles, type and number of cytokines, and how these differences may relate to the efficiency of CAR T-cell therapy and immunotherapy.[31–33] Current work in single-cell EV secretion consists of either antibody-based capture of secreted EVs, which may miss EVs lacking expression of certain proteins, or culturing single cells in droplets to accumulate all EVs for quantification. However, these single-cell, droplet microfluidic techniques require pure populations of cells as input for droplet generation.[34,35] Therefore, in this study we show not only the selective isolation of specific cell populations using the CellMag-CARWash system, but also the potential of using this system to study the heterogeneous secretion of EVs in cells treated with a therapeutic on the single-cell level. We demonstrate successful collection of EVs secreted from single cells in droplets and analyze them to show the varied responses of cells to stimulation.

2.2 Materials and Methods

2.2.1 Cell culture

All cell lines were cultured at 37 °C, 5% CO2 under normoxic conditions. NK92mi cells were cultured in a T75 flask with 10 mL of minimum essential medium alpha (MEM-α, Thermo Fisher) supplemented with fetal bovine serum (Sigma), horse serum (Thermo Fisher), myo-inositol (Sigma), folic acid (Sigma) and antibiotic-antimycotic (Thermo Fisher). Jurkat cells (T-cells) were cultured in a T75 flask with 10 mL of Roswell Park Memorial Institute (RPMI, Thermo Fisher) supplemented with fetal bovine serum and antibiotic-antimycotic. MCF7-GFP cells were cultured in a T75 flask with 10 mL of Dulbecco's Modified Eagle's Medium (DMEM, Thermo Fisher) supplemented with fetal bovine serum and antibiotic-antimycotic. NK-92mi cells and Jurkat cells were subcultured every 2-3 days by removing 80-90% of the cell solution and replacing it with fresh media. MCF7-GFP cells were subcultured when they reached 70-80% using Tryp-LE. All cell lines were tested and reported negative for mycoplasma using MycoAlert Mycoplasma Detection Kit (Lonza, Basel, Switzerland).

To better visualize cells and improve the analysis, NK cells and T-cells were fluorescently labeled with CellTracker dye (Thermo Fisher). Cells were removed from culture, washed with PBS to ensure no serum remained and resuspended in 5mls of serum free media and 5μL of CellTracker. The cells incubated for 30 minutes at 37℃ before being washed twice with PBS to remove the remaining CellTracker.

2.2.2 Magnetic bead preparation and attachment to cells

To isolate cells using magnetic beads, cell-specific antibodies were first conjugated on to magnetic beads before attaching the beads to the cells. First, the streptavidin coated M280, 2.8μm Dynabeads™ (Thermo Fisher) were removed from the sterile bottle and rinsed 5x with 0.2μm filtered PBS by pressing a magnet to the side of the tube, allowing the liquid to be removed and the beads left behind. The clean beads were then resuspended in their original volume of 0.1% BSA (Sigma) in PBS. For NK cell attachment, biotinylated anti-CD56 antibodies (R&D Systems, cat# BAF2408) were then incubated with the beads at room temperature for 30 minutes on a rocker, allowing the biotinylated antibodies to bind with the streptavidin coated Dynabeads™. For MCF7 GFP cell attachment, biotinylated anti-EpCAM (R&D Systems, cat# BAF960), anti-CD133 (Miltenyi Biotec, cat# 130-113-185) and anti-EGFR (RayBiotech, cat# MD-02-0006) antibodies were incubated with beads. Following antibody binding, excess antibody was rinsed off by diluting the bead-antibody solution with 1mL of 0.1% BSA in PBS. The beads are then again trapped using a magnet, allowing the solution to be removed. The anti-CD56 conjugated beads are rinsed 4 times. After conjugation, beads are incubated with the cells of interest at room temperature on the rocker for either 30 minutes (NK cell attachment) or 1.5 hours (MCF7 GFP attachment). Before further experimentation, bead-tagged cells are imaged to ensure effective bead attachment.

2.2.3 Microfluidic device fabrication

Device fabrication has been described previously.[36] Masters are fabricated using standard photolithography techniques. SU-8 2025 negative epoxy photoresist is spin coated to a thickness of ~40 μm on a silicon wafer and baked. It is exposed to UV light

through a design mask transparency obtained from CAD/Art Services, Inc. Device designs are constructed using AutoCAD software. Unpolymerized photoresist is removed via development in propylene glycol monomethyl ether acetate. After baking, wafers are treated with tridecafluoro-1,1,2,2-tetrahydrooctyl trichlorosilane using chemical vapor deposition. To fabricate devices, polydimethylsiloxane (PDMS) is mixed at a 10:1 ratio of base to curing agent, degassed, and poured onto the master. Once cured, the PDMS stamp is cut out and ports are punched out using a 30-gauge needle or a 0.75mm biopsy punch (Robbins Instruments, cat# RBP-075). The stamp is bonded to a glass slide (droplet generation) or coverslip (CellMag-CARWash) via oxygen plasma activation.

2.2.4 Microfluidic device set-up

All devices are treated prior to the experiment with aquapel (Pittsburg Glass Works, cat#47100); this incubates for one minute before being flushed and replaced with FC-40 oil (Sigma Aldrich, cat#F9755). Pieces of #30 PTFE Masterflex tubing (Masterflex, cat# 06417-11) are inserted into the device ports then their respective pressure vial. The output tubing of each device collects into a 0.6-mL Eppendorf tube. 1% (w/v) Fluorosurfactant-008 (RAN Biotechnologies, Inc, 008-FluoroSurfactant-1G; abbreviated F008) in Novec 7500 oil (The 3M Company; Novec 7500) serves as the oil phase for droplet generation and CellMag-CARWash processing.

Reagents are delivered on device using a custom-built pressure controller. Nitrogen gas is directed into two splitting manifolds that connect to several two-stage regulators. These regulators allow for pressure selection. The gas then passes through an array of LHDA0531115H solenoid valves that actuate in response to LabView

signals from an NI PCIE-6251 multifunction data acquisition device. The headspaces of reagent vials are pressurized via steel pins, and reagent is driven onto the devices via 20-centimeter-long pieces of #30 PTFE tubing. Both droplet generation and CellMag-CARWash devices are imaged on a Leica DMi8 light microscope, and videos are captured using a VEO 640L high-speed camera from Vision Research Inc. Image processing occurs using ImageJ software from the National Institute of Health (NIH).

2.2.5 Single-cell droplet generation

We have previously described the droplet generation process,[37] thus here we described the specifications for this system. The cell solution is pipetted to mix the contents before 30-50 µL is aspirated to load into the “sample hopper”. The hopper consists of a cut 200 µL pipette tip placed inside a pressure vial and connected to the device via 5 cm length of #30 PTFE tubing and 5 mm length of Tygon tubing (Masterflex, cat# 06460-18). This vial is inverted to contain the sample inside the pipette tip. Typical pressure settings would be 75 kPa for the oil and 60 kPa for the cell solution.

Device operation takes between 5 and 15 minutes, depending on sample size. At the end of operation, air enters the device, at which point the cell solution pressure is turned off to allow the oil to rinse the sample hopper. At this point, sample loading and device operation can be repeated. The device can be re-used several times for identical samples. Device usability is determined through brightfield imaging of the device to check for blockages or contamination. Output droplets are rinsed with oil phase before the tube cap is cut off and the tube placed inside a vial to be pressurized to deliver droplets onto the following device.

2.2.6 CellMag-CARWash processing

Droplets are injected (~35 kPa) into the device and initially spaced out with an oil spacer (~45 kPa). Droplets enter the washing chamber and coalesce with the wash buffer (~45 kPa) due to application of an electric field. The electric field is delivered via a ground electrode channel filled with 3 M sodium chloride. A platinum wire inserted into the wash buffer solution serves as the positive electrode. After coalescence, cells are carried along by the washing buffer. Magnetic-bead-tagged cells are attracted towards the eight Neodymium magnets installed on the device, approximately 400 μm away from the washing channel. An oil coflow (~45 kPa) is used to prevent cells and magnetic beads from sticking to the channel walls. Cells and magnetic beads in the lowest streamline will be resegmented into new droplets at the end of the device. All other material in the buffer stream will be sent into waste (~15 kPa). The sizing of output droplets can be adjusted by varying the pressure of a 2% (w/v) F008 in Novec 7500 oil phase input (~30 kPa) at the resegmenting junction. Output droplets can be collected for imaging analysis or sent to downstream processing steps at this point. For future magnetic droplet splitting, droplets are collected into a 12-well plate and incubated overnight at 37 °C. Extra oil phase is added as necessary to keep droplets hydrated and prevent breakage and merging.

Operation time typically takes between 15 and 45 minutes, depending on sample size. Wash buffer and the oil phases are used to rinse the sample input tubing and carry all resegmented droplets into collection. Each CellMag-CARWash device can be reused for replicate samples, but a new device is set up for different sample types or in response to debris collecting within the channel.

2.2.7 Magnetic droplet splitter processing

Following overnight incubation, samples are collected into Eppendorf tubes and prepared for processing on a magnetic droplet splitting device as they were prior to processing via CellMag-CARWash. On device, droplets (~30 kPa) are spaced out by an oil flow (~25 kPa; 2% (w/v) F008 in Novec 7500 oil) before traveling through a channel lined by eight Neodymium magnets installed in the coverslip and encountering a channel wall that juts into the channel. Droplet volume splits into two output channels, with magnetic bead-tagged cells entering the right-most output, due to their attraction to the lower channel wall. One of the output channels is contained in a vial that can be pressurized to assist with troubleshooting fibers stuck in the device. A second oil flow (~20 kPa; 2% (w/v) F008 in Novec 7500 oil) is applied at the splitting junction to enable real-time adjustment of the volumes sent into each output channel.

2.2.8 Droplet manipulation and analysis coalescence

Following droplet generation, CellMag-CARWash processing, and/or magnetic droplet splitting, cells in droplets (referred to as simply droplets) are either kept intact to investigate droplet stability and cell viability in live cell experiments, or coalesced using 1H, 1H, 2H, 2H-perfluoro-1-octanol (Sigma Aldrich, cat# 370533) to gather the cells into the aqueous phase for ease of counting.

Droplets that have coalesced combine to form one aqueous phase that can be distinguished as a layer on top of the oil phase. The aqueous phase with cells is removed and put into a well plate for imaging. Droplets were coalesced from the CellMag-CARWash product and waste streams, as well as from the droplet splitter EV and magnetic outputs. After coalescence, cells were imaged at 30x in fluorescent

channels to identify cell types and quantities, and in brightfield to quantify the number of beads per cells using a Nikon Ti2 Eclipse microscope.

2.2.9 Live/dead analysis

Live/Dead Viability Kit (Invitrogen Kit #L3224) was used to determine the viability of cells within the droplets. However, as it was not possible to easily introduce the assay to the droplets, a portion of the droplets were placed in a well plate and excess PBS was added. By mixing the droplets with the excess PBS, this caused the droplets to break and cells to gather in the PBS solution. The PBS solution was then removed from the oil, placed in a new well and 0.5 µL of calcein-AM and 0.25ul of ethidium homodimer-1 per 200 µL of PBS was added to the cell suspension. The solution incubated for 30 minutes in the dark before being imaged using fluorescent microscopy. Cells were counted as either live or dead based on the presence of FITC (green/calcein/live stain), PE (red/ethidium homodimer-1/dead stain).

2.2.10 Bulk EV quantification using nanoparticle tracking analysis (NTA)

NTA for EVs secreted from cells with and without beads (Fig. 2.6) was performed using the Malvern NanoSight system. A diluted EV solution obtained from ultracentrifugation was injected into the machine to obtain five 60-second-long videos of EVs in scatter mode. Data acquisition and processing was performed using the NanoSight NS300 control software. For each video, the concentration of the particles in the size range of 30 -1000 nm was determined. The average concentration and particle size for each sample was determined and reported.

NTA for EVs secreted from a bulk solution of cells cultured with and without β-Estradiol (Fig. 2.7, Fig. 2.9A) was performed using the Zetaview (Particle Metrix). A diluted EV solution obtained from ultracentrifugation was injected into the machine and the concentration and particle size was determined across 11 positions in the chamber. This was repeated three times for each sample. To account for diffusion limitations in the chamber, the average of the three highest concentrations from each replicate were used to determine an overall sample concentration. The concentration was normalized to the original volume and a relative concentration based on samples cultured without β-Estradiol was determined.

2.2.11 Single-cell secreted EV droplet analysis

To evaluate the single-cell EV concentration in droplets, after processing with the droplet splitter, droplets were placed in the 50 μm tall imaging chamber device. The imaging chamber consist of the PDMS top that previously described in Yoon et al, but briefly is a 50 μm tall single chamber that is approximately the dimensions of a 1”x3” glass slide. The difference in this imaging chamber used here is that the PDMS chamber is bonded using an O_2 plasma etcher directly to a glass slide, creating one large chamber. Imaging chambers are first primed with oil before loading the droplets using a Harvard syringe pump at 10 μL min^{-1}. Once droplets are loaded into the chamber, the device was imaged at a 60x objective. Post imaging analysis was done on the Nikon elements software. Briefly, 100+ droplets from each sample were manually identified and their border circled. Any droplet that contained a cell was removed from analysis. The fluorescent intensity of each circled object was recorded. Additionally, regions with no droplets were identified and circled to obtain the background fluorescent

intensity of the device. This average background intensity was subtracted from each droplet to obtain the normalized fluorescent intensity for each droplet.

2.3 Results

Figure 2.1 shows the overall workflow of our study, consisting of two parts: the isolation of single cells from a mixed population into droplets, and further analysis of the EV secretion from these cells using a droplet splitter device with additional imaging and analysis. Cells of interest within a complex mixture were first tagged via the “CellMag” portion of the workflow through incubation with antibody-coated, magnetic Dynabeads. The cell mixtures were emulsified into droplets to distribute cells throughout the solution volume and prevent them from settling due to gravity. Droplets were processed through the CARWash device to isolate target cells in product droplets, followed by overnight incubation and secretion of EVs. Due to the large size difference between secreted EVs (~150 nm) and cells (15 - 30 μm), a magnetic, droplet splitter device was incorporated to split droplets and facilitate fluorescent imaging of EV-only-containing droplets.

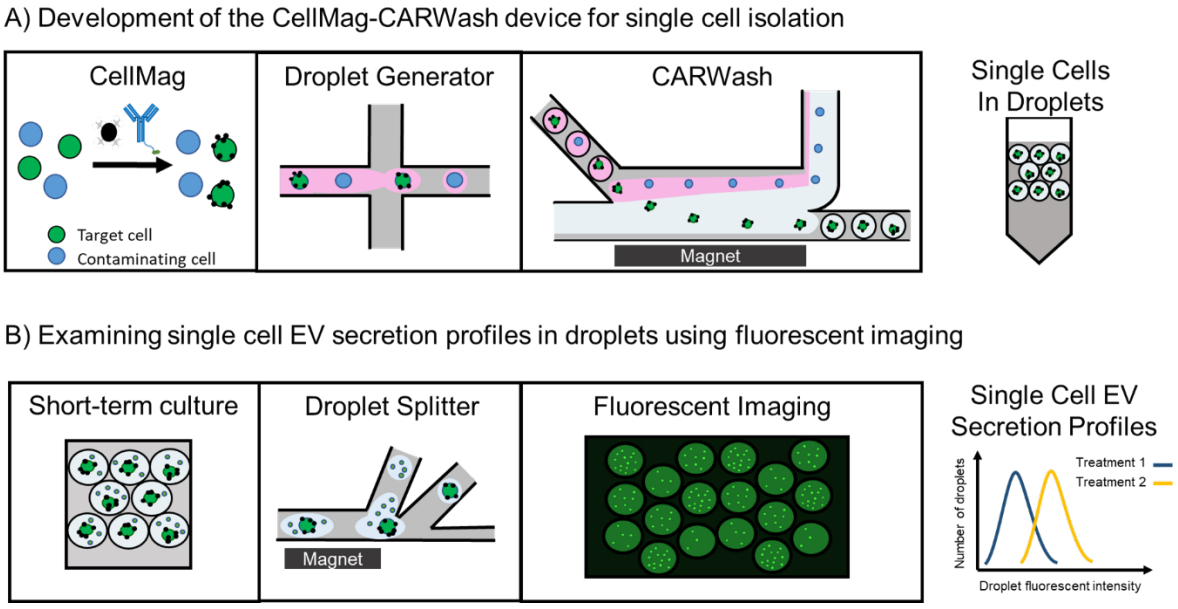

Figure 2.1. Process Overview. A) Development of the CellMag-CARWash device for single-cell isolation. Cells are incubated with 2.8 µm Dynabeads coated with cell type specific antibodies. After incubation with the cells, Dynabeads attach to the desired cell population. The cell mixture is then emulsified into droplets, which are inputted into the CARWash to separate cells attached to Dynabeads into droplets containing a single cell. New media and other cell culture reagents can be used as a wash buffer and added to the newly resegmented droplets. B) Examining single-cell EV secretion profiles in droplets using fluorescent imaging. Cells in droplets are incubated to allow for single-cell EV secretion. After short-term culture, droplets are inputted into a Droplet Splitter device to divide each droplet into two smaller droplets, one containing the cell and another containing EVs. Droplets containing EVs are placed into a 50 µm tall chamber and imaged. Fluorescence intensity of the droplets is recorded and used to determine relative EV concentration inside the droplets.

2.3.1 Attachment of magnetic beads to cells using target specific antibodies

To test the CellMag-CARWash system, two samples composed of mixed cell populations were made; a Natural Killer (NK)/T cell mixture to examine the isolation of specific immune cells and a MCF7 GFP/NK cell mixture to examine the isolation of cancer cells from immune cells. The target cell population was distinguished and later separated by attaching streptavidin coated magnetic Dynabeads to their surface using biotinylated antibodies specific for their surface antigens. Anti-CD56 was used to isolate NK cells as it has previously been shown to be a reliable marker for NK cell isolation.[38] Optimization experiments were performed using the NK92mi and Jurkat (T) cell line. First, a ratio of 1:2 antibody to bead by volume was incubated for 30 minutes to attach

biotinylated antibodies to streptavidin coated beads. This was followed by a 30-minute incubation of cells and antibody coated beads and was found to result in bead attachment to ~90% of all NK cells. Figure 2.2Ai shows representative images of a mixture of NK (red) and T cells (blue) after incubation with Dynabeads. The Dynabeads are attached specifically to NK cells and have minimal attachment to T cells. The number of Dynabeads attached to each cell was counted using brightfield images. The distribution of the number of beads per cell is shown in Figure 2.2Aii (NK cells) and Figure 2.2Aiii (T cells). Anti-CD56 coated Dynabeads show variable attachment to NK cells, with approximately 10% of NK cells having no attached beads and over 10% of cells having 10+ beads attached (average 5.3 beads per cell). Additionally, there was limited nonspecific binding of anti-CD56 beads, as 90% of T-cells (CD56 negative cells) showed no attachment to anti-CD56 Dynabeads (average 0.125 beads per cell).

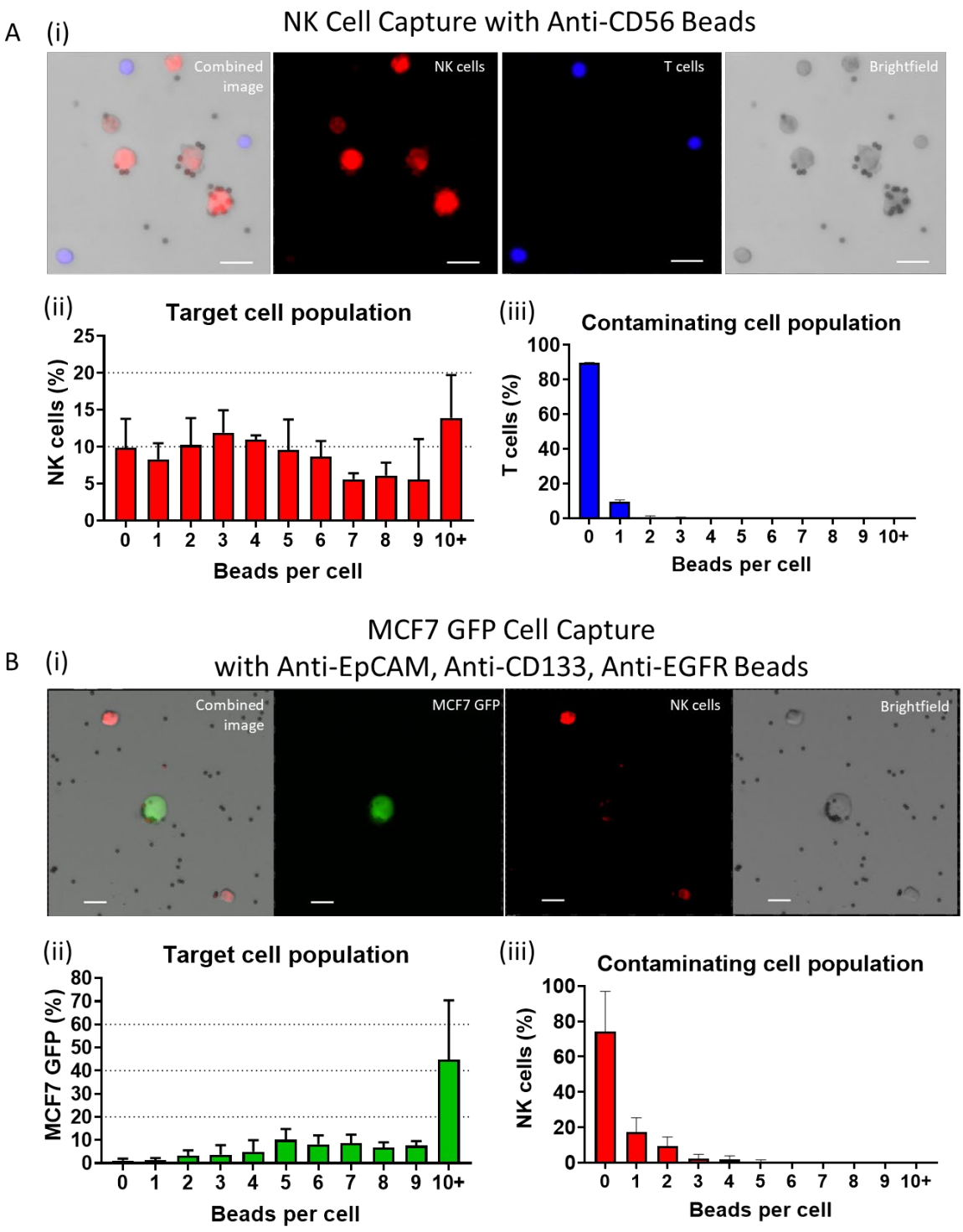

Figure 2.2. Attachment of 2.8 µm Dynabeads to a desired cell population within a mixed population. A) Anti-CD56 coated Dynabeads attached to NK92mi cells in a mixture of NK cells and T-cells. i) Images of Dynabeads attached to NK cells (red). T cells are shown in blue. Scale bar 20 µm. ii) Percentage of NK cells with various amounts of anti-CD56 Dynabeads. N=3 iii) Percentage of T-cells with various amounts of anti-CD56 coated Dynabeads. N=3 B) Anti-EpCAM/ anti-EGFR/ anti-CD133 coated Dynabeads

attached to MCF7 GFP cells in a mixture of MCF7 GFP cells and NK cells. i) Images of Dynabeads attached to MCF7 GFP cells (green). Scale bar 20 µm. ii) Percentage of MCF7 GFP cell population with various amounts of anti-EpCAM/ anti-EGFR/ anti-CD133 coated Dynabeads. N=4 iii) Percentage of NK cell population with various amounts of anti-EpCAM/ anti-EGFR/ anti-CD133 coated Dynabeads. N=4

As cancer cells can have heterogeneous expression of surface markers, a cocktail of biotinylated antibodies, anti-EpCAM, anti-CD133, anti-EGFR, was added to the Dynabeads intended for cancer cell isolation. An optimized ratio of 2:3 antibody to bead by volume with a 1.5-hour incubation of antibody coated beads with cells was shown to be sufficient for the attachment of Dynabeads to MCF7 GFP cells (Fig. 2.2Bii). After incubation, over 20% of MCF7 GFP cells have 10+ beads attached, while <5% of cells had less than two beads attached (average 9.8 beads per cell). When mixtures of MCF7 GFP cells and NK cells were introduced to cancer-specific beads, ~75% of NK cells had less than two beads attached (average 0.51 beads per cell). Mixtures of cells with attached Dynabeads were then inputted into the CellMag-CARWash device to determine the minimum number of beads per cell needed to recover cells in the product stream.

2.3.2 CAR-Wash design adjustments for expansion to cell isolation

CARWash was previously shown to enrich biological molecules attached to 10 µm, streptavidin coated beads in product droplets, exchanging >99% of the initial droplet contents.[37] We anticipated two potential challenges in successfully recovering magnetic bead tagged cells from the device. First, we expected cells to experience increased drag forces compared to 10 µm beads alone, due to Stokes law. Stokes law (Eqn. 2.1) describes the drag force on small particles in dense solutions, such as media, and states that the drag force, F_d, is proportional to the object's radius, r. Therefore, as bead-tagged cells would be >10 µm, they will experience more resistance to moving

towards the magnet and the product stream, reducing recoveries. Second, the smaller size of the Dynabeads (2.8 μm in our system) versus the original 10 μm streptavidin beads results in smaller magnetic force applied per bead, and the beads would not be drawn as quickly to the magnet. This is due to the proportional relationship between magnetic force, F_m (Eqn. 2.2), and a particle's volume via the magnetic moment, **m**. We chose to extend the washing chamber length so that bead-tagged cells would have a longer residence time inside the chamber, which would allow them to traverse further across the washing buffer streamline, towards the magnet (Fig. 2.3A). Additional changes, such as removing serpentine features and adding in additional oil spacer flows, were incorporated to improve the device's resilience to fibers but had no effect on overall cell recovery.

$$F_d = 6\pi\eta r\boldsymbol{\Delta v} \tag{2.1}$$

$$F_m = (\frac{1}{\mu_0})(\boldsymbol{m}\cdot\nabla)\boldsymbol{B} \tag{2.2}$$

2.3.3 CellMag-CARWash processing of cell mixtures

Magnetic bead-tagged cells were emulsified into ~200 pL sized droplets by flowing the cell solution and an oil phase through a flow focusing droplet generator. Droplet samples were subsequently loaded and processed through the CellMag-CARWash device to isolate cells of interest (NK cells and MCF 7 GFP cells, respectively) into resegmented droplets. Coalescence of initial droplet samples into a wash buffer can be seen in the Blue box in Figure 2.3A and in Video 2.1. Resegmentation of cells with Dynabeads into new droplets is shown in the Yellow box of Figure 2.3A and Video 2.2. Initial mixtures containing approximately equal amounts of the desired cell type and a contaminating cell type were processed through the CellMag-CARWash. The respective output product streams were enriched for the desired cell type, achieving over 93% purity for both cell types of interest (Fig. 2.3B, D).

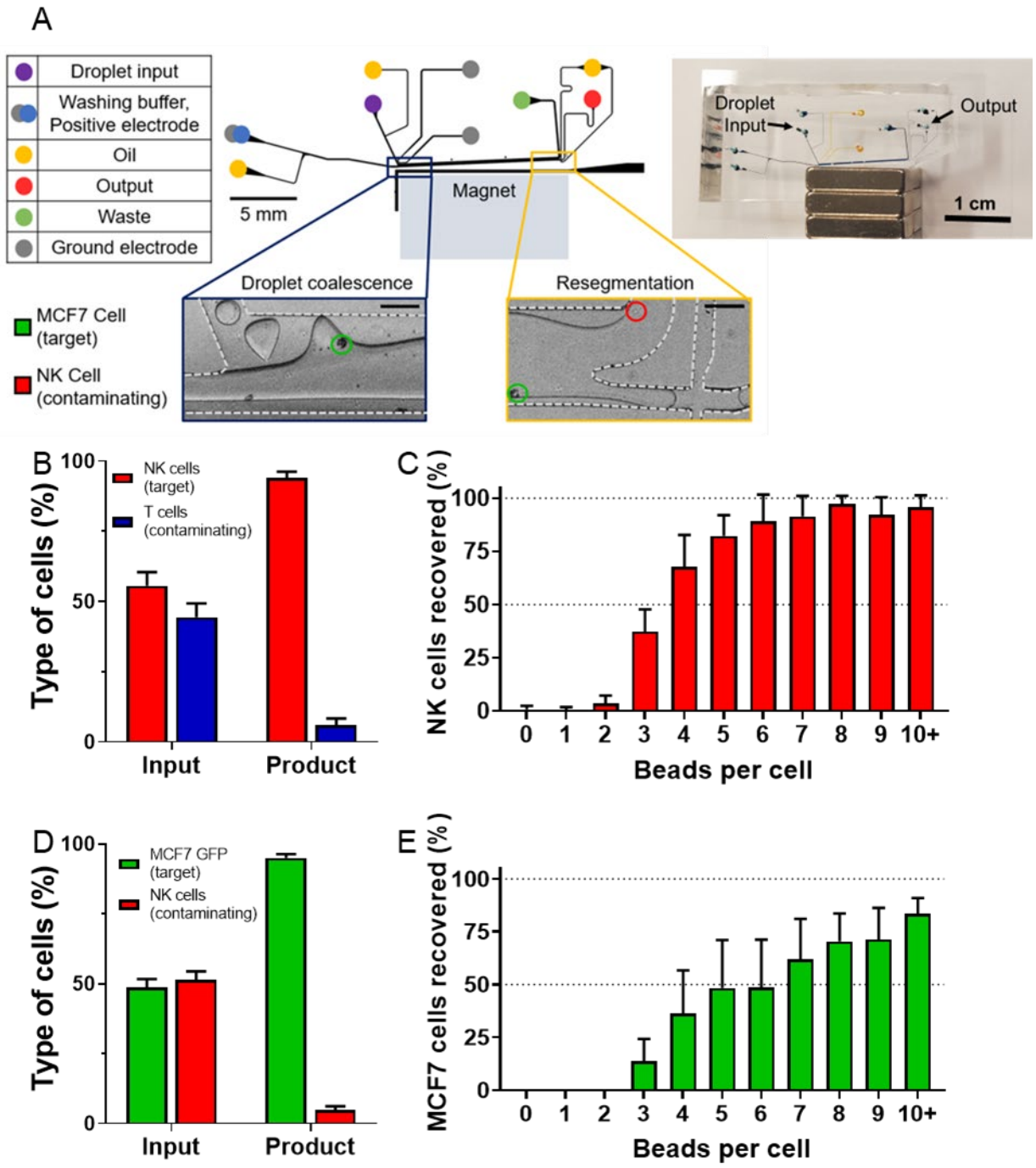

Figure 2.3. CellMag-CARWash cell recovery. A) Diagram of the CellMag-CARWash with labeled inlet and outlet streams. Blue box shows premade droplets containing cells coalescing with the wash buffer upon entering the device. Cells with beads will be attracted to the magnet and resegmentation of droplets containing media (yellow box bottom right). Cells without beads and other waste components will exit into the waste stream (yellow box top right). MCF7 GFP cells (target cells) are circled in green. NK cells (contaminating cells) are circled in red. Side panel of (A) shows an image of CellMag-CARWash with channels filled with dyes. Blue food coloring fills the fluid handling channels; yellow food coloring fills the electrode channel. Droplet input and output are labeled. B) The percentage of each cell type in the

solution, with anti-CD56 beads, inputted into the CellMag-CARWash and recovered from the CellMag-CARWash in the product stream. N=4 D) The percentage of NK cells resegmented and recovered from the CellMag-CARWash based on the number of anti-CD56 beads attached to cells. N=5 E) The percentage of each cell type in the solution, with anti-EpCAM/anti-CD133/anti-EGFR, inputted into the CellMag-CARWash and recovered from the CellMag-CARWash in the product stream. N=6 F) The percentage of MCF7 GFP cells resegmented and recovered from the CellMag-CARWash based on the number of anti-EpCAM/anti-CD133/anti-EGFR Dynabeads attached to cells. N=6.

Video 2.1. Droplet Coalescence: Mixed cell populations with magnetic beads attached were placed into droplets and inputted into the CellMag-CARWash system. Upon entering the wash chamber, droplets were coalescence with a wash buffer due to the application of an electric field via a ground electrode channel filled with 3 M sodium chloride and a positive electrode from a platinum wire inserted into the wash buffer solution. Cells then moved through the wash chamber due to magnetic force from the attached magnet and/or force from the moving wash buffer. Scale bar depicts 100 µm.

Video 2.2. Droplet Resegmentation: At the end of the wash chamber, cells would either exit through the waste stream, top right or product stream, bottom right, where they would be resegmented into droplets. Due to laminar flow within the device and the placement of the cell input, cells without attached magnetic beads remained in the top portion of the chamber and were carried into the waste stream. Cells with magnetic beads attached were attracted to the product stream where they could be collected and resegmented into single-cell droplets. Scale bar depicts 100 µm.

To determine the number of attached beads needed to recover cells in the product stream, the resulting output droplets and waste streams were separately collected, imaged, and analyzed. Figure 2.3C and E show the percentage of cells recovered in the product stream based on the number of beads attached, where percentage of cell recovered is defined as

$$\%\ of\ cells\ recovered = \left(\frac{\#\ of\ cells\ in\ product\ stream\ (droplets)}{\#\ of\ cells\ in\ product\ stream + \#\ of\ cells\ in\ waste\ stream}\right) * 100 \qquad (2.3)$$

A minimum of four attached beads was needed to recover over half of the NK cells, with near 100% recovery of NK cells achieved when six or more beads were attached. A minimum of five beads was needed to recover over half of the MCF7 GFP cells and a maximum recovery of 83% was achieved when 10+ beads were attached to a cell. We attribute the higher number of beads required to recover the MCF7 GFP cells to their larger size (Fig. 2.4), which increases the amount of drag forces they experience when traveling across the streamlines of the CellMag-CARWash device.

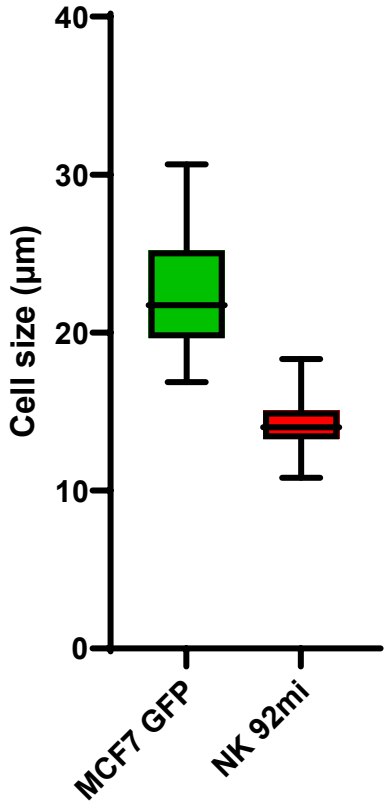

Figure 2.4. Measured size of desired cell populations. Brightfield images of cells were taken after beads were attached and Nikon Elements software was used to measure the size of each cell population.

2.3.4 Optimizing a magnetic droplet splitter device to collect EVs from cell-containing droplets

To study EV secretion from cells, we propose using fluorescent cells capable of secreting fluorescent EVs that can then be imaged using a fluorescent microscope and analyzed. However, due to size differences between cells and EVs, µm vs nm diameters respectively, the fluorescent intensity of the cell could overpower the fluorescent signal of EVs contained within the same droplet. Therefore, it was necessary to incorporate a device capable of separating cells from secreted molecules and cargo of interest. The droplet splitter device was designed to take droplets after an overnight incubation and divide them into two droplets, one containing the cell.

Figure 2.5A shows the device junction where beaded MCF7 GFP cells were attracted to the magnet on device and sent to the magnetic output, while the EV output contains the excess droplet solution with EVs. Cells can be seen entering the magnetic output as droplets are split in Video 2.3. For each experiment, droplets were collected from both the magnetic and EV output, coalesced, and imaged for cells. Figure 2.5B shows the percentage of cells recovered from the magnetic (waste) output under different parameter conditions, including high or low droplet velocities, and various carrier phases (oils). Lower velocities appeared to have a higher percentage of cells recovered in the magnetic outlet, though this difference is not statistically significant due to the small sample size. The two carrier phases tested were 2% w/w fluorosurfactant-008 (F008, a fluorinated surfactant used to stabilize droplet-in-fluorinated-oil emulsions) in Novec 7500 oil and fluoroinert FC-40 oil (FC-40). Novec 7500 oil possesses a lower interfacial tension relative to water compared to FC-40.[39] As interfacial tension increases, the capillary number of a system decreases, which makes droplet splitting more likely to occur. We theorized that using a carrier phase with a higher interfacial tension relative to the droplet phase would increase our rate of droplet splitting and consequently increase the desired recovery of cells in the magnetic output. Empirically, we found that 2% F008 in Novec 7500 oil compared to FC-40 did not show a statistically significant difference in cell recovery (87.3% vs 86.3%). However, as 2% F008 in Novec 7500 was shown to have high recoveries at relatively higher velocities compared to FC-40, Novec 7500 used for sample processing. We also noted that the lower interfacial tension of the Novec 7500 oil phase could help stabilize droplets after they exited the

splitting device, preventing discreet droplets from merging together prior to fluorescence imaging.

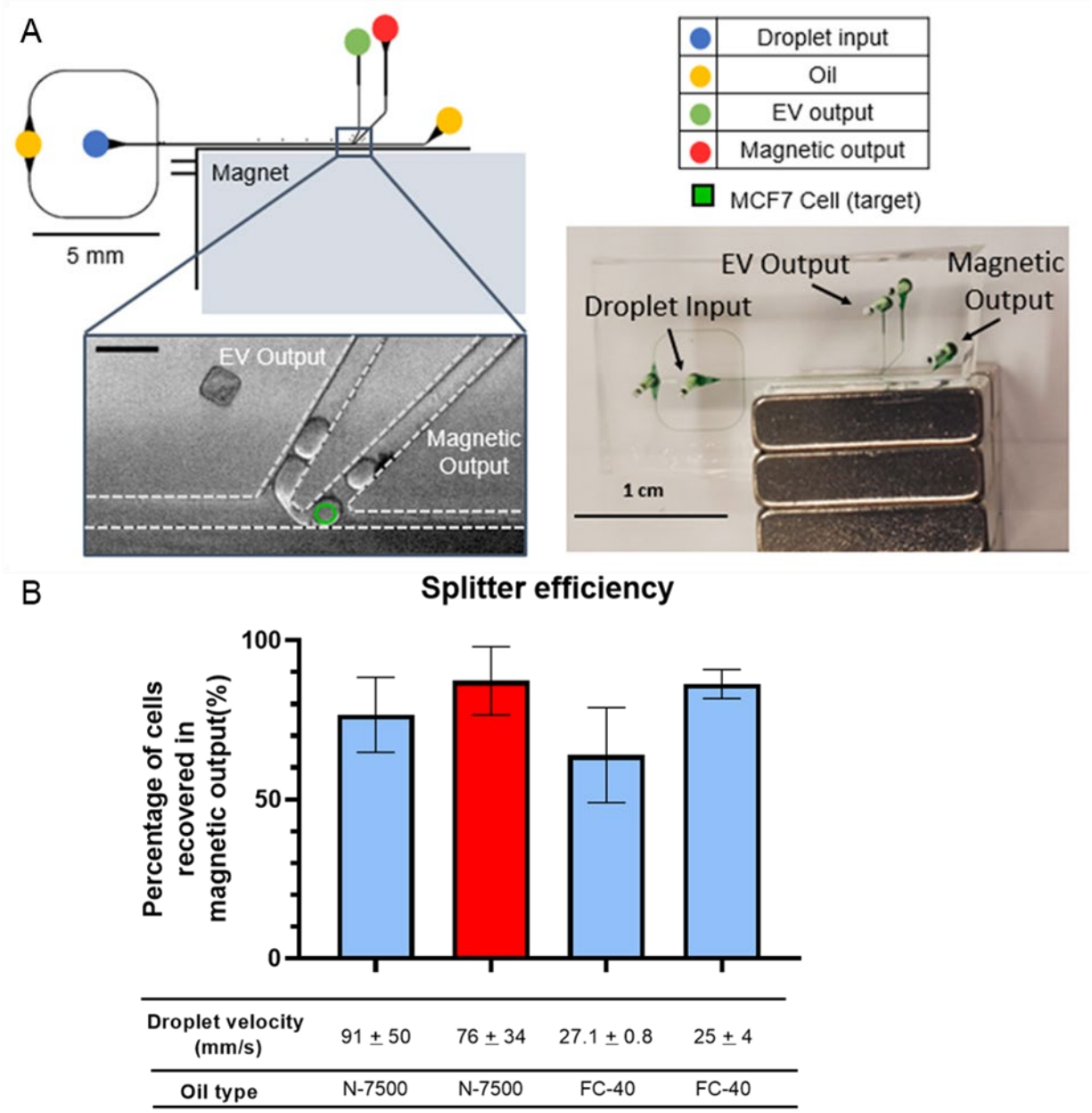

Figure 2.5. Droplet splitter recovery. A) Diagram of the droplet splitter device. Box shows the junction of the device where droplets are divided into two smaller droplets, with the cell being recovered in the magnetic output. Scale bar indicates100 μm. Side panel of (A) shows an image of the droplet splitter device. Channels are filled with green food coloring, and droplet input, EV output, and magnetic output ports are labeled. B) Recovery of beaded MCF7 GFP cells in the magnetic output based on droplet velocity in the device and the type of oil used. Either fluoroinert FC-40 (FC-40) or 2% F008 in Novec 7500 oil (N-7500) was used. N=3. The red bar indicates the condition that was used for future experiments.

Video 2.3. Magnetic Droplet Splitter: After short-term incubation to allow for cells to secrete extracellular vesicles, droplets were inputted into the splitter device which contains two output streams, the EV output (first output) and Magnetic output (second output). Cells, which have magnetic beads attached, will be attracted to the magnet in the device and move to the bottom of a droplet, thereby forcing cells to exit into the magnet output when the droplet reaches the junction. Free floating EVs, which have no magnetic beads attached will remain suspended in the droplet solution and exit the device in the EV output droplet. Scale bar depicts 100 μm.

2.3.5 Single-cell EV quantification in droplets

MCF7 GFP is a cell line developed from an estrogen receptor positive breast cancer patient. B-Estradiol, a form of estrogen, has been previously shown to induce cell proliferation in MCF7 cells. However, the effect of β-Estradiol on cell EV secretion has not been studied. We show that using both traditional (ultracentrifugation) and single-cell methods of EV isolation (the CellMag-CARWash system), the addition of β-Estradiol increases EV secretion in bulk MCF7 GFP cell culture and single-cell culture (Fig. 2.9A and B, respectively).

To confirm that our CellMag workflow was not affecting EV secretion, we cultured bulk NK cells with or without beads attached and collected the secreted EVs, which were isolated from cell culture supernatant using ultracentrifugation. Nanoparticle tracking analysis (NTA) of the collected EV secretions showed relatively consistent

concentrations and size distributions (Fig. 2.6) across both conditions. This suggests that bead attachment does not affect EV secretion.

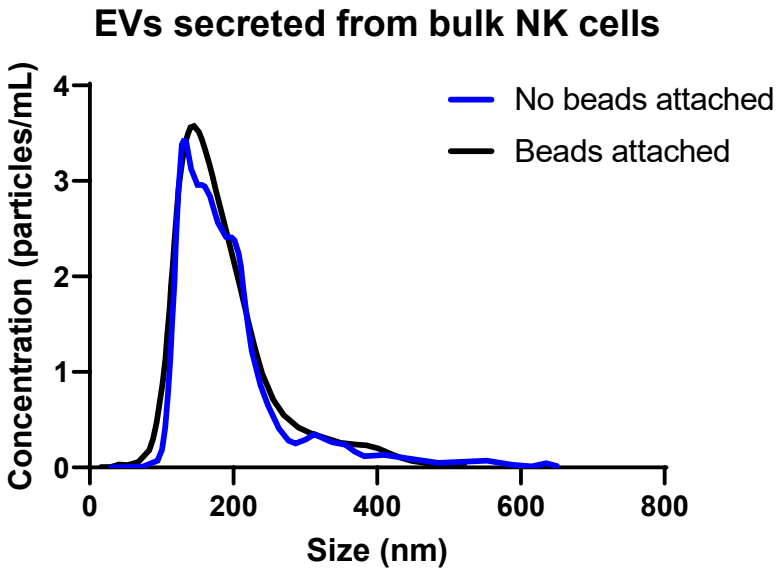

Figure 2.6. Comparison of extracellular vesicle size and concentration from bulk NK cells cultured with and without anti-CD56 beads attached. NK cells were cultured in bulk and the supernatant ultracentrifuged to obtain EVs. EV concentration and size was determined using NTA analysis via the NanoSight. N=5

Bulk EV secretion was obtained from MCF7 GFP cells supernatant after culturing in DMEM with and without β-Estradiol. EVs were then isolated using ultracentrifugation before quantification using NTA (see Fig. 2.7). We observed an increase in the concentration of EV particles with the addition of β-estradiol, but no change in particle size distribution, indicating an increase in EV secretion. For single-cell secretion studies, media with or without β-Estradiol was used as the wash buffer during the CellMag-CARWash processing, allowing the separated cells to be resegmented directly into the desired buffer. Cells were left in droplets for 18 hours before processing with the splitter. Finally, cell depleted droplets were placed in a chamber device and imaged (Fig. 2.8A). Distribution of the fluorescent intensity of droplets appeared to be mostly Gaussian with

a slight skew to the right (Fig. 2.8B – D) for cells cultured without β-Estradiol. Cells cultured with 1 μM β-Estradiol showed a slight multimodal distribution and right skew. These distributions suggest that cells heterogeneously secrete EVs, with some cells being high EV secretors. B-estradiol addition induced a shift to higher overall droplet fluorescence, indicating stimulation of EV secretion from MCF7 GFP cells.

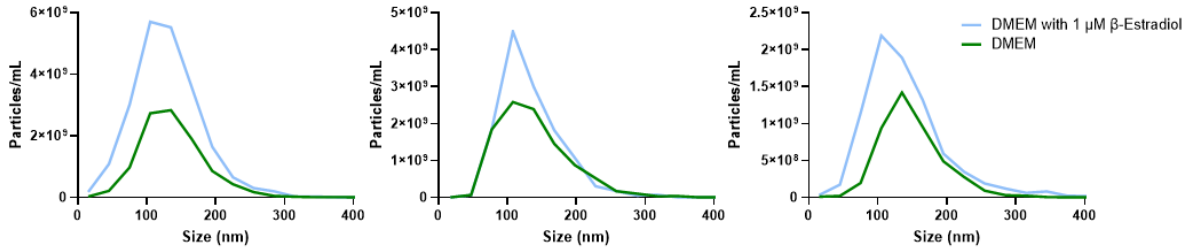

Figure 2.7. Comparison of extracellular vesicle size and concentration from NK cells cultured with and without supplemental β-Estradiol. The experiment was performed in triplicate across different days, with each run corresponding to one graph. For each run, NK cells were cultured in bulk with or without supplemental β-Estradiol for the same period of time. After culturing, the supernatant ultracentrifuged to obtain EVs. EV concentration and size was determined using NTA analysis via the Zetaview.

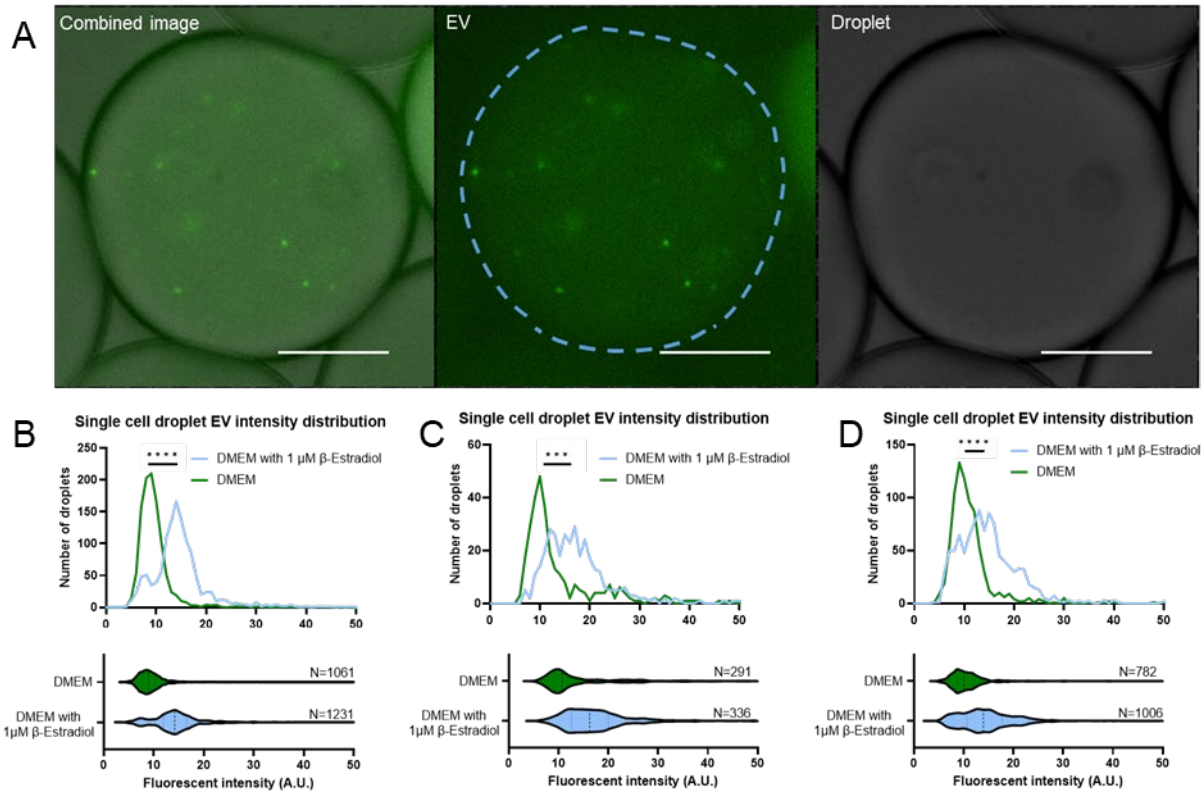

Figure 2.8. Full system runs of MCF7 GFP purified and isolated into single-cell droplets using the CellMag-CARWash system before short term incubation with or without supplemental β-Estradiol. After incubation, cells were removed using the droplet splitter device and the fluorescent intensity of the remaining EVs was analyzed. A) Image of droplet with fluorescent EVs taken at 60X magnification. Dotted line indicates droplet border. Scale bar 20 μm. B, C, and D show the distribution of fluorescent intensities of droplets containing EVs secreted by single cells obtained using the workflow on different days. B) P-value <0.0001. C) P-value =0.003. D) P-value <0.0001.

Normalization of the mean, β-estradiol stimulated cell EV fluorescence intensities to media treated cells enables comparison of bulk and single-cell EV isolation methods. Figure 2.9A shows a 2.1x increase in the relative EV concentration when cells were cultured in bulk with 1 μM β-Estradiol compared to when no β-Estradiol added. Figure 2.9B shows a 1.74x increase in EV secretion from single cells in the presence of 1 μM β-Estradiol based on mean fluorescent intensity for the entire droplet. The comparable increases in these values suggests that we are observing a common stimulation phenomenon through both techniques, however, CellMag-CARWash reveals the underlying heterogeneity of EV secretion dynamics.

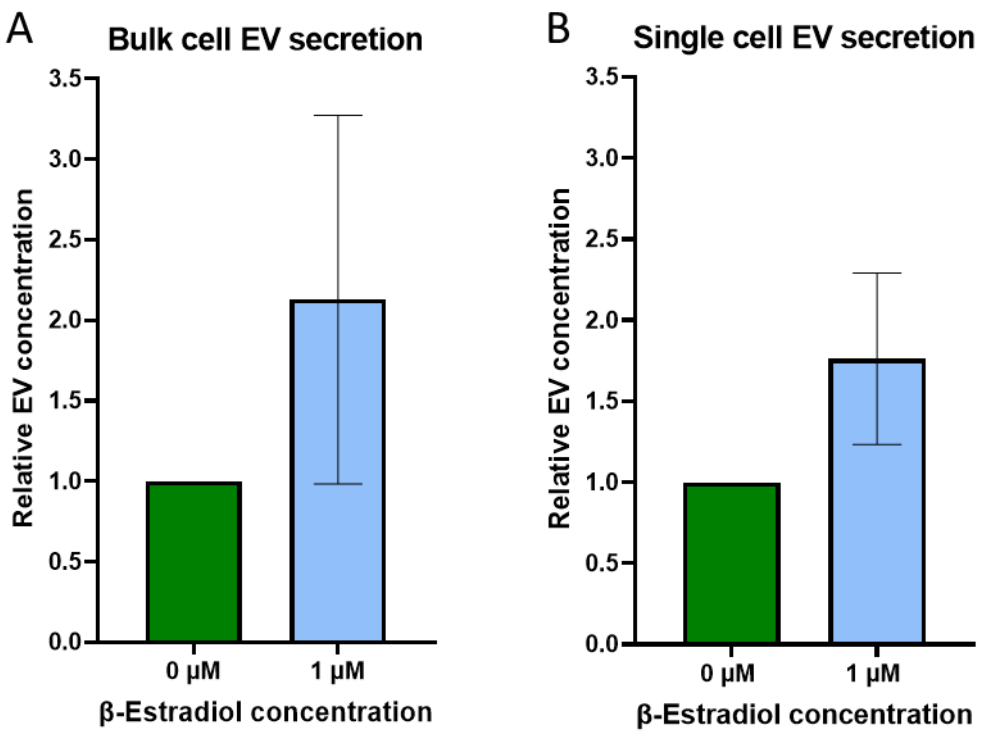

Figure 2.9. MCF7 GFP EV secretion with various concentrations of β-Estradiol. A) Relative EV concentration obtained from the supernatant of bulk MCF7 GFP cells cultured with various concentrations of β-Estradiol. N=3 B) Relative EV concentration of EVs secreted by single cells based on the mean fluorescent intensity of the droplets post droplet splitter, compared to the background fluorescent intensity. N=3

2.4 Discussion

In this study, we presented a high throughput, droplet microfluidic device, the CellMag-CARWash, for the specific isolation of single cells to examine heterogeneity. By using antibodies that target antigens on the surface of the desired cell population, we were able to isolate cells of interest from a mixed cell population and encapsulate the cells within droplets to study them at a single-cell level. We further examined the heterogeneity of single-cell EV secretions by culturing individual cells in droplets short-term to allow for EV secretion before imaging and analysis. This analysis showed

differences in the EV secretion profiles within cells from the same population in response to molecular stimulation.

To expand the CARWash technology for cellular isolation, methods for bead attachment to cells were developed, the design was adjusted, and the performance of the CARWash with cells was determined. Two sets of antibody coated Dynabeads were made and tested for specific applications: NK cell recovery from other immune cells and cancer cell recovery from immune cells. As the Dynabeads were streptavidin coated, the application and desired target cell population recovered can be changed by the user by adjusting the biotinylated antibodies used. In cases where cell surface expression may be variable, multiple antibodies could be added to beads to improve attachment.

Cell recovery of the CellMag-CARWash device was determined by calculating the percent recovery of two different target cell populations, NK cells and MCF7 GFP cells, based on the number of antibody-coated magnetic beads that were attached to the cells. Over half of the NK cells processed through the device were recovered when four or more beads were attached, with the recovery of cells with six or more beads attached increasing to 90%. However, MCF7 GFP cells required five or more cells to achieve 50% recovery and the maximum recovery was limited to 83% with ten or more beads attached. As the MCF7 GFP cells used in these experiments were on average 8.3μm larger in diameter compared to NK cells (Fig. 2.4), we believe the different performance is due to the cell size and the corresponding increase in drag force. Further lengthening of the CellMag-CARWash washing chamber and slowing down the velocity to allow cells more time to be attracted to the product stream or increasing the magnetic field strength of the permanent magnet to draw cells more rapidly to the

product stream could further improve recoveries. However, as there was some non-specific binding of beads to the contaminating cell population, the current thresholds of three or more beads per cell needed for recovery limits the recovery of contaminating cell populations in the product stream, resulting in a purity of over 93%.

A magnetic droplet splitter was incorporated to separate fluorescent cells from droplets with EVs, post EV secretion, to reduce the fluorescent background and improve EV quantification. Operational conditions tested in this device were (1) velocity of droplets in the device and (2) type of oil used for emulsion. The magnet was positioned below the junction, to attract cells towards the bottom of the droplet, which would then flow into the magnetic outlet. We found that slower velocities improved recovery of cells into the magnetic output, suggesting that at lower speeds, the cells had more time to move into the correct position within the droplet or that internal vortices present in the droplet were reduced, stabilizing the cell's position inside the droplet. The two oils tested have different interfacial tensions, which we hypothesized may affect the likelihood of the droplet to split, as failure to split could result in cells exiting the wrong output. However, this appeared to have little difference in the overall recoveries, suggesting that droplets were consistently splitting in both oil phases.

To validate the whole system, a mixture of MCF7 GFP cells and NK cells was inputted into the CellMag-CARWash, incubated for 18 hours, and split using the droplet splitter before imaging of droplets with EVs. The cells were kept in either DMEM or DMEM with β-estradiol, which was added via the wash buffer during CellMag-CARWash processing. The mean single-cell EV secretion in droplets, measured by fluorescent intensity of the droplets, was compared to bulk cell EV secretion obtained from

ultracentrifugation and NTA analysis. Both methods showed a similar increase in EV concentration when β-Estradiol was added, indicating that we observed the same stimulation phenomenon. However, the profiling of single droplets provided additional insight into the distribution of EV secretions. A small peak in the distribution of cells cultured with β-Estradiol suggests that a portion of cells did not respond to β-Estradiol and increase their EV secretion. However, as all droplets without cells were included in this analysis, some of these droplets may not have contained a cell originally, and therefore no EVs were secreted. Increasing the amounts of droplets with cells present, improving imaging, and determining better threshold intensities could improve analysis and provide a better quantification of EVs in droplets.

The CARWash device offered several additional advantages for single-cell work due to the buffer exchange design. Passing cells through a wash buffer before their resegmentation into droplets allows for both the removal of other cell populations and waste components and can introduce new reagents to the cells necessary for downstream applications. The washing design is especially beneficial for solutions such as blood, which have multiple cell types and components, such as platelets, that complicate further analysis. Buffers used in the device are interchangeable, provided the solution has an ionic charge, so that it can function as the positive electrode in the device. This flexible buffer choice also enables the addition of treatments at the single-cell level in product droplets. Therefore, multiple different buffers or additives could be used in the device for a broad range of downstream applications.

While the CellMag bead attachment step offers incredible selectivity for specific cell types due to the use of specific antibodies, successful recovery of cells from the

CellMag-CARWash device will be intimately linked to antibody choice. Thus, the technique requires a strongly binding antibody or mixture of antibodies. CellMag also inherently assumes consistent expression of surface markers to target and does not take into account natural fluctuations of membrane protein expression. This could bias our single-cell measurements if cells with low surface marker expression are not reliably recovered through the CellMag-CARWash. Additionally, the need to remove cells from droplets to reduce fluorescent background for EV imaging limits the utility of the analysis, since we cannot link individual cells to their EV secretion levels. Identification and selection of cells with uniquely high or low EV secretion responses would be desirable for studies on therapeutic effects, so that the basis of these differences can be further studied and leveraged. Improvements to the fluorescent imaging and analysis workflow could eliminate the need to remove cells from droplets so these relationships can be identified.

2.5 Conclusions

The CellMag-CARWash technique offers a modular, droplet microfluidic workflow to isolate single cells in product droplets at high purity and enable downstream droplet processing and analysis. We have applied this technique to uncover heterogeneity in EV secretion from cells in response to molecular stimulation. We envision next steps will include increasing the complexity of input samples to mimic the natural complexity of biological samples and studying various therapeutic effects on isolated cells, such as a treatment to reduce EV secretion. CellMag-CARWash fills the gap for a high-throughput, straightforward, scalable technique that enables isolation of single cells from complex mixtures and analysis of their heterogeneous cellular responses.

2.6 Acknowledgements

We gratefully acknowledge the National Science Foundation (Understanding the Rules of Life Epigenetics: 1921677) and the Forbes Institute for financial support for C.D. Cook and B.T. Rupp, respectively, to complete this work. E.A. Purcell and N. Mesyngier were supported by the Microfluidics in Biomedical Sciences Training Program. This research was also funded by the National Institute of Health (R01-CA-208335-01-A1 to S.N. and V.S.), a Lefkofsky Scholar award and Rogel Scholar award to S. Nagrath. We also thank the Lurie Nanofabrication Facility for access to their microfabrication equipment.

2.7 Attribution Information

B.T. Rupp and E.A. Purcell were responsible for performing cell sample preparation, fluorescence imaging and analysis of microfluidically processed samples, and all extracellular vesicle characterizations and analysis. C.D. Cook led the microfluidic workflow design and operation. All three authors participated heavily in manuscript preparation. M. Pop and A.E. Radomski helped complete optimization experiments, and N. Mesyngier participated in project design and manuscript editing.

Chapter 3 Development and Characterization of the FADS-MNase, Droplet Microfluidic Workflow to Enrich and Epigenetically Profile *S. Pombe*-Containing Droplets

Claire D. Cook, J. Damon Hoff, Meng Sun, Vishal Sahore, Kaushik Ragunathan, Ryan C. Bailey

3.1 Introduction:

The DNA molecule contains genetic information vital for building proteins and structures needed for the life and function of cells. DNA compacts to fit within a cellular nucleus by wrapping ~146 base pairs (bp) around an octamer of histone proteins to form a nucleosome.[85] Nucleosomes are the basic, repeating unit of chromatin. They coil around themselves repeatedly to form smaller and more compact chromatin structures, until eventually reaching chromatin's most compact state: the chromosome. Within an organism, all cells possess identical DNA but exhibit different phenotypes resulting from cellular differentiation. These different phenotypes arise through differential regulation of access to the DNA molecule at various regions or genes, known as epigenetic regulation. Epigenetic regulation occurs via the choreography of chemical groups, proteins, and RNA molecules to extend or "open" gene regions, so they are accessible to transcription machinery or, on the other hand, to compact and block unnecessary gene regions from being transcribed. These competing processes balance to enable

cells to respond to new environmental stimuli. Additionally, epigenetic modifications made in response to stimuli can be inherited in daughter cells or organisms. [137]

Slight variations in the epigenome can lead to varied responses to stimuli from cells within a population.[11] These “outliers” can often have clinical or biological importance, such as individual tumor or bacterial cells that are resistant to therapeutics.[8,12] A recent example of the importance of heterogeneity was observed during the COVID-19 pandemic, where heterogeneity in the immune response of individual cells was linked to disease severity.[9] However, these differences are often lost in bulk epigenetic profiling techniques. The gold standard for assessing the location of epigenetic “players” like nucleosomes throughout the genome is micrococcal nuclease digestion paired with sequencing (MNase-seq).[114,115,138] MNase-seq utilizes the endo-exonuclease MNase to digest chromatin down to nucleosome- or chromatin associated protein-occupied DNA fragments, which are sequenced to obtain genome-wide nucleosome and chromatin protein positions. The ability of MNase to digest chromatin samples down to blocked DNA was discovered in 1974 and was used as evidence to support the notion of a repeating chromatin subunit.[117] The advent of next generation sequencing (NGS) techniques in the early 2000’s expanded the utility of MNase digestions and enabled rapid mapping of nucleosome and chromatin associated protein locations throughout genomes.[36] MNase-seq mapping using NGS has revealed differential nucleosome organizational principles dependent on RNA polymerase II binding and whether the region is in an active versus repressed expression state.[4,114] MNase-seq commonly uses 1+ million cells[115,118,124,139] per sample, though, to offset losses incurred through sample coatings on pipette tips and containers as well as poor

reaction efficiencies to produce fragmented chromatin.[126] However, its ability to reveal nucleosome distribution throughout the genome as well as locations of accessible chromatin regions, by inference, has allowed it to remain a technique of interest in the epigenetic field.

Several variations on the classic MNase-seq protocol have been developed to maximize the information gained from cells or decrease the number of cells needed for analysis.[112,140] Lion *et al* developed a low-input MNase Accessibility of Chromatin (MACC) assay that incorporates MNase titrations (increasing units of enzyme) to profile different regions of nucleosomes, from longer, higher order features that tend to be more “fragile” down to mononucleosome-length DNA fragments.[118,128,133] Low-input MACC-seq improved on the original MACC-seq technique, by scaling down the volumes of reagents used, allowing them to assess nucleosome positioning in as few as 50 pre-isolated cells. Each MNase titration reaction requires 50 cells, so the total number of cells needed will actually scale with the number of titration steps included. Single-cell MNase-seq (scMNase-seq) has also been developed to investigate heterogeneity of nucleosome positioning, revealing different principles of nucleosome organization in silent versus active gene regions.[4] Each single-cell reaction is performed in a 40 µL volume at 37 °C; however, reaction efficiency would be improved by further reducing the reaction volume.

All these low-input or single-cell techniques rely on fluorescence activated cell sorting (FACS) to obtain cell samples. FACS applies an electric field to fluid flow in response to cellular fluorescence signals, causing single cells to be electrostatically diverted into collection.[141] FACS has enabled studies into cancer cell drug resistance,[142]

immunophenotyping of cells,[143] and epigenomic and lipidomic analysis of single cells.[4,143] Unfortunately, mechanical stress and radiation of cells during the sorting process has been shown to cause cellular damage, leading to concerns about cellular viability and homeostasis.[25] Fluorescence activated droplet sorting (FADS) has been developed as a gentler approach.[26,63] Cells or biological material are encapsulated in droplets, which are carried in an oil phase past excitation radiation and detection. Here, the radiation and electrical field are distributed over the entire, aqueous droplet, rather than individual cells, providing a physical barrier to cells from destructive effects. Cells and their droplet vehicles divert dielectrophoretically within the oil flow into separate collection. Droplets also compartmentalize secreted components along with cells, so components that exit the cell can still be analyzed in the context of their origin cell or used as a novel sorting target. The gentler processing of cells and expanded panel of potential sorting targets sets FADS up as an attractive alternative for isolating cells of interest for biological assays.

The Bailey Lab recently reported a droplet microfluidic, digestion device that processes whole cells within ~200 pL droplets to generate mononucleosomal DNA fragments useable for nucleosome positioning assays.[134] Droplets were generated containing cells, lytic components and MNase to access and fragment chromatin simultaneously at room temperature. The activity of MNase stopped following injection with quenching buffer containing EDTA into droplets. EDTA chelates calcium ions present in solution, which are needed for MNase to continue digesting DNA. Xu *et al.* found that the optimized droplet processing format produced higher ratios of mononucleosomal DNA fragments compared to bulk processing. This device produced

mononucleosomes with a shorter, room temperature incubation (3.5 min at ambient temperatures for cell lysis and MNase digestion) compared to conventional MNase processing techniques (5 min at 37 °C for MNase addition only). [115,134] Xu *et al* also demonstrated input independency and assessed nucleosome positioning for as few as 2500 cells by reducing the cell solution concentration loaded on device. The low droplet volume facilitates single-cell processing while also automating several experimental steps, reducing the number of pipetting steps needed. These features are desirable for studying subsets of cell populations to assess heterogeneity.

In this chapter, I discuss the combination of the FADS technique with our droplet MNase digestion device to profile mononucleosomal DNA fragments from droplet populations enriched for fluorescent cells. FADS enables gentler isolation of cells based on differential fluorescence emission, here shown with distinct *Schizosaccharomyces pombe* (*S. pombe*) strains. The function, throughput, and discretion of FADS was characterized with droplets of fluorescent solution. And the ability of FADS to divert fluorescent yeast cell-containing droplets from a mixture was assessed through quantitative polymerase chain reaction (qPCR) analysis. The MNase digestion device was expanded to process yeast cells—and other cells that possess cell walls—through the incorporation of zymolyase, and the resulting digestion profile was evaluated with Bioanalyzer capillary electropherograms. Finally, the entire workflow was applied to produce mononucleosomal-length DNA fragments from enriched, cell-containing droplet populations generated from FADS. The workflow described in this chapter was applied to *S. pombe* yeast as a proof of concept but could be used to separate subpopulations of cells based off of epigenetically-controlled expression of a fluorescent protein.

3.2 Materials and Methods:

3.2.1 Buffer, media, and oil phase formulations

All cell strains were cultured in YEA media: yeast extract was prepared with 30 g D – (+) glucose (Sigma-Aldrich) and 5 g yeast extract powder (Gibco) and supplemented with 225 mg/L adenine hemisulphate (Sigma-Aldrich). Sorbitol-tris buffer (STB) and optiprep-sorbitol-tris buffer (optiSTB) were prepared on the days of experiments for washing cell pellets and resuspending for droplet generation. STB is comprised of 1 M sorbitol (Fisher Scientific) and 50 mM tris hydrochloride (tris-HCl, Fisher Scientific), pH 7.5. OptiSTB maintains the same concentrations of sorbitol and tris-HCl, adding 21.88% v/v optiprep density gradient (Sigma-Aldrich). Earlier experiments used optiPBS (21.89% optiprep density gradient and 88.12% phosphate buffered saline (PBS, Lonza) for droplet generation.

For DNA extraction, a digestion cocktail was prepared from pre-made lysis buffer (pH 7.9), nuclei digestion buffer (pH 7.5), MNase, and zymolyase. The cocktail contained 6.40 mM 2-[4-(2-hydroxyethyl)piperazin-1-yl]ethanesulfonic acid (HEPES, Fisher Scientific), 0.96 mM magnesium chloride (Fisher Scientific), 21.76 mM potassium chloride (Fisher Scientific), 5.12 mM tris-HCl, 3.84 mM sodium chloride (Fisher Scientific), 1.28 mM calcium chloride (Fisher Scientific), 0.04 mM spermine (Sigma Aldrich), 0.13 mM spermidine (Sigma Aldrich), and 0.32% w/v IGEPAL-CA630 (Sigma Aldrich). MNase (New England Biolabs, Inc.) was added at a concentration of 127.99 gel units per µL, and zymolyase (Amsbio LLC, resuspended in M/15 phosphate buffer (Sigma Aldrich)) was added to a concentration of 4.01 mg/mL. For genomic DNA extractions instead of mononucleosomal digestions, the storage buffer for MNase was

recreated with 10 mM tris-HCl, 50 mM sodium chloride, 1 mM EDTA, and 50% (v/v) glycerol (Sigma Aldrich). Digestion cocktails for No Zymolyase control samples used M/15 phosphate buffer in place of zymolyase. Quenching buffer was also prepared at a pH of 8.0 with 100 mM tris-HCl, 20 mM EDTA, 200 mM sodium chloride, 2% (v/v) triton-X-100 (Alfa Aesar), and 0.2% (w/v) sodium dodecyl sulfate (Fisher Scientific). One tablet of cOmplete, Mini, EDTA-free protease inhibitors (Roche) was added to the quenching buffer (10 mL) prior to experiments. Every buffer was prepared using DNase/RNase-free distilled water (Invitrogen).

The oil phases in droplet microfluidic processing were made up of 2% (w/v) fluorosurfactant-008 (RAN Biotechnologies) diluted in 3M Novec 7500 oil (Gallade Chemical). All buffers and oil phases, aside from cell media, were filtered through 0.2 µm nylon syringe filters (VWR).

3.2.2 Cell Culture

S. pombe strains were cultured in 3 mL liquid YEA media from frozen glycerol stocks two days prior to experiments and back diluted to 0.01 – 0.05 OD roughly every 12 hours. Cells were incubated in a benchtop shaker at 32 °C, 250 rpm. Cells were grown to an OD between 0.4 and 0.8 on the day of the experiment before being pelleted and washed with STB and resuspended in 1 mL of STB. Cells were counted in a disposable hemocytometer (INCYTO) then diluted to 6 – 7 million cells per mL with optiSTB. Initial experiments for the MNase digestion device used higher concentrations of cells (20 million/mL) for validation. Synthetic cellular mixtures were prepared by combining proportional volumes of the green fluorescent protein (GFP) expressing SP180 (GFP +) and non-GFP expressing SP327 (GFP -) cells in a total volume of 1 mL

optiSTB. Thirty microliters of solution were used for the control strains and synthetic mixtures.

3.2.3 Microfluidic device fabrication

Device designs were created in AutoCAD and sourced from Cad Art Services. Standard photolithography and soft lithography techniques were used to fabricate templates and microfluidic devices; however, it is briefly summarized here.[144] SU-8-2025 negative photoresist (Kayaku Advanced Materials) was spin coated onto a silicon wafer (University Wafer) to a thickness of 40 μm. Following soft baking, the wafer was exposed to UV light through the respective design mask to crosslink device features. Development occurred in propylene glycol monomethyl ether acetate (PGMEA, Sigma Aldrich) to remove non-crosslinked photoresist. For the digestion device, a second layer was needed. SU-8-2050 photoresist was spin coated to a thickness of 100 μm. Similar soft baking, exposure, and development steps were performed, although wafers needed to be aligned to first layer design features prior to UV exposure. Following development of wafers, features were hard baked on by heating for 15 minutes at 150 °C.

Devices were fabricated by pouring polydimethyl siloxane (PDMS, Momentive) at a ratio of 10:1 base to curing agent onto the masters. The PDMS cured for 1 hour at 70 °C before the slabs were peeled off the wafers. Tubing ports were punched using 0.75 mm biopsy punches (Robbins Instruments), and holes were rinsed with water to remove any debris in the ports. Droplet generation and digestion devices were plasma bonded to glass microscope slides (Fisherbrand) while the FADS devices were plasma bonded to 48 x 65 mm No. 1 coverslips (Gold Seal Thermo Scientific). Metal electrodes were fabricated on the FADS devices by melting rods of Roto144F low melt fusible ingot alloy

(RotoMetals) into the electrode channels, inserting pins of custom-made jumper wire-to-banana plug adapters, and allowing the metal to solidify the connection. All devices were treated prior to experiments by injecting pure aquapel (Pittsburg Glass Works) into the channels followed by a rinse with fluorinated FC-40 (Sigma-Aldrich).

3.2.4 Microfluidic device operation

For all devices, fluid was delivered via syringe pump flow (Harvard Apparatus) through #30, PTFE tubing (Masterflex). The oil phase was stored within glass syringes (Hamilton Company). 30 ga PTFE tubing was connected to the oil syringes with ~1 cm-long pieces of Tygon tubing (Masterflex).

3.2.5 Droplet generation

A 3-mL BD syringe delivered desired aqueous solution onto a flow focusing droplet generator. The aqueous solution was pinched off by the oil phase to form ~200-pL sized droplets. Aqueous sample was flown at 3 µL/min and the oil phase was set to 10 µL/min. Droplets were collected in custom-prepared collection chambers that facilitate reinjection of droplets into downstream devices. For initial FADS experiments, 10 nM fluorescein (Sigma Aldrich) in optiPBS was used as the aqueous solution, and droplet generation ran for 10 minutes (~30-µL output). The 1:10 mixture of fluorescein to optiPBS droplets was prepared by generating fluorescein droplets for 2 minutes then non-fluorescent optiPBS droplets for 20 minutes. For yeast cell experiments, the 3 mL syringe was filled with filtered FC-40 which was used to fill a piece of #30 PTFE tubing. A gap of air was left before drawing up 30 µL aliquots of the cell solution.

3.2.6 Fluorescence Activated Droplet Sorting

3.2.6.1 Optical setup:

FADS experiments were performed in the Single Molecule Analysis in Real-Time (SMART) Center at the University of Michigan on an Olympus IX81 Confocal Microscope with a 60X, 1.20 numerical aperture water immersion objective. Droplets were irradiated with a 100 mW, 477.5-nm LED fiber optic (ThorLabs) focused with appropriate filters. A 488/561-nm dichroic beamsplitter (Semrock) was used to reflect excitation and brightfield light between the microscope stage and back input but transmit fluorescent emission through to the detector. Emission from fluorescein and GFP proteins expressed in cells was captured on an ISS Alba avalanche photodiode (APD) aligned to the LED beamspot on the device. Simultaneous video imaging of microfluidic device operation was collected on a high-speed camera (Phantom Miro Ex2; 640 x 480 resolution, 990 µs exposure time). This optical setup can be seen in Figure 3.2.

3.2.6.2 Electrical setup:

Signal from the APD was delivered to a Teensy 2.0 Arduino where a code assessed whether the signal was higher than the set threshold, and, if so, sent a pulse to a function generator (Agilent) to trigger a 60-cycle burst of 30 kHz square waves. This burst was amplified via a high voltage amplifier (Trek) and applied on device via the previously described solid metal electrodes. The trigger and amplified signal were visualized on an oscilloscope (Agilent). The electrical circuit is shown in Figure 3.2B.

3.2.6.3 Microfluidic setup and operation:

The oil phase was set to a flow rate of 10 uL/min, and the droplets are set to a rate of 0.3 uL/min. The sorting device design was based on previous work by Mazutis *et al.*[26] Droplets were collected either in Eppendorf tubes (for qPCR analysis) or in custom droplet containers (for further microfluidic processing).

3.2.7 qPCR sample and data processing

Droplets were coalesced by adding 1H,1H,2H,2H perfluoro-1-octanol (Sigma-Aldrich) and centrifuging to separate the aqueous and oil phases. The aqueous layer was aspirated out into a DNA LoBind tube (Eppendorf). For genomic DNA studies, 30 µL of the digestion cocktail sans MNase was added, mixed, and incubated with each sample for 20 minutes before being quenched. Two microliters of 10 mg/mL proteinase K (VENDOR) were added and incubated at 65 °C for two hours up to overnight. Samples were then purified via the MinElute PCR Purification kit (Qiagen). Quantitative PCR plates were prepared in 384-well plates (Thermo Scientific) with SybrGreen master mix (Applied Biosystems), primers obtained from Integrated DNA Technologies, and template DNA. qPCR was performed on a CFX Opus 384 real-time PCR system (Bio-Rad). Quality assurance of performance was completed via Bio-Rad's cloud platform, BR.io, and delta delta Ct/fold enrichment values were calculated in Excel.

3.2.8 Nucleosome positioning device

Pre-made or FADS-processed droplets were reinjected into the digestion module at a flow rate of 0.5 - 2 µL/min, depending on backpressure. They were spaced out with an oil flow (2X, 1 – 2 µL/min) prior to being injected with lysis components, zymolyase,

and MNase (X, 0.5 – 1 µL/min). Droplets incubated through delay channels for 20 minutes while spheroplasting, cell lysis, and chromatin digestion occurred until the addition of the quenching buffer (2X, 1 - 2 µL/min) at the end of the device. Droplets were collected into an Eppendorf tube and merged through the addition of perfluorooctanol, and the aqueous phase was aspirated into a new, clean tube.

Samples were treated with proteinase K at 65 °C overnight to release DNA fragments from nucleosome and chromatin associated proteins. DNA was purified with the MinElute PCR kit from Qiagen, before amplification via the ThruPlex DNA-seq kit from Takara Bio. Following amplification, a SPRI bead-based NGS cleanup step was performed (Takara Bio, NucleoMag). DNA concentration was measured through the Qubit dsDNA HS assay (ThermoFisher), and fragmentation patterns were assessed through capillary electrophoresis on an Agilent Bioanalyzer high sensitivity chip. Percent mononucleosomal fragment generation was assessed using ImageJ in conjunction with the Bioanalyzer gel images, and comparing the area under the curve for mononucleosomal fragments versus all DNA generated up to 1000 bp.

3.3 Results and Discussion:

To investigate heterogeneity within cellular populations, we used a multi-device workflow, shown in Figure 3.1. Cells were initially compartmentalized within droplets before being injected onto the FADS device. FADS separated cell-containing droplets from empty droplets based on differential fluorescence emission. The droplets outputted from FADS were then injected into our modified digestion device, where cells were treated simultaneously with zymolyase, lytic components, and MNase to simultaneously remove the cell wall, lyse the cell membrane, and fragment chromatin into

mononucleosomal length pieces, respectively. Following this, DNA fragments were purified and prepared for analysis.

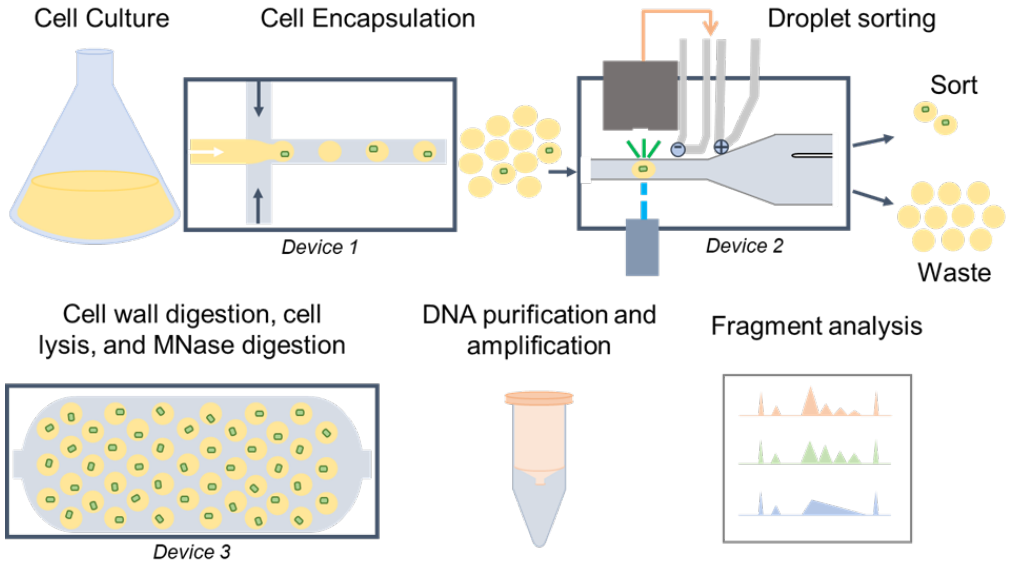

Figure 3.1. Diagram for the FADS-MNase, droplet microfluidic workflow. Following culture, cells are encapsulated into droplets (Device 1) which are sorted via FADS (Device 2). Fluorescent cell-containing droplets are enriched in the "Sort" output, while empty and low fluorescent droplets are collected into the "Waste" output. The output droplets from FADS can then be processed through the MNase digestion device (Device 3) to perform simultaneous cell wall digestion, cell lysis, and DNA fragmentation before the MNase enzyme is quenched through the injection of EDTA at the end of the device. DNA is subsequently purified and amplified prior to analysis of DNA fragments.

3.3.1 FADS validation

FADS experiments were completed in the SMART Center at the University of Michigan. Figure 3.2 depicts the organization of optical elements for excitation and detection of fluorescent emission and the circuit of electrical components needed to trigger the application of an AC field to divert droplets. The excitation source and high-speed camera were positioned behind the microscope and directed into the back of the microscope turret. Using our beamsplitter and FITC dichroic mirror, we were able to simultaneously excite cells, detect fluorescence, and image the microfluidic device allowing for real-time adjustments. Droplets were spaced out initially at a flow focusing junction on the FADS device (Fig. 3.3A) before being sent across the excitation beam

spot. With no detected fluorescent signal, or signal below the set threshold (10,000 – 40,000 counts per second or cps), droplets flowed straight into the “Waste” outlet. However, for signals above the threshold, aqueous droplets were diverted into the “Sort” outlet due to dielectrophoretic forces induced by the application of an AC field. Thresholds were manually set each experiment day at levels above noise from the detector every 100 μs time block.

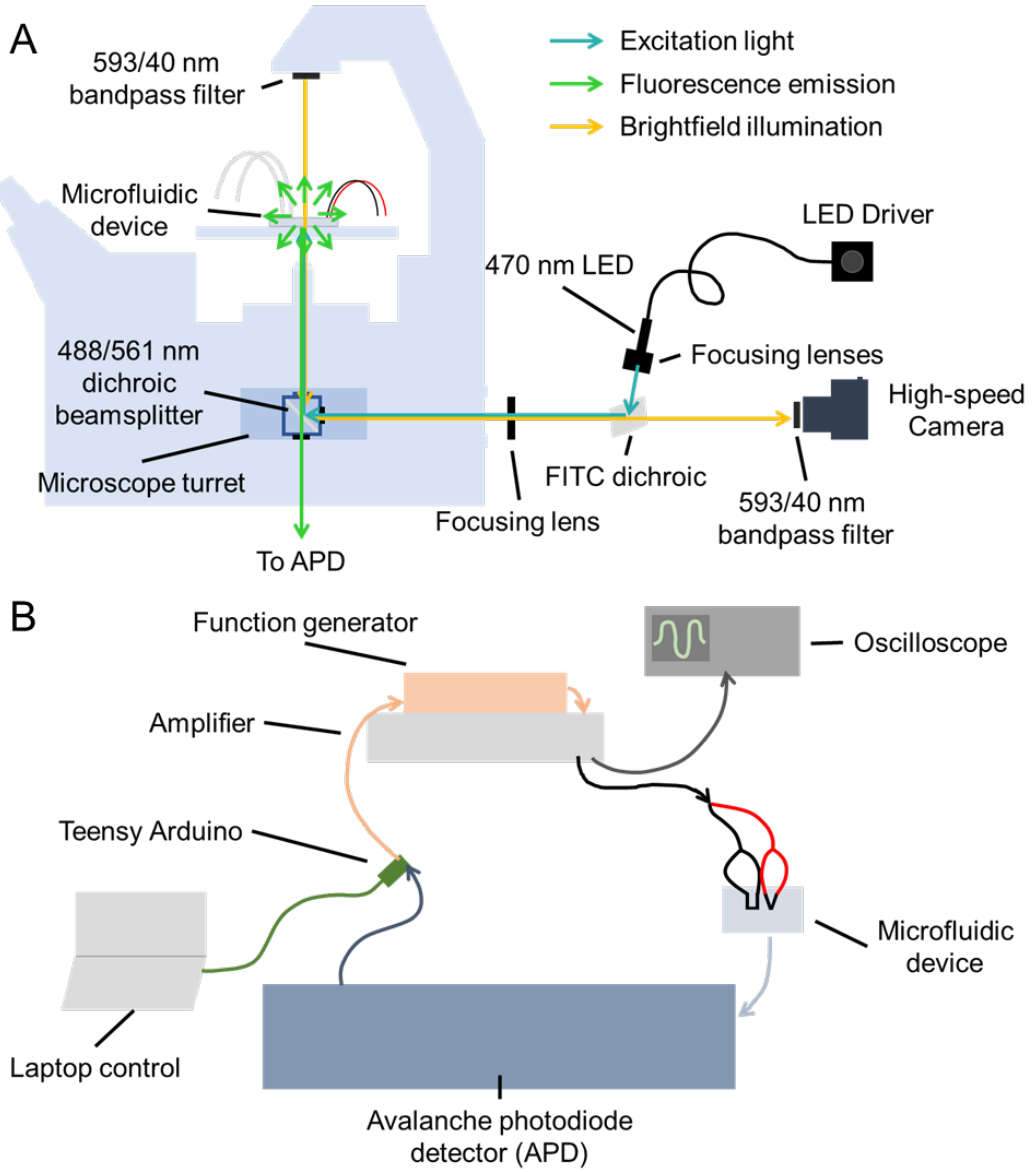

Figure 3.2. Diagrams of optical and electrical components used for FADS sorting. (A) Excitation light is directed from the LED source to the microscope stage using filters and mirrors. The excitation path is filtered to narrow the wavelength range that reaches the microfluidic device. Brightfield light is filtered to facilitate imaging of the device during operation with a high-speed camera without impacting the excitation and emission of fluorescent droplets. A dichroic beamsplitter is used to filter out excitation and brightfield light from droplet fluorescence emission that travels to an avalanche photodiode detector (APD). (B) Fluorescence emission is detected by the APD whose signal outputs to a Teensy Arduino running the FADS sorting script. A threshold for sorting can be set on the script; above this threshold, a signal is sent to the function generator to trigger an AC pulse, which is amplified and delivered onto the microfluidic device via solid-metal electrodes. The AC burst from the function generator and amplifier can be visualized on an oscilloscope. Application of the AC field on device results in diversion of oil away from the electrodes, which displaces droplets passing through the device towards the electrodes and into the Sort output.

To confirm the FADS system's ability to divert fluorescent droplets, 10 nM fluorescein-optiPBS droplets were generated and processed through the device. Fluorescent emission from droplets was observed as evenly spaced peaks through APD detection (Fig. 3.3B), indicative of consistent droplet passage through the sorting device. The spacing of these peaks indicates a throughput of 30 droplets processed per second. Representative video imaging showed consistent diversion of droplets into the Sort output (Video 3.1) and demonstrated successful performance of the FADS setup. A 1:10 mixture of 10 nM fluorescein-optiPBS and optiPBS droplets was processed next to confirm sorting occurred in response to fluorescent signals, not just droplet occurrence, and assess how well the system could divert individual droplets. Indeed, Figure 3.3C and a synchronized Video 3.2 confirmed decreased numbers of peaks detected above the threshold and droplets diverted into the Sort output, supporting the lower proportion of fluorescently active droplets in the sample. The video imaging and APD trace were synchronized by passing a hand or object behind the microscope, through the excitation and illumination light paths. Comparison of the synchronized data showed sorting of individual droplets in response to peaks observed in the APD trace. These observations confirm our FADS setup was able to divert single droplets following their fluorescence emission and detection.

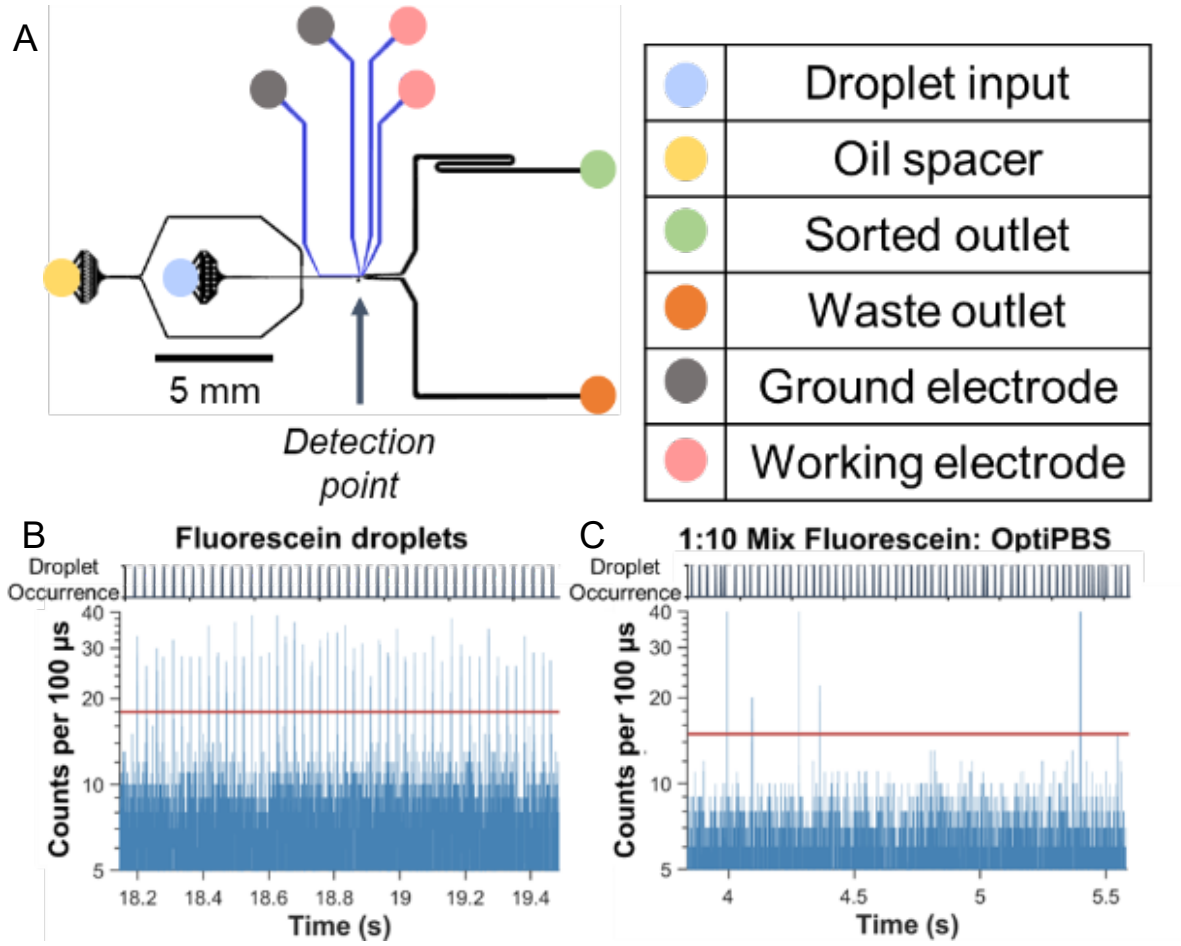

Figure 3.3. Validation of the FADS device. (A) FADS device diagram with inputs and outputs labeled. Fluorescent signal from fluorescein-optiPBS droplets (B) and a 1:10 mixture of fluorescein-optiPBS and optiPBS droplets (C). APD signal is shown for a subset of the collection time (18.1 – 19.5 s and 3.8 – 5.6 s, respectively). The time windows correspond to synchronized videos collected of droplets passing through the device. Droplet occurrence in the device is indicated with peaks in the graphs above the fluorescent signal traces. Fluorescent peaks above the set thresholds (red lines) correspond to fluorescein droplets passing through the detection point.

Video 3.1. Video imaging of FADS processing of a pure sample of 10 nM fluorescein-optiPBS droplets. Droplets consistently diverted into the Sort output channel. A shadow appears across the channel which results from the edge of a filter passing through the camera's field of view – this shadow has no effect on the excitation light path or sorting of droplets.

Video 3.2. Synchronized imaging of FADS processing of a 1:10 mixture of 10 nM fluorescein-optiPBS and optiPBS droplets. Individual droplets were observed diverting into the Sort output channel. A shadow appears across the channel which results from the edge of a filter passing through the camera's field of view – this shadow has no effect on the excitation light path or sorting of droplets.

Initial validation of the FADS system was performed with a manufactured fluorescent signal. Fluorescent yeast cells were encapsulated and processed to begin assessing the system's ability to respond to biological signals. An *S. pombe* yeast strain modified to express green fluorescent protein (GFP) in the nucleus was used as the fluorescent cell population. There was concern that the small size (4 X 10 μm) and heterogeneous GFP expression of these *S. pombe* cells would lead to challenges during FADS. However, we were able to detect and divert droplets in response to fluorescent *S. pombe* yeast cells contained in droplets, as shown in Figure 3.4. Three

snapshots can be seen of a cell-containing droplet entering the video imaging field of view and being diverted into the Sort output. These snapshots correspond to the fluorescence peak observed at 55.07 s. Video 3.3 depicts the droplets processed during the APD trace segment shown in Figure 3.4A. Several cases were observed where an individual, cell-containing droplet was diverted in between adjacent, empty droplets, indicating appropriate timing parameters employed for the sorting.

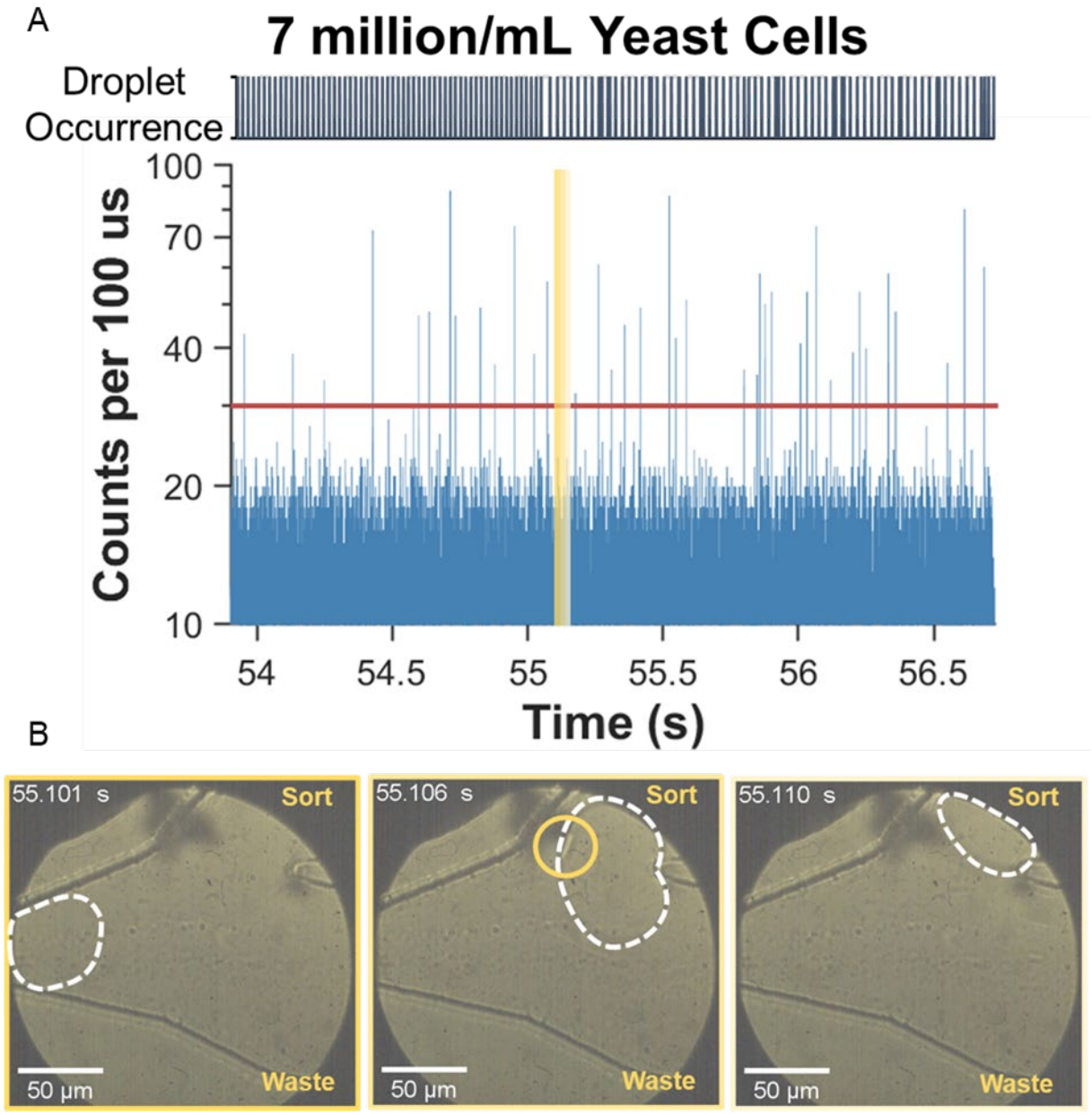

Figure 3.4. Fluorescent signal and corresponding snapshots of video imaging for FADS processing of yeast cell-containing droplets. (A) Fluorescent signal of yeast cell-containing droplets during FADS processing for a subset of the APD collection time (53.9 – 56.7 s). The time window corresponds to a synchronized video collected of droplets passing through the device. Droplet occurrence in the device is depicted as peaks in the graph above the fluorescence trace. Fluorescent peaks above the threshold (red line) correspond to droplets containing yeast cells. (B) Snapshots a yeast-cell-containing droplet being diverted into the Sort output. The cell is circled in the middle frame. This droplet corresponds to the peak present at 55.07 highlighted in the fluorescence trace.

Video 3.3. Synchronized video imaging for FADS processing of yeast cell containing droplets. Droplets were generated at a concentration of 7 million cells per mL and sorted on the same day. Individual droplets containing a yeast cell were observed entering the Sort output between adjacent empty droplets. However, several droplets containing yeast cells were not diverted. It was determined that the fluorescence emission from these cells was not high enough to trigger a sorting event.

3.3.2 qPCR analysis of FADS processed S. pombe mixtures

The biological complexity of the system needed to be increased to reach our goal of using FADS as a method for enriching droplet populations for cells of interest. Mixtures were prepared containing the GFP expressing strain and a non-fluorescent *S. pombe* strain. The latter possessed a gene encoding Ura4, an enzyme involved in synthesis of pyrimidine nucleobases, in place of the GFP gene encoded in the fluorescent strain genome. Processing mixtures of these two strains allowed us to mimic sorting of epigenetic subpopulations, where fluorescence emission from cells depends on epigenetic regulation of a fluorescent gene. Incorporation of the non-fluorescent yeast cell line exposed the limited assessment power of our synchronized imaging setup since fluorescent and non-fluorescent cells were undifferentiated in video imaging. Thus, we incorporated an offline, qPCR measurement to assess the purity of cells present in product droplets from each output.

Quantitative PCR analysis reveals the amount of a specific DNA sequence present in a sample relative to a control. Primers for the sequence of interest are added

to selectively amplify matching DNA fragments until their concentration passes a selected threshold (monitored through the intercalation of fluorescent dyes within DNA molecules). The number of amplification cycles needed to pass the threshold (C_t) for a treated sample can be compared with a control to calculate a $\Delta\Delta C_t$ value (Eqn. 3.1) and fold enrichment value (Eqn. 3.2). These numbers express whether the DNA sequence is present in high or low abundance relative to the control. For ease of visualization, fold enrichment values were used and interpreted as the contribution of each gene of interest (either GFP or Ura4) to the total DNA content at the specific, genomic locus. Since individual cells will contain only one of these genes, this allowed us to assess cell purity following FADS processing, indicating how accurately fluorescent cells were diverted into the Sort output. Controls were made up of pure cell populations (fluorescent yeast cells for GFP; non-fluorescent yeast cells for Ura4). Differences in the total amount of DNA present in the qPCR samples were corrected by comparing the C_t values of the genes of interest (GOI) and the reference gene, Tub1, whose expression was expected to be relatively constant in both strains (Eqn. 3.3).

$$\Delta\Delta C_t = C_{t_{mixture}} - C_{t_{control}} \quad \text{(Eqn. 3.1)}$$

$$Fold\ enrichment = 2^{-\Delta\Delta C_t} \quad \text{(Eqn. 3.2)}$$

$$C_{t_{sample}} = C_{t_{GOI}} - C_{t_{Tub1}} \quad \text{(Eqn. 3.3)}$$

Output droplets from FADS processing were merged, and DNA was extracted to perform qPCR analyses. Bulk mixtures were also prepared, extracted, and analyzed to demonstrate what an averaged measurement would produce (Fig. 3.5A). Bulk qPCR analysis showed that the fold enrichment of genes was a function of the cell mixture composition. As an example, the fold enrichment value for GFP decreased as the

fluorescent, GFP-expressing cell content in the mixture decreased. This trend was observed for the nonfluorescent cell strain as well. Unexpectedly, the ratios of the fold enrichment values did not change proportionally with the mixture content (e.g., the fold enrichment values for the 50% GFP cell mixture were not equal for both GFP and Ura4). This could indicate that there are differences in cell proliferation rates in tube or unaccounted biases occurring during amplification for the two genes.

On the other hand, FADS-processing resulted in higher fold enrichment values for GFP in Sort outputs (Fig. 3.5B), indicating successful enrichment of fluorescent cells in the sample obtained from the Sort output. For both a 50% and 25% fluorescent cell mixture, the Sort output showed a fold enrichment for the GFP gene region comparable to the fold enrichment of the Sort output for the fluorescent cell control, indicating high amounts of DNA from fluorescent cells and high purity of cells diverted into that output. The resulting fold enrichment for the Waste output (Fig. 3.5C) more closely resembled bulk processing of cell mixtures, which indicates that we are not significantly de-enriching the Waste output for fluorescent cells.

While fluorescent cells were successfully enriched in the Sort output, a fold enrichment value of 0.14 ± 0.04 intensity was also observed for the Ura4 gene in the Sort output (Fig. 3.5B). This demonstrated that non-fluorescent cells were present in droplets diverted to the Sort output. It is believed that these non-fluorescent cells could be present with fluorescent cells in droplets during FADS processing. Based on our 6 million cells per mL concentration and an estimated droplet size of 200 pL, the average number of cells per droplet is expected to be 1.2, with about 34% being occupied by 2 or more cells (Fig. 3.6A). Thus, it is reasonable that both cell strains might occupy the

same droplet and reduce sample purity. Additionally, droplet merging during FADS processing has been observed in the tubing leading to the microfluidic device (Fig. 3.6B). These larger droplets are re-segmented by the oil spacer, but cells likely collect together due to gravity instead of remaining evenly dispersed throughout the solution.

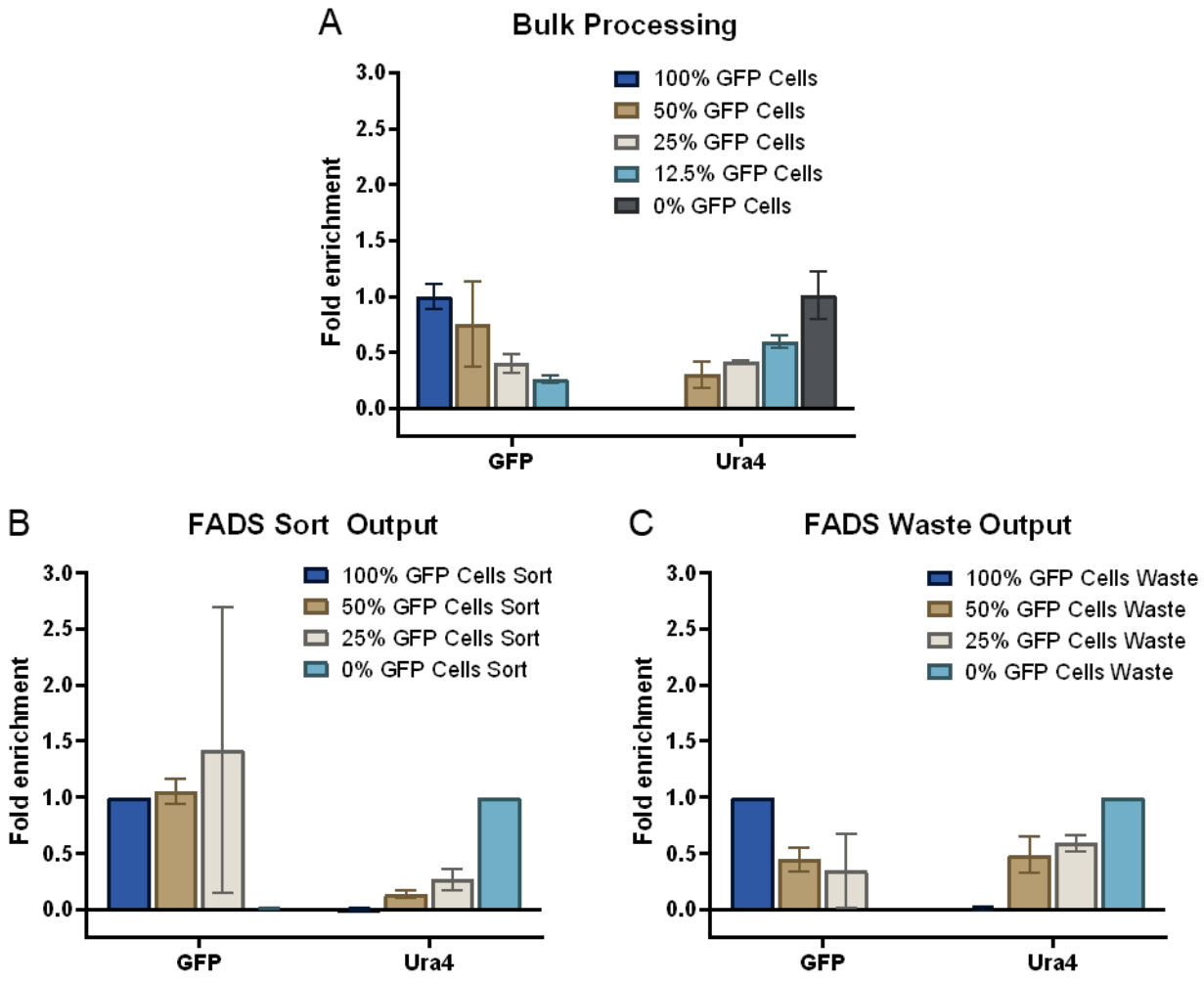

Figure 3.5. Quantitative PCR analysis of bulk (A) versus FADS-processing (B, C) of synthetic cell mixtures. The fold enrichment of the FADS-processed samples is split with respect to samples obtained from the Sort (B) and Waste outputs (C).

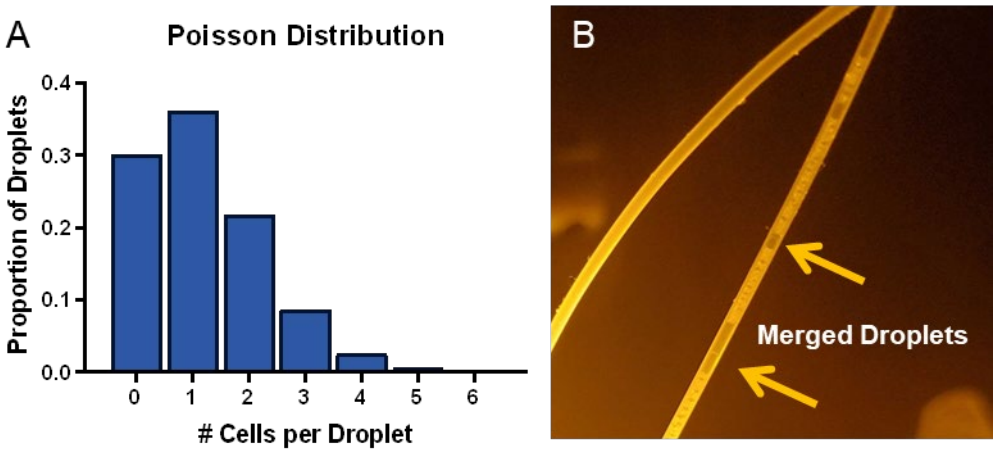

Figure 3.6. Possible causes for non-fluorescent cells entering the Sort output. (A) The expected distribution of cells in droplets based on calculated Poisson statistics from 6 million cells/mL sample segmented into 200 pL droplets. Only 36% of droplets are expected to contain a single cell, with 30% of droplets being empty and 34% of droplets containing 2 or more cells. (B) Merged droplets observed in tubing headed into the FADS device. Droplets are delivered onto the FADS device as soon as 1 hour following generation. However, processing of samples takes 1.5 – 2 hours, so droplets could be sitting in the reinjection container for up to 3 hours or more for subsequent samples.

3.3.3 MNase module application to yeast cells and pairing with FADS

The MNase digestion module has previously been used in the Bailey Lab to obtain nucleosome positioning information from human cells.[134] Cells, lytic components, and MNase were segmented into droplets. These droplets mixed through a serpentine channel and incubated at room temperature through delay channels for 3.5 minutes. During this incubation, cell lysis and chromatin digestion occurred simultaneously. MNase cleaves and digests double stranded DNA preferentially at open regions; however, DNA attached to nucleosomes or other chromatin associated proteins is protected and remains intact for longer. At the end of the device, a picoinjector added quenching buffer containing EDTA to droplets to chelate calcium ions present in solution which quenched MNase's digestion activity. Droplets were then merged for DNA purification, library preparation, and sequencing analysis.

For this work, the module's design was modified to accommodate pre-made droplets (Fig. 3.7A). The droplet generator of the initial device was replaced by a droplet input and oil spacer, and a pico-injector was incorporated to add digestion components to each droplet. To expand what cell types could be processed through this module, I incorporated zymolyase into the digestion cocktail. Zymolyase is an enzyme mixture designed to degrade the integrity of cell walls, facilitating access to the plasma membrane by lytic components. Typical zymolyase treatments last for 15 – 30 minutes at high temperatures, so the incubation time for this simultaneous digestion on device was increased from 3.5 minutes to 20 minutes. Following the initial injection, droplets were mixed through the serpentine feature before incubating for 20 minutes through delay channels, during which time zymolyase digested the yeast cell wall, lytic components broke open the plasma and nuclear membranes, and MNase digested down linker DNA between nucleosomes. At the end of the device, quenching buffer was injected through the second picoinjector to halt the activity of MNase before droplets exited the device.

Following device processing, droplet samples were merged and separated from the oil phase. DNA fragments were released with Proteinase K treatment and purified prior to amplification. Amplification of DNA samples was incorporated to counteract the low DNA output from yeast cells. This ensured that there was enough DNA to be observed through bioanalyzer analysis, which was used to assess the quality of each DNA digestion. In bioanalyzer chip processing, nucleic acids separate based on size in response to a voltage gradient applied to induce electrophoretic movement.[145] DNA and RNA molecules possess a constant mass-to-charge ratio, so movement through the

chip matrix depends solely on size. Shorter fragments travel through the matrix faster than longer fragments. During movement through the chip matrix, fluorescent dyes intercalate within nucleic acid strands to enable fluorescent detection of fragments as they exit the chip. The goal of our digestion was to produce high proportions of mononucleosomal fragments relative to higher order features. This would be observed as intense peaks located at 267 bp, accounting for a 146 bp mononucleosome fragment length with 121 bp of primers adapted on during amplification, and low intensity peaks present at 413 bp, 559 bp, and 705 bp, which represent di-, tri-, and tetra-nucleosome-length fragments.

Bioanalyzer analysis of the size distribution of DNA fragments produced from microfluidic samples, bulk-processed samples, and No Cell controls are shown in Figure 3.7B. Mononucleosomal fragment peaks were observed between 200 and 350 bp, which fits with the anticipated fragment length for proof-of-concept purposes. All samples exhibited a shoulder on the mononucleosomal peak, beginning at ~ 200 bp, demonstrating slight over-digestion of DNA samples or “nucleosome sliding”. Nucleosome sliding occurs as nucleosomes naturally move along short sections of DNA.[146,147] During MNase digestion, this phenomenon can lead to shorter apparent DNA fragments, due to previously blocked DNA being made available to the digestion enzyme, showing shorter than expected nucleosomal fragment lengths. Droplet processed samples showed a higher percentage of mononucleosomal fragments produced relative to bulk processed samples, 75% vs 28% ± 3%, demonstrating more efficient digestion of DNA in the droplets (Table 3.1). A small peak was observed in the No Cell control and droplet-processed samples beginning at ~175 bp (Fig. 3.7C).

However, upon preliminary sequencing of the No Cell control samples (Appendix C), an extremely low percentage of DNA fragments aligned to the *S. pombe* genome. These fragments are assumed to derive from DNA contaminants in kit buffers and on pipette tips during processing, which will amplify in the absence of other, larger DNA sources. Decreasing the ratio of SPRI beads used for library purification could help remove the contribution of this peak from droplet-processed samples.

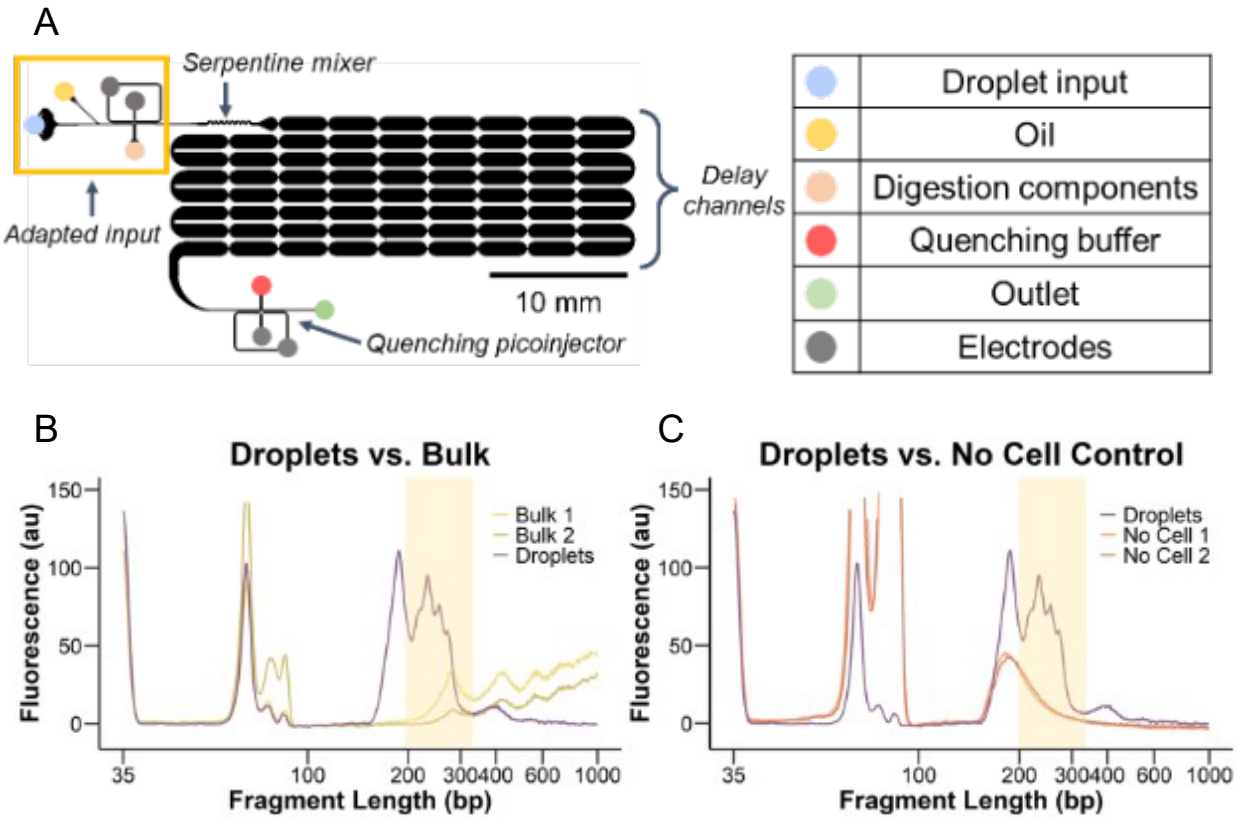

Figure 3.7. Expansion of the MNase droplet device to process cell-wall containing cells. (A) The adapted design features an adjustment of the inputs to facilitate processing of pre-made droplet samples with a droplet input, oil spacer, and picoinjector for adding digestion and lysis components (outlined in yellow). Following the digestion injection, droplets are mixed through a serpentine channel, incubated through delay channels, and injected with quenching buffer. Digestion profiles from bioanalyzer analysis are shown for droplet versus bulk processing (B) and droplet processing versus No Cell controls (C). The location of mono-nucleosome-length DNA fragments (200 – 350 bp) is highlighted in yellow. Some fluorescence intensity for primer dimers at < 100 bp is cut off. 720,000 S. pombe cells emulsified for data shown.

Table 3.1. Percent production of mono-nucleosome DNA fragments for microfluidic versus bulk processing. The number of replicates per sample type is indicated.

Processing	% Mono-nucleosome Fragment Production	Replicates
Droplets	75	1
Bulk	28 ± 3	2

Finally, fluorescent yeast cell droplet samples were enriched through FADS processing and processed through the MNase digestion module to demonstrate cohesive operation of the entire droplet microfluidic workflow. Droplets were generated, processed through the FADS device with a threshold of 12,000 cps, then each output was injected into its own digestion device to produce mononucleosomal DNA fragments. Figure 3.8 shows the digestion profiles for FADS-processed samples in comparison to bulk processed samples and No Cell controls. All sample processing techniques resulted in 70% mononucleosome production (Table 3.2), indicating successful performance of the droplet microfluidic workflow. No Cell control samples showed a contaminating peak again beginning at ~175 bp that contributes slightly to the FADS-MNase droplet processed samples. This continued contamination indicates the extra peaks seen in the Bioanalyzer data in Figure 3.7 are likely due to the presence of DNA fragments on pipette tips and in kit buffers as hypothesized.

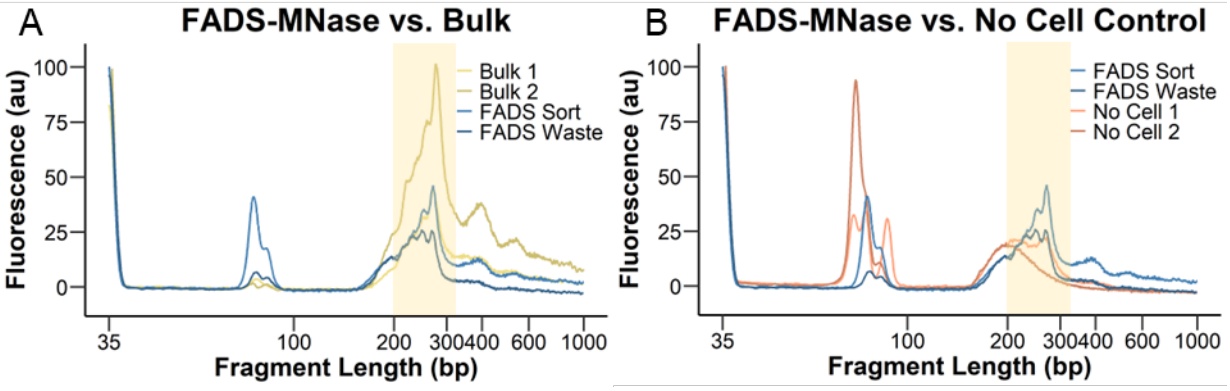

Figure 3.8. Digestion profiles from bioanalyzer analysis are shown for the full FADS-MNase droplet processing versus bulk processing. (A) and versus No Cell controls (B). The location of mono-nucleosome-length DNA fragments (200 – 350 bp) is highlighted in yellow. 180,000 S. pombe cells emulsified for experiment.

Table 3.2. Percent production of mono-nucleosome DNA fragments for FADS versus bulk processed samples. The number of replicates per sample type is indicated.

Processing	% Mono-nucleosome Fragment Production	Replicates
FADS Sort	70 ± 20	2
FADS Waste	70	1
Bulk	70 ± 10	4

3.4 Conclusion:

Nucleosome positioning assays provide insights into the global storage of DNA under different environmental stimuli. Conventional assays, such as MNase-seq, require millions of cells to offset samples losses that occur throughout processing steps. Droplet microfluidic techniques enable movement towards smaller sample sizes, due to the ability to compartmentalize cells within small volumes and obtain better reaction efficiencies. Additionally, the automation of multiple reagent additions helps reduce sample loss. Here, I report the development of a droplet microfluidic FADS-MNase workflow to study nucleosome positioning in yeast cell subpopulations.

The FADS setup enabled simultaneous excitation, detection, and video imaging of the microfluidic device, allowing us to perform adjustments in real-time. Droplets composed of fluorescent solution as well as droplets containing *S. pombe* cells were detected and diverted at a throughput of 30 droplets per second. Synthetic cell mixtures of fluorescent and non-fluorescent yeast cells were enriched through FADS, showing enrichment of GFP gene sequences in Sort outputs. However, the presence of the Ura4 gene from the non-fluorescent cell in the Sort outputs also indicates further optimization is needed to reduce the average number of cells per droplet and prevent droplet merging prior to FADS processing. Generation of smaller droplets initially and an increase in the fluorosurfactant used to stabilize droplets would help decrease the cases where multiple cells are present in droplets.

The MNase design was modified to facilitate processing of pre-made droplets. Additionally, zymolyase was incorporated into the digestion cocktail to expand the possible cell types compatible with this method to include cell wall-possessing cells. This addition was performed simultaneously with cell lysis and DNA digestion both to maintain the current simplicity of the device but also to reduce sample handling requirements before input onto the device. Specifically, a simultaneous cell wall digestion, lysis, and DNA fragmentation step enables usage of the FADS and MNase devices directly in series. The fragmentation patterns showed production of mononucleosomal fragments at a higher proportion in droplet processed samples versus bulk processing (75% vs 28% ± 3%, respectively), indicating an improved reaction efficiency achieved in droplets. Lastly, the full FADS-MNase droplet microfluidic workflow was applied for the first time ever to obtain mononucleosomal DNA fragments

from droplets enriched for fluorescent yeast cells. Bulk and droplet-processed samples both generated 70% mononucleosomal DNA fragments.

While this chapter shows effective progress for this modular workflow, additional work is needed to achieve its full potential. The parameters employed for FADS sorting need to be delicately balanced to reduce the presence of off-target cells in the Sort output while maintaining practical output volumes. Adjusting the FADS device design to increase the throughput and decrease total sample processing time would permit processing of larger sample sizes. This would increase the output volume obtained for downstream steps. Once optimized, the workflow can be applied to an *S. pombe* strain that epigenetically controls the expression of a fluorescent protein. This would uncover insights into the extent to which cells can fine-tune heterochromatin formation.

3.5 Acknowledgements:

Funding for this work was provided by the National Science Foundation (NSF Grant No. 1921677). We acknowledge NSF MRI-ID grant DBI-0959823 to N.G.W. for seeding the SMART Center. J. Damon Hoff was vital in providing training, expertise, and assistance while optimizing the FADS setup in the SMART Center. We would like to acknowledge Anna L. Calkins for providing molecular biology expertise for performing cell culture. The University of Michigan Biomedical Research Core Facilities Advanced Genomics Core was vital in performing Bioanalyzer analysis of DNA samples. We also acknowledge Douglas Dickey from the Chemistry Department Electronic Shop for fabricating the high voltage adapters to connect our amplifier to the sorting device. Lastly, we would like to thank Brittany Bowman for providing training and access to the BioRad Opus CFX instrument in Biological Chemistry.

3.6 Attribution Information

This research project has been worked on by multiple generations of students in the Bailey Laboratory. M. Sun wrote the script used for sorting droplets in FADS; V. Sahore implemented some of the setup and protocol steps utilized for sorting in the SMART Center and digesting yeast cells using the MNase digestion device. C.D. Cook made alterations to the sorting setup to enable simultaneous sorting and imaging—these changes were made in consultation with J.D. Hoff from the SMART Center. C.D. Cook generated all data presented in this chapter and brought together the two device workflows to isolate fluorescent yeast cells and generate mono-nucleosomal DNA fragments. *S. pombe* strains were provided by K. Ragunathan.

Chapter 4 Modular Droplet Microfluidic Workflows for Isolation and Analysis of Limited Cell Samples

4.1 Dissertation Motivation

Natural variations in cell cycle, epigenetic state, and environmental cues lead to measurable differences in phenotype between cells within a genetically identical population. These differences have been shown to have important implications for biological processes and clinical health monitoring.[2,4,9,13] Thus, there is a need for tools to study the range of cellular responses to stimuli. Several isolation and analysis tools have been developed to prepare and study small populations of cells, down to the single-cell level.[14,36] However, these techniques typically require large volumes of reagents, long times for analysis, and expensive equipment.

The field of microfluidics has developed tools to fill the gap of low cost, miniaturized, rapid, and high throughput cellular isolation and analysis tools. Scientists have creatively designed arrays, chambers, and channels to separate cells of interest from complex mixtures,[47,53,55] compartmentalize cells for individual processing, and analyze a variety of cellular features.[4,55,65,148] The incorporation of an immiscible fluid to aqueous microfluidic devices enables generation of nanoliter to attoliter droplets to compartmentalize cells within further reduced volumes.[39] Droplet microfluidic devices are easily scalable, mix efficiently, and prevent dilution of reagents or analytes. Many

channel geometries have been developed to accomplish reagent manipulations in droplet microfluidic devices.[60–64,149] However, a limited number of them are incorporated into devices that focus on singular assay steps. Benchtop protocols require a variety of processing steps to produce desired results, so single-step microfluidic devices rely on benchtop processing techniques to prepare input or finalize the output sample.[150] To fully automate benchtop assays, multiple steps must be completed in microfluidic features, which leads to complex devices that are difficult to operate or that are sensitive to alterations in back pressure and can decrease the uniformity with which droplets are processed.[151,152]

To reduce the reliance on benchtop processing for cellular analysis, this dissertation detailed the development of modular, droplet microfluidic workflows that combine multiple droplet microfluidic devices in series to isolate cells of interest and process or treat them for downstream analyses. These workflows are comprised of individual microfluidic devices that focus on separate portions of the protocol and can be mixed and matched in a “plug and play” format to customize the assay as desired. In particular, two workflows were developed. The first focused on an expansion of the CAR-Wash device[62] to isolate cells of interest from multi-cell mixtures. This adaptation to the CellMag-CARWash workflow demonstrates the versatility of the device’s concept and takes an important step forward in expanding its utility. Cells were segmented into individual droplets that are suitable for many downstream, droplet processing workflows. Specifically, we leveraged the ability to incorporate molecular treatments into the CellMag-CARWash buffer to study the effect of β-estradiol on extracellular vesicle (EV) secretion from MCF7 GFP cells. The second workflow combined a fluorescence

activated droplet sorter (FADS) device with the Bailey Lab's MNase digestion module.[134] Validation of and adaptations to these devices focused on improving their ability to be used together cohesively. The FADS setup was adjusted to enable simultaneous imaging and detection to facilitate real-time troubleshooting during sorting. The MNase module design and operation were adapted to process pre-made droplets and a wider variety of cell types. These changes improved the plug-and-play friendliness of these devices and expanded their usability for modular workflows. Overall, these two workflows expand the applicability of these devices and demonstrate the usefulness of modular, droplet microfluidic workflows to study biological phenomena in single-cell samples. Key steps remain, however, to streamline workflow logistics and deepen their biological applicability.

4.2 CellMag-CARWash workflow for cellular isolation and EV studies

Droplet microfluidics is an attractive platform for single-cell studies due to its ability to compartmentalize and process individual cells in a scalable, high throughput fashion. However, most single-cell, droplet microfluidic assays require pre-purification of the desired cell type prior to encapsulation with reaction components.[65] To fill this gap, we developed the CellMag-CARWash workflow to selectively label cells of interest in a mixture with magnetic beads and magnetically isolate them into droplets through positive selection in the CellMag-CARWash device (Chapter 2). Output droplets from the workflow contained highly pure populations of single cells that can be used for further downstream assays and analyses. Cell mixtures were initially incubated with pre-functionalized magnetic beads that attach to cells of interest through antibody-driven interactions with cell surface markers. Antibody cocktails were curated to selectively

isolate a variety of cell types. Labeled cell mixtures were encapsulated within droplets initially to distribute them evenly throughout the sample volume and prevent gravitational settling. Droplets were processed through the CellMag-CARWash device, which features an extended washing channel to account for the anticipated increased residence time needed to recover cells in the output. Indeed, output droplets contained single cells with a high degree of purity (>93%) that were suitable for a variety of downstream analyses. We applied the workflow to study the distribution of EVs secreted from individual cells.

EVs are a trending research field, with the number of studies being published on them increasing rapidly beginning in 2015.[153] They facilitate cellular communication by ferrying proteins, molecules, lipids, and nucleic acids to other cells to elicit changes.[70] There is specific, clinical interest in EVs as potential biomarkers and drug delivery vehicles due to their long half-life within the body, presence in many biological fluids, function in ferrying multiple cargo types, and ability to target specific cells or regions of the body.[71] We wanted to study the effect of β-estradiol, a form of estrogen that has been shown to induce cell proliferation in estrogen receptor positive cell lines,[154] on EV secretion from MCF7 GFP cells. MCF7 GFP cells are a modified, breast cancer cell line that produce green fluorescent protein (GFP), and the effect of β-estradiol on their EV secretion dynamics has not been well studied. The washing buffer used in CellMag-CARWash can be exchanged for any buffer as long as it is able to conduct electricity. We leveraged this feature by spiking β-estradiol into our washing buffer to apply a single-cell level treatment to MCF7 GFP cells as they entered new droplets. Due to the small size of EVs relative to human cells (~150 nm versus ~15-30 μm), it was necessary

to remove the cells from droplets following incubation. I incorporated a magnetic droplet splitter to separate the droplets into two outputs: one with the magnetically tagged cell and one with droplet contents only, including secreted EVs. These latter droplets were fluorescently imaged to reveal the distribution of EV secretion dynamics from MCF7 GFP cells. We found that both media-only and β-estradiol spiked media treated cells secreted EVs in a Gaussian distribution. However, β-estradiol treatment increased EV secretion overall. Comparison with bulk EV isolation methods confirmed a similar increase in levels of secreted EVs following β-estradiol treatment, however, we obtained finer details regarding the heterogeneity of cellular responses using the CellMag-CARWash workflow. This points to the suitability of novel droplet microfluidic workflows such as CellMag-CARWash to process complex samples and study heterogeneity within cellular processes.

4.2.1 Future directions for CellMag-CARWash

Immediate next steps for this workflow include increasing the complexity of the initial cell mixture processed by CellMag-CARWash and assessing potential biases inherent in the technique. Two-cell mixtures were used exclusively to validate the workflow; however, isolation from multi-cell mixtures would bring it nearer to clinical contexts where native cell samples and biological fluids are directly processed.[155–157] It is anticipated that the antibody cocktail used to target desired cell types would take on an even greater importance, due to overlaps in expression markers on multiple cell types and greater heterogeneity in expression levels. Considering the heterogeneity of surface marker expression, it is assumed that the positive selection used in CellMag-CARWash biases downstream techniques towards cells with higher expression

levels.[158] The requirement for 3 or more beads to attach per cell to recover them in output droplets limits analysis to cells with higher levels of surface markers. Three changes could help lower the number of beads required for isolation: slowing the velocity of solutions within the device, further lengthening the washing chamber, and increasing the magnetic field strength of the permanent magnet. Unfortunately, the number of recovered, off-target cells with nonspecifically bound beads may increase from these changes, so the purity of cells in output droplets could be diminished.

It would be interesting to assess whether these differences in cell surface marker expression influence cellular dynamics. Separation of desired cells into subpopulations based on the number of beads attached through CellMag-CARWash could enable this analysis. Cells with different numbers of beads attached have different trajectories within the magnetic field, which I observe as cells reaching the bottom of the washing streamline at different points throughout the channel. This could be leveraged to separate cells based on the number of beads attached by incorporating multiple outlets along the washing channel (Fig. 4.1). However, resegmentation into droplets at each output would be challenging to maintain. Currently, an oil co-flow separates the washing buffer from the magnet-adjacent channel wall to prevent sample from sticking to the PDMS. This flow barrier would need to be considered when trying to allow cells to exit prior to the current resegmentation location. Additional oil flows would also need to be incorporated to ensure reproducible droplet generation at all outputs, which would increase the complexity in operating the device.

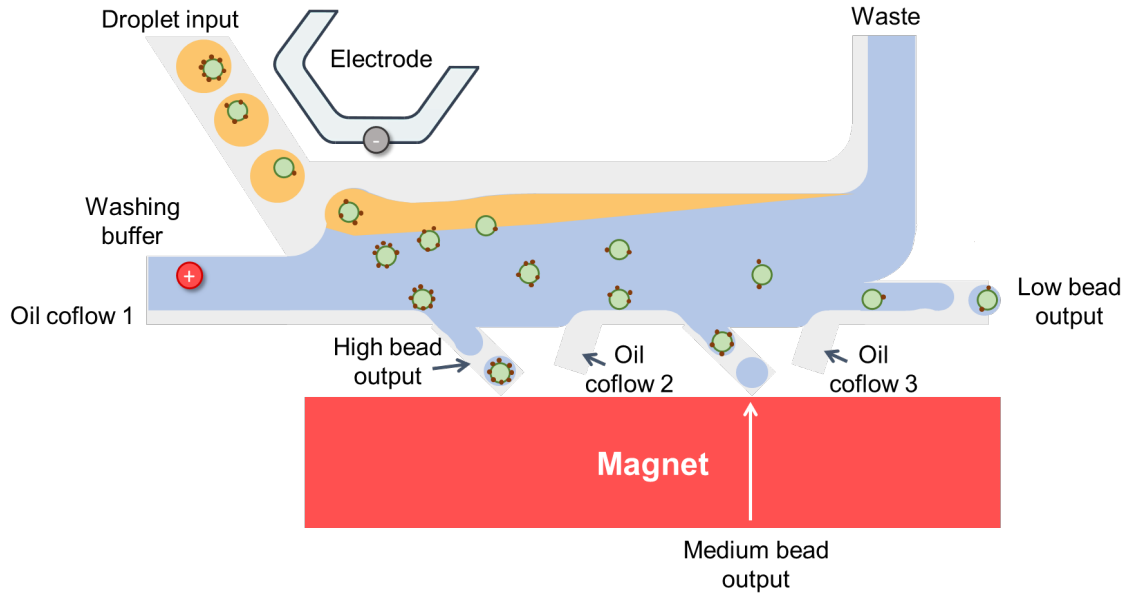

Figure 4.1. Proposed design for a multi-output CellMag-CARWash device. Extra outputs along the magnet-facing wall have been incorporated to collect cells with different numbers of beads attached. To maintain the oil barrier that prevents sample from sticking to the PDMS wall, extra oil coflow inputs have also been incorporated between each output.

Another interesting application to study using CellMag-CARWash would be cell-cell communication effects on cellular dynamics. The compartmentalization of cells within droplets isolates them, so typical responses that would be observed *in vivo* are hindered due to the removal of cells from their native communication context. Specifically, only autocrine, or cell-to-self, signaling can occur while cells are isolated in droplets, which is rare in normal physiology.[159] However, it is no longer believed that droplet contents are completely isolated after encapsulation. Droplet crosstalk has been observed for small molecules in several high throughput screening cases.[160–162] It has been shown that the fluorosurfactants used to stabilize droplets actually mediate transfer of small molecules between droplets. This feature could be leveraged to observe cellular changes in response to small-molecule mediated signaling between cells.[163,164] I envision isolation of multiple cell types into droplets via CellMag-CARWash and collection into a two-part array, where oil can flow past droplets that contain cells

treated to increase secretion of a small molecule towards droplets containing recipient cells, whose response can be imaged over time (Fig. 4.2). In principle, the oil applies shear forces to the original droplets which produce small micelles containing the secreted signaling molecule and carries them to recipient cells. The specific geometry of this device would need to be optimized so that droplets are easily captured within the arrays and direct connections between origin and receptor cells are controlled. Additionally, the transfer of small molecules between droplets would need to be characterized before cell studies could be completed. However, this concept is an exciting approach to expand the biological similarity of cell studies in droplets using a characteristic typically deemed an inconvenience.

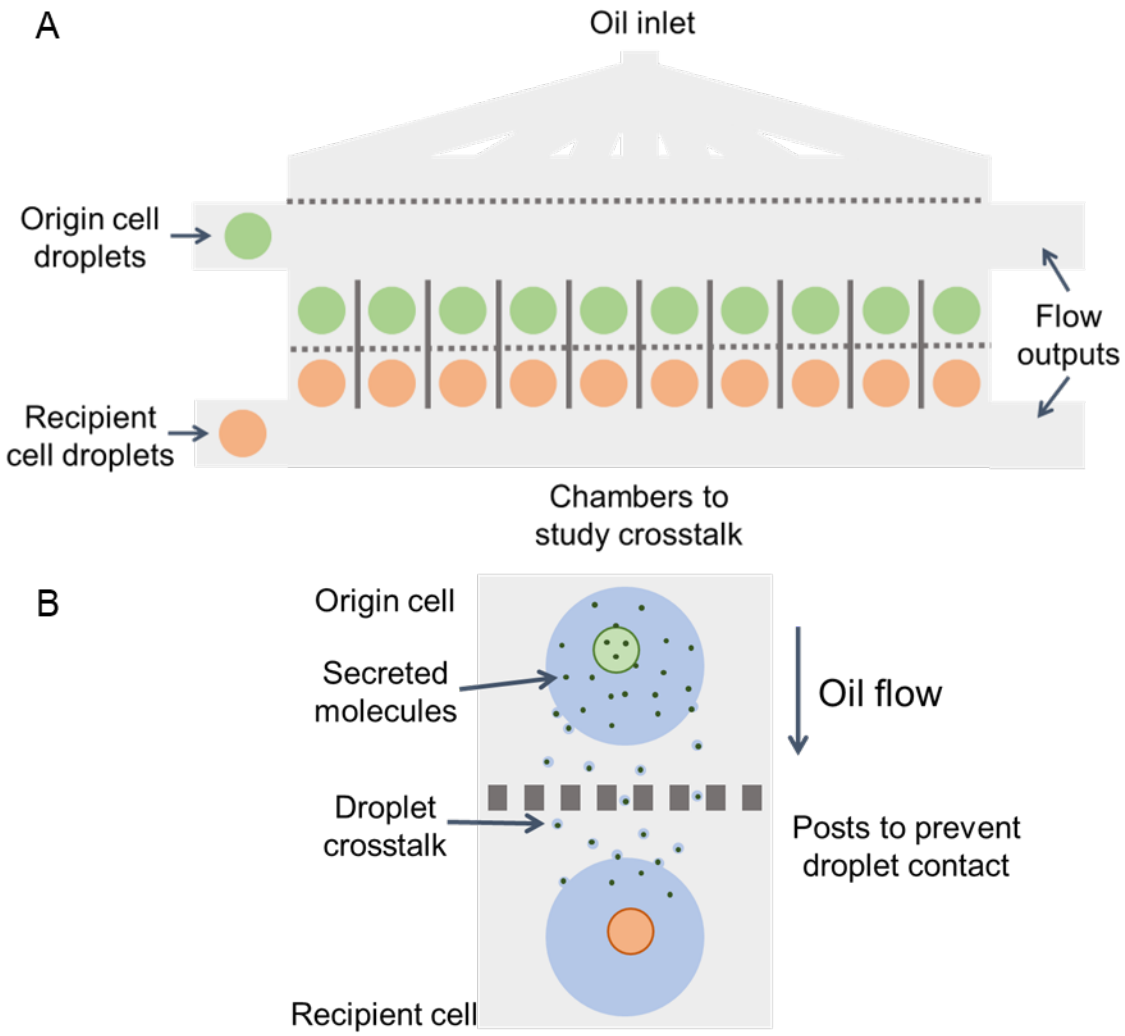

Figure 4.2. Initial device design for an array to study cell-cell communication between droplets using droplet crosstalk. (A) The overall device design features two inlets to feed in the two droplet types (green = origin cell droplets; orange = recipient cell droplets), an oil inlet, and two flow outputs. Droplets will be immobilized in the chambers over time. Oil flows from the top of the device to the bottom to induce droplet crosstalk. (B) A zoomed in image of individual chambers. Oil flows from the origin cell droplet (light green) to the recipient cell droplet (orange). Secreted molecules from the origin cell (dark green dots) are encapsulated in shear-created micelles due to oil flow and merge with the recipient cell droplet. Responses from the recipient cell could then be observed through imaging.

4.3 FADS-MNase workflow development and characterization

The organization of nucleosomes throughout the genome reveals insights into how genes are regulated in response to stimuli. MNase-seq analysis of large cell samples reveals the predominant nucleosome positioning in use throughout the entire cell sample, but it lacks the resolution to identify important cases of unique organization

applied within individual cells. Low-input and single-cell variants of MNase-seq have been developed to uncover fundamental differences in nucleosome organization between active and repressed chromatin regions. However, they rely on fluorescence activated cell sorting (FACS) to generate pure cell samples, which isolates cells with harsh application of voltage, which can harm cell viability and homeostasis. Chapter 3 describes our work to develop the FADS-MNase droplet microfluidic workflow, which isolates cells of interest and generates mono-nucleosomal fragments from output populations at a single-cell level. Fluorescence activated droplet sorting, or FADS, is a droplet microfluidic alternative to FACS that incorporates droplets to reduce the forces experienced by cells during the sorting process and maintain homeostasis. Our FADS system was validated for its ability and accuracy in sorting out cells of interest in output droplets. A previously published, MNase digestion device was expanded to facilitate processing of a wider variety of cell types as well as pre-made droplets.[134] The cohesive operation of the two devices in series was assessed.

I set up a FADS system that could be imaged and operated simultaneously to allow for troubleshooting during experiments. This system was validated for its ability to divert individual droplets in response to a variety of fluorescence signals. It was shown that droplets could be diverted following fluorescence emission detected from contained *Schizosaccharomyces pombe* (*S. pombe*) cells. To mimic the isolation of epigenetic subpopulations, I processed pre-prepared mixtures of fluorescent and nonfluorescent *S. pombe* cells and studied the purity of the outputs. Quantitative polymerase chain reaction (qPCR) analysis revealed successful enrichment of fluorescent cells in the droplets from the Sort output. Unfortunately, a small response was observed for non-

fluorescent cells in the Sort output. I believe multiple cell occupancy within droplets due to Poisson statistics and droplet merging are the source of this false positive signal. Further work is needed to attempt reducing droplet volume and decreasing cell concentrations to see if those changes could mitigate the presence of non-fluorescent cells in the Sort output. The main difficulty of those changes is that they will increase the device operation time needed to generate enough droplets from the Sort output to reliably recover cells for analysis. Currently, device operation time is extensive, so investment in changes to increase the throughput should be explored. Another change that would help decrease any false positive droplet sorting events would be the incorporation of a “bias oil” that further prevents droplets from entering the Sort output stochastically.[165] Random diversion of empty droplets is rarely observed during video imaging, so it remains to be seen whether this addition would benefit the method.

The original MNase digestion device automated multiple steps of the MNase protocol, from encapsulation of cells with lytic and digestion components to perform a consolidated incubation step to quenching of the reaction by injecting droplets with EDTA. Cells are essentially processed at the single-cell level and the entirety of the DNA fragment generation protocol is completed automatically. However, the MNase device requires pure cell samples as input and is limited to the analysis of human cell lines. Thus, we adapted the design and reagent compositions to expand its utility. First, the inlet was modified to facilitate processing of pre-prepared droplets. Droplets were inputted, spaced out, and injected with the lytic and digestion cocktail to start the lysis and digestion step that occurred within the delay channels. To expand the cell types that could be processed through the device, we incorporated zymolyase to digest cell

walls present on cells simultaneously with the automated lysis and digestion step. Removal of the cell wall for yeast and bacterial cell profiling is typically performed as a separate, sample preparation step in microfluidic assays, so incorporation to the MNase device allows us to process these cell types directly from other droplet isolation methods. Cells are fully processed down to DNA fragments in approximately half the time required for benchtop and other microfluidic techniques due to the elimination of sample preparation steps between each individual reaction. Application of the modified MNase digestion module to *S. pombe* cells resulted in successful production of mononucleosome-length DNA fragments, as shown through Bioanalyzer analysis. The device was also successfully used in combination with FADS to generate DNA fragments from droplet samples enriched for fluorescent *S. pombe* cells. These modifications position the MNase digestion module for an expanded set of sample inputs and incorporation into other droplet microfluidic workflows to customize sample processing.

4.3.1 Future Directions for FADS-MNase

Overall, the FADS-MNase droplet workflow has successfully been tested with proof-of concept experiments and is ready to move forward with real experimentation. The workflow is well-positioned to isolate and profile epigenetic subpopulations, that is, cellular populations that express a fluorescent protein as a function of epigenetic regulation. FADS's ability to separate cells into epigenetic subpopulations could initially be assessed through reverse transcription and qPCR (RT-qPCR) analysis of outputs, where the expression level of a fluorescent reporter gene ("ON" state) and surrounding genes could be quantified. Ideally, MNase processing of these samples will support RT-

qPCR results by showing a higher number of DNA fragments collected for the non-sorted or “OFF” output, consistent with higher nucleosome occupancy along the fluorescent reporter gene, preventing its active transcription. Assessment of other genes surrounding the fluorescent reporter gene should reveal higher expression levels of transcripts for genes lacking high nucleosome occupancy. Following initial validation, more interesting research questions can be investigated. Of particular interest to me would be studying the resolution of nucleosome positioning as a regulation method within gene regions. It has been shown in *Saccharomyces cerevisiae* that pairs of co-regulated genes exist—where one gene is transcriptionally enriched, the adjacent gene is as well.[165] FADS-MNase offers a platform to pair transcriptional data, from RT-qPCR analysis following FADS, with epigenetic nucleosome positioning maps, produced via the MNase digestion device, to begin articulating the precision of epigenetic control among adjacent and distal genes along a chromosome.

4.4 Broader impacts of the dissertation

This dissertation demonstrates the potential of modular, droplet microfluidic device workflows to automate the single-cell isolation and processing steps for high-throughput, cellular heterogeneity assays. The CellMag-CARWash and FADS-MNase droplet workflows were developed, characterized, and applied in proof-of-concept applications. These workflows are comprised of “plug-and-play” devices that focus on singular assay portions. The combination of multiple devices allows users to automate multiple protocol steps to limit sample handling without over-complicating device design and operation. Logistical challenges, such as ensuring cohesion throughout the workflow and limiting sample loss during device transfers, are inherent in developing

modular workflows.[166] However, the ability to substitute in different modules achieves a customizable platform that gives users more control over sample processing. Overall, this work has expanded the utility of several droplet microfluidic modules to be applied individually or in series to isolate cells of interest from complex samples and automatically process them to study cellular heterogeneity in multiple biological applications.

These workflows made major strides toward full automation of single-cell assay protocols. While automation of the analysis step was outside the scope of this work, further adjustments to device reagent compositions could enable combination of these technologies with next generation sequencing (NGS) analysis. NGS analysis is an unbiased, high-throughput method that has revolutionized epigenomic and transcriptomic assays.[32] Single-cell sequencing of total mRNA molecules (scRNA-seq)[167] and chromatin accessible DNA regions (scATAC-seq)[136] have been accomplished using microfluidic technologies by isolating single cells with unique barcode beads and appropriate reagents inside droplets using 10X Genomics's Chromium platform technology. However, these techniques still require pre-isolation of cell samples or must spend bioinformatics resources to remove unwanted cells from sequencing results. CellMag-CARWash has been demonstrated for single-cell isolation from complex mixtures; plus, we incorporated single-cell level treatments into the resulting droplets during device operation. This feature could be leveraged to inject scRNA-seq or scATAC-seq reagent components into resulting single-cell droplets, achieving a fully automated, high-throughput technology to study cellular heterogeneity within the transcriptome or epigenome. CellMag-CARWash paired with sequencing

would expand the types of cell samples that could be studied with scRNA-seq or scATAC-seq while maximizing the information collected from cells of interest.

The technologies developed through this dissertation could also benefit sample processing workflows employed in clinical applications. Patient samples are composed of complicated cell mixtures and the exact number of cells obtained is unknown, so scalable, single-cell technologies that can physically isolate cells while accommodating a flexible input are desirable. Additionally, patient samples are difficult to obtain, so all cells present are of interest for study, regardless of cell type. Most microfluidic tools advertise their ability to scale down reactions to small cell numbers. However, this strength is commonly tarnished by an upper limit to the number of cells that can be processed through each device. Integrated fluid circuits[168] and the DEPArray,[53] specifically, are limited to processing < 384 or < 30,000 single cells based on the respective size of their arrays, so multiple devices are needed to process entire patient samples at the single-cell level (~1 million cells).[169] The droplet microfluidic tools described in this dissertation can easily scale to larger sample sizes while maintaining single-cell level processing. They maintain automated sample processing while accepting varying cell input sizes by simply modulating the number of droplets generated. The MNase device, specifically, has already been demonstrated to cover three orders of magnitude of cell input numbers.[134] Incorporation of unique barcodes into the reagents injected into single-cell droplets as they pass through the device would enable production of single-cell nucleosome positioning libraries from patient samples. This input independence paves the way for incorporation of these devices into clinical sample processing workflows.

Modular, droplet microfluidic workflows provide high-throughput avenues to perform all portions of cellular assays automatically, reducing hands-on processing while maintaining simple and robust device operation. The CellMag-CARWash and FADS-MNase workflows are comprised of individual devices that can be substituted and rearranged to achieve customized sample processing. Further integration with single-cell NGS analysis would widely expand the impact of these devices, since NGS analysis matches the high-throughput nature of the workflows. Additionally, these modules are input independent and can scale to larger numbers of cells, which would translate well to processing and analyzing clinical, patient samples. These many beneficial characteristics position the devices and workflows described herein to be further applied to help researchers study the diversity of cellular responses to new experiences.

Appendices

Appendix A: Droplet Generator Device Schematics

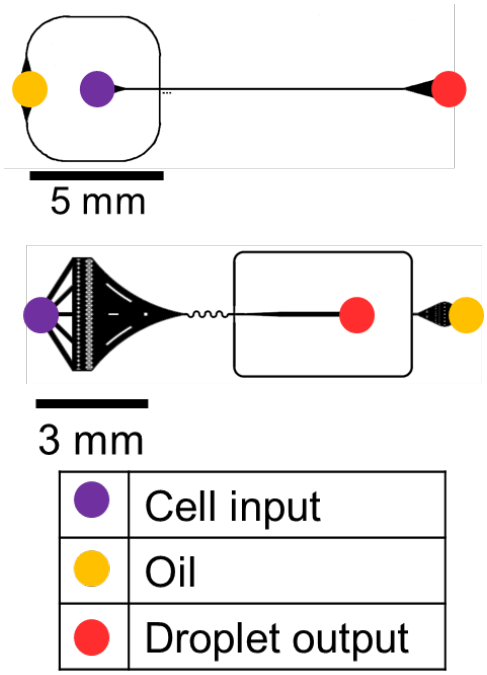

Appendix Figure A.1 Schematics for droplet generator devices used in these projects. The top device was used to generate droplets for the CellMag-CARWash project, and the bottom device was used to produce droplets for the FADS-MNase project. Cell input, oil input, and droplet outputs are labeled with colored dots.

Appendix B: Device Schematics Involved in Optimization of the CellMag-CARWash Droplet Microfluidic Workflow

The figures included in this appendix represent previous iterations for the devices used in Chapter 2. Specific design changes are explained in figure captions to explain why further iterations and the eventual final design were used.

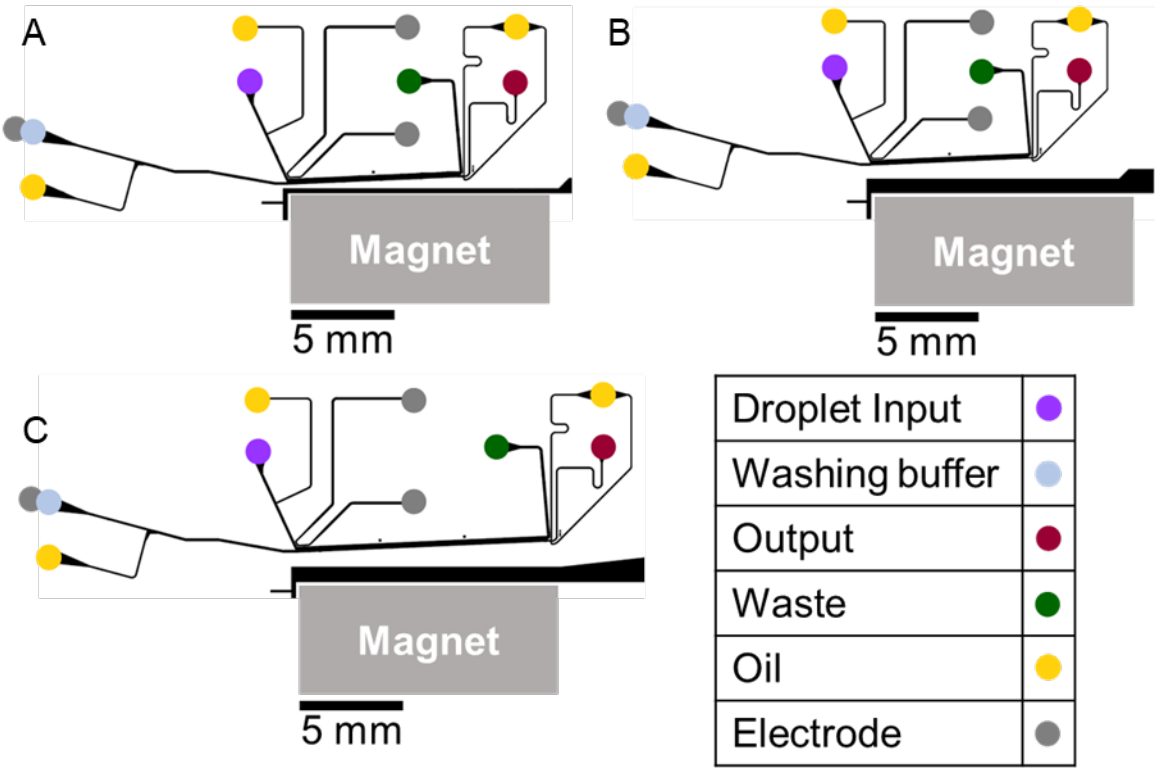

Appendix Figure B.1. Schematics for previous iterations of the CellMag-CARWash device. (A) Initial extension of the washing chamber to accommodate smaller magnetic bead sizes. This design was created by Dr. S.R. Doonan, a previous member of the Bailey Lab to wash Dynabeads. (B) Same as A, but the magnet is placed 1 mm farther from the washing channel. The distanced magnet position was incorporated to enable potential interactions with the washing buffer. (C) Same as B, but the washing

chamber was extended 1.5X. The distanced magnet position still offers potential for interactions with the washing buffer, but the longer channel accounts for the longer time needed to divert cells across the streamlines due to their increased size. C was initially observed to recover high numbers of cells through video imaging, but offline measurements of cell recovery later revealed poor reproducibility. Thus, the magnet was moved back closer to the washing channel (as in A) to increase the magnetic force experienced by cells and improve recovery. This final design was used for the experiments in Chapter 2. The various inputs are labeled with colored dots shown in the table.

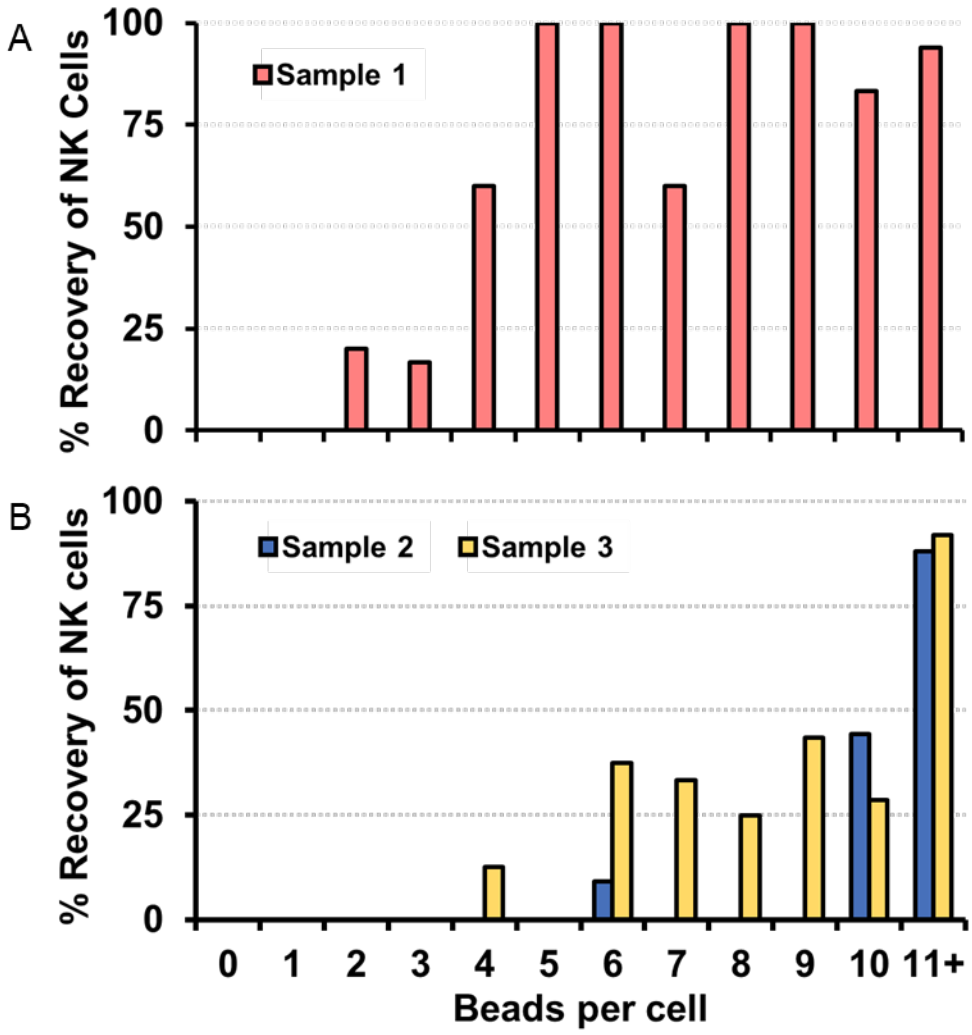

Appendix Figure B.2. Percentage of cells recovered from processing with the chosen CellMag-CARWash design (Figure B.1C) as a function of the number of beads attached per cell. (A) shows an initial sample result, indicating promising levels of recovery. However, subsequent processing of two additional samples (B) revealed poor reproducibility in recovering cells. Thus, the decision was made to bring the magnet closer to the washing channel in the final design used in Chapter 2.

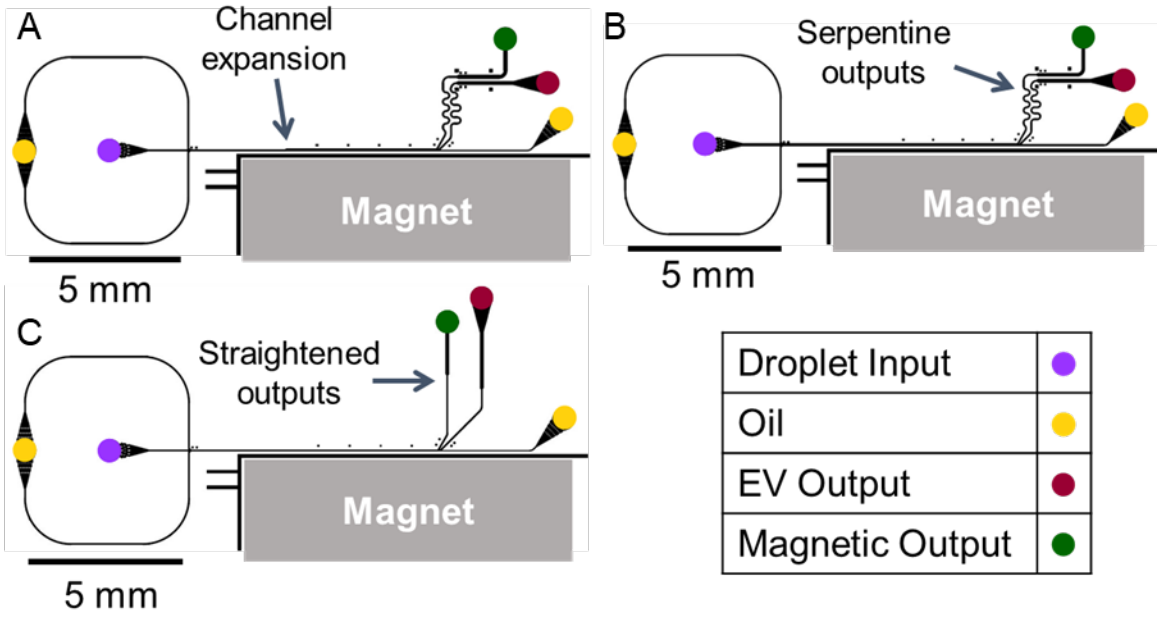

Appendix Figure B.3. Representative schematics of major feature changes in previous iterations of the magnetic splitter device. (A) The initial design featured a channel expansion after the droplet spacer and serpentine outputs that were useful for mixing droplet contents to ensure equal distribution. (B) The channel expansion was removed, since it did not add to the function of the device. (C) The serpentine outputs were removed to improve device robustness in processing fibers that entered samples. Each design iteration featured designs with different channel widths to facilitate processing of different droplet volumes, and the final design used in Chapter 2 possessed wider channels compared to (C) due to its appropriateness for processing the ~200 pL droplets from CellMag-CARWash while minimizing blockage by fibers at the splitting junction. Various inputs and outputs are indicated with colored dots.

Appendix C: No Cell Control Troubleshooting Data

The following data was produced by preliminary Mi-Seq analysis of selected samples to determine whether the presence of nucleic acid peaks in the Bioanalyzer traces were of concern. It was determined based on the extremely low percentage of reads aligned to the *S. pombe* genome and distinct GC content of the No Cell controls that they could be filtered out if the FADS-MNase project ever reached sequencing analysis.

Appendix Table C.1. Averaged Percentage of Reads Aligned to S. pombe genome for various sample types. No Cell controls consistently exhibit <0.2% reads aligned to the genome, indicating the majority of DNA present in these samples is a contaminant. Since it is not changed with fresh buffers, the initial buffers are assumed to not be the source of contamination. Interestingly, the droplet processed samples exhibit a higher percentage of aligned reads for the 10 min incubation time than bulk, indicating improved reaction efficiency in the droplet processing context.

Processing type	Incubation Length	Average Percentage of Reads Aligned
Bulk	10 min	68 ± 4
No Cell	10 min	0.18 ± 0.03
Microfluidic	10 min	75 ± 3
Bulk	20 min	92 ± 1
No Cell	20 min	0.15 ± 0.03
Fresh Buffers – Bulk	20 min	82 ± 1
Fresh Buffers – No Cell	20 min	0.15 ± 0.03

Appendix Table C.2. Averaged GC content for various sample types. All cell-containing samples exhibit two peaks of GC content prevalence, one around 40% and one around 62%. The latter matches the prominent peak present within all No Cell controls.

Processing type	Incubation Length	Mean GC Content Peak 1	Mean GC Content Peak 2
Bulk	10 min	37 ± 0	62 ± 0
No Cell	10 min	63 ± 1	N/A
Microfluidic	10 min	39 ± 0	65 ± 0
Bulk	20 min	39.8 ± 0.4	67 ± 2
No Cell	20 min	63 ± 3	N/A
Fresh Buffers – Bulk	20 min	42 ± 2	69 ± 0
Fresh Buffers – No Cell	20 min	64.5 ± 0.7	N/A

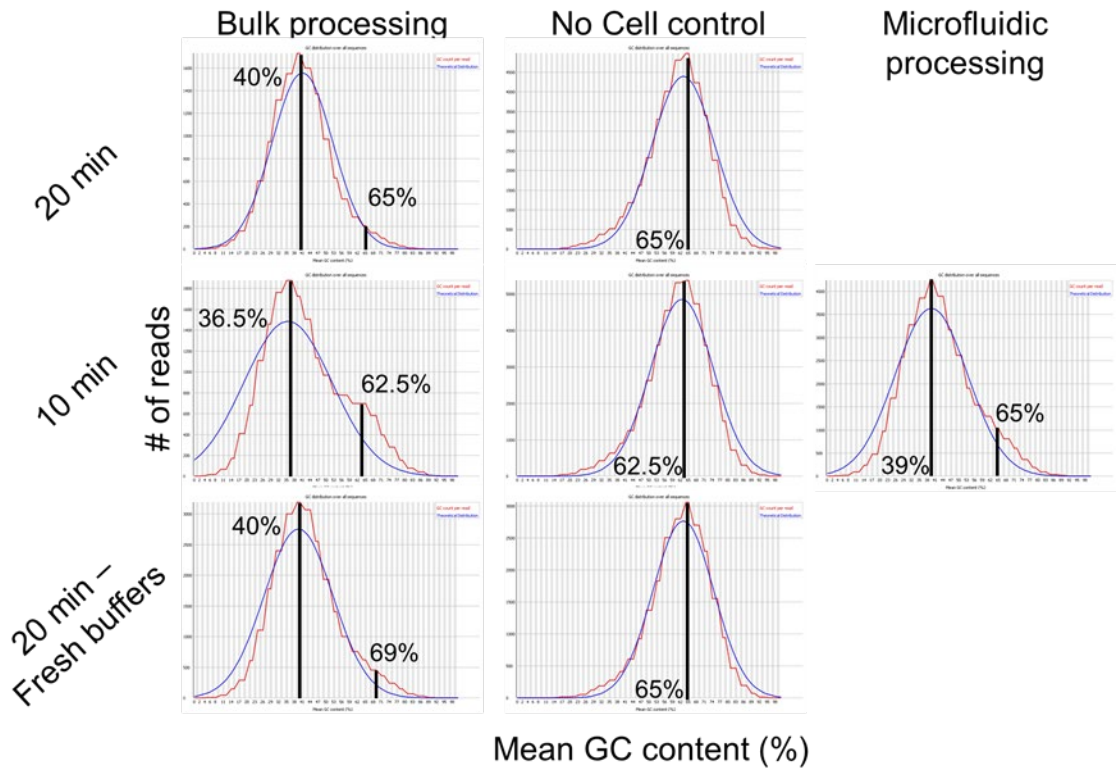

Appendix Figure C.1. Representative graphs showing mean GC content of sequenced samples. Peak locations are indicated with black lines and labels. Cell containing samples exhibited 2 peaks of GC content prevalence, indicating multiple species of DNA present. The higher GC containing shoulder peaks aligned well with the location of the No Cell control peaks. The prevalence of the shoulder peak decreases with incubation time and microfluidic processing. Note that the # of reads axes do not match – data was considered qualitatively for the prominent peak GC contents.

Bibliography

(1) Elsasser, W. M. Outline of a Theory of Cellular Heterogeneity. *Proceedings of the National Academy of Sciences* **1984**, *81* (16), 5126–5129. https://doi.org/10.1073/pnas.81.16.5126.

(2) Rubin, H. Early Origin and Pervasiveness of Cellular Heterogeneity in Some Malignant Transformationsli. *Proc Natl Acad Sci U S A* **1984**, *81*, 5121–5125.

(3) Liu, Y.; Jeraldo, P.; Jang, J. S.; Eckloff, B.; Jen, J.; Walther-Antonio, M. Bacterial Single Cell Whole Transcriptome Amplification in Microfluidic Platform Shows Putative Gene Expression Heterogeneity. *Anal Chem* **2019**, *91* (13), 8036–8044. https://doi.org/10.1021/acs.analchem.8b04773.

(4) Lai, B.; Gao, W.; Cui, K.; Xie, W.; Tang, Q.; Jin, W.; Hu, G.; Ni, B.; Zhao, K. Principles of Nucleosome Organization Revealed by Single-Cell Micrococcal Nuclease Sequencing. *Nature* **2018**, *562* (7726), 281–285. https://doi.org/10.1038/s41586-018-0567-3.

(5) Nguyen, Q. H.; Lukowski, S. W.; Chiu, H. S.; Senabouth, A.; Bruxner, T. J. C.; Christ, A. N.; Palpant, N. J.; Powell, J. E. Single-Cell RNA-Seq of Human Induced Pluripotent Stem Cells Reveals Cellular Heterogeneity and Cell State Transitions between Subpopulations. *Genome Res* **2018**, *28* (7), 1053–1066. https://doi.org/10.1101/gr.223925.117.

(6) Slack, M. D.; Martinez, E. D.; Wu, L. F.; Altschuler, S. J. Characterizing Heterogeneous Cellular Responses to Perturbations. *Proceedings of the National*

Academy of Sciences **2008**, *105* (49), 19306–19311. https://doi.org/10.1073/pnas.0807038105.

(7) Kim, E.; Kim, J.-Y.; Smith, M. A.; Haura, E. B.; Anderson, A. R. A. Cell Signaling Heterogeneity Is Modulated by Both Cell-Intrinsic and -Extrinsic Mechanisms: An Integrated Approach to Understanding Targeted Therapy. *PLoS Biol* **2018**, *16* (3), e2002930. https://doi.org/10.1371/journal.pbio.2002930.

(8) Alizadeh, A. A.; Aranda, V.; Bardelli, A.; Blanpain, C.; Bock, C.; Borowski, C.; Caldas, C.; Califano, A.; Doherty, M.; Elsner, M.; Esteller, M.; Fitzgerald, R.; Korbel, J. O.; Lichter, P.; Mason, C. E.; Navin, N.; Pe'er, D.; Polyak, K.; Roberts, C. W. M.; Siu, L.; Snyder, A.; Stower, H.; Swanton, C.; Verhaak, R. G. W.; Zenklusen, J. C.; Zuber, J.; Zucman-Rossi, J. Toward Understanding and Exploiting Tumor Heterogeneity. *Nat Med* **2015**, *21* (8), 846–853. https://doi.org/10.1038/nm.3915.

(9) Khare, K.; Pandey, R. Cellular Heterogeneity in Disease Severity and Clinical Outcome: Granular Understanding of Immune Response Is Key. *Front Immunol* **2022**, *13*. https://doi.org/10.3389/fimmu.2022.973070.

(10) Altschuler, S. J.; Wu, L. F. Cellular Heterogeneity: Do Differences Make a Difference? *Cell* **2010**, *141* (4), 559–563. https://doi.org/10.1016/j.cell.2010.04.033.

(11) Carter, B.; Zhao, K. The Epigenetic Basis of Cellular Heterogeneity. *Nat Rev Genet* **2021**, *22* (4), 235–250. https://doi.org/10.1038/s41576-020-00300-0.

(12) Stewart, C. A.; Gay, C. M.; Xi, Y.; Sivajothi, S.; Sivakamasundari, V.; Fujimoto, J.; Bolisetty, M.; Hartsfield, P. M.; Balasubramaniyan, V.; Chalishazar, M. D.; Moran,

C.; Kalhor, N.; Stewart, J.; Tran, H.; Swisher, S. G.; Roth, J. A.; Zhang, J.; de Groot, J.; Glisson, B.; Oliver, T. G.; Heymach, J. V; Wistuba, I.; Robson, P.; Wang, J.; Byers, L. A. Single-Cell Analyses Reveal Increased Intratumoral Heterogeneity after the Onset of Therapy Resistance in Small-Cell Lung Cancer. *Nat Cancer* **2020**, *1* (4), 423–436. https://doi.org/10.1038/s43018-019-0020-z.

(13) Ferrell, J. E.; Machleder, E. M. The Biochemical Basis of an All-or-None Cell Fate Switch in *Xenopus* Oocytes. *Science (1979)* **1998**, *280* (5365), 895–898. https://doi.org/10.1126/science.280.5365.895.

(14) Hwang, B.; Lee, J. H.; Bang, D. Single-Cell RNA Sequencing Technologies and Bioinformatics Pipelines. *Exp Mol Med* **2018**, *50* (8), 1–14. https://doi.org/10.1038/s12276-018-0071-8.

(15) Yilmaz, S.; Singh, A. K. Single Cell Genome Sequencing. *Curr Opin Biotechnol* **2012**, *23* (3), 437–443. https://doi.org/10.1016/j.copbio.2011.11.018.

(16) Fröhlich, J.; König, H. Rapid Isolation of Single Microbial Cells from Mixed Natural and Laboratory Populations with the Aid of a Micromanipulator. *Syst Appl Microbiol* **1999**, *22* (2), 249–257. https://doi.org/10.1016/S0723-2020(99)80072-1.

(17) SKERMAN, V. B. D. A New Type of Micromanipulator and Microforge. *J Gen Microbiol* **1968**, *54* (2), 287–297. https://doi.org/10.1099/00221287-54-2-287.

(18) Espina, V.; Milia, J.; Wu, G.; Cowherd, S.; Liotta, L. A. Laser Capture Microdissection; 2006; pp 213–229. https://doi.org/10.1007/978-1-59259-993-6_10.

(19) Navin, N.; Hicks, J. Future Medical Applications of Single-Cell Sequencing in Cancer. *Genome Med* **2011**, *3* (5), 31. https://doi.org/10.1186/gm247.

(20) Hulett, H. R.; Bonner, W. A.; Barrett, J.; Herzenberg, L. A. Cell Sorting: Automated Separation of Mammalian Cells as a Function of Intracellular Fluorescence. *Science (1979)* **1969**, *166* (3906), 747–749. https://doi.org/10.1126/science.166.3906.747.

(21) Herzenberg, L. A.; Parks, D.; Sahaf, B.; Perez, O.; Roederer, M.; Herzenberg, L. A. The History and Future of the Fluorescence Activated Cell Sorter and Flow Cytometry: A View from Stanford. *Clin Chem* **2002**, *48* (10), 1819–1827. https://doi.org/10.1093/clinchem/48.10.1819.

(22) Mirabelli, P.; Scalia, G.; Pascariello, C.; D'Alessio, F.; Mariotti, E.; Noto, R. Di; George, T. C.; Kong, R.; Venkatachalam, V.; Basiji, D.; Vecchio, L. Del. ImageStream Promyelocytic Leukemia Protein Immunolocalization: In Search of Promyelocytic Leukemia Cells. *Cytometry Part A* **2012**, *81A* (3), 232–237. https://doi.org/10.1002/cyto.a.22013.

(23) Piyasena, M. E.; Graves, S. W. The Intersection of Flow Cytometry with Microfluidics and Microfabrication. *Lab Chip* **2014**, *14* (6), 1044–1059. https://doi.org/10.1039/C3LC51152A.

(24) George, T. C.; Basiji, D. A.; Hall, B. E.; Lynch, D. H.; Ortyn, W. E.; Perry, D. J.; Seo, M. J.; Zimmerman, C. A.; Morrissey, P. J. Distinguishing Modes of Cell Death Using the ImageStream® Multispectral Imaging Flow Cytometer. *Cytometry Part A* **2004**, *59A* (2), 237–245. https://doi.org/10.1002/cyto.a.20048.

(25) Binek, A.; Rojo, D.; Godzien, J.; Rupérez, F. J.; Nuñez, V.; Jorge, I.; Ricote, M.; Vázquez, J.; Barbas, C. Flow Cytometry Has a Significant Impact on the Cellular

Metabolome. *J Proteome Res* **2018**, acs.jproteome.8b00472. https://doi.org/10.1021/acs.jproteome.8b00472.

(26) Mazutis, L.; Gilbert, J.; Ung, W. L.; Weitz, D. A.; Griffiths, A. D.; Heyman, J. A. Single-Cell Analysis and Sorting Using Droplet-Based Microfluidics. *Nat Protoc* **2013**, *8* (5), 870–891. https://doi.org/10.1038/nprot.2013.046.

(27) Miltenyi, S.; Müller, W.; Weichel, W.; Radbruch, A. High Gradient Magnetic Cell Separation with MACS. *Cytometry* **1990**, *11* (2), 231–238. https://doi.org/10.1002/cyto.990110203.

(28) Carr, C.; Espy, M.; Nath, P.; Martin, S. L.; Ward, M. D.; Martin, J. Design, Fabrication and Demonstration of a Magnetophoresis Chamber with 25 Output Fractions. *J Magn Magn Mater* **2009**, *321* (10), 1440–1445. https://doi.org/10.1016/j.jmmm.2009.02.064.

(29) Adams, J. D.; Kim, U.; Soh, H. T. Multitarget Magnetic Activated Cell Sorter. *Proceedings of the National Academy of Sciences* **2008**, *105* (47), 18165–18170. https://doi.org/10.1073/pnas.0809795105.

(30) Poli, A.; Michel, T.; Thérésine, M.; Andrès, E.; Hentges, F.; Zimmer, J. CD56bright Natural Killer (NK) Cells: An Important NK Cell Subset. *Immunology* **2009**, *126* (4), 458–465. https://doi.org/10.1111/j.1365-2567.2008.03027.x.

(31) Poznanski, S. M.; Ashkar, A. A. Shining Light on the Significance of NK Cell CD56 Brightness. *Cell Mol Immunol* **2018**, *15* (12), 1071–1073. https://doi.org/10.1038/s41423-018-0163-3.

(32) Hurd, P. J.; Nelson, C. J. Advantages of Next-Generation Sequencing versus the Microarray in Epigenetic Research. *Brief Funct Genomic Proteomic* **2009**, *8* (3), 174–183. https://doi.org/10.1093/bfgp/elp013.

(33) Chiang, M.-K.; Melton, D. A. Single-Cell Transcript Analysis of Pancreas Development. *Dev Cell* **2003**, *4* (3), 383–393. https://doi.org/10.1016/S1534-5807(03)00035-2.

(34) Kalisky, T.; Quake, S. R. Single-Cell Genomics. *Nat Methods* **2011**, *8* (4), 311–314. https://doi.org/10.1038/nmeth0411-311.

(35) Aird, D.; Ross, M. G.; Chen, W.-S.; Danielsson, M.; Fennell, T.; Russ, C.; Jaffe, D. B.; Nusbaum, C.; Gnirke, A. Analyzing and Minimizing PCR Amplification Bias in Illumina Sequencing Libraries. *Genome Biol* **2011**, *12* (2), R18. https://doi.org/10.1186/gb-2011-12-2-r18.

(36) Barba, M.; Czosnek, H.; Hadidi, A. Historical Perspective, Development and Applications of Next-Generation Sequencing in Plant Virology. *Viruses* **2014**, *6* (1), 106–136. https://doi.org/10.3390/v6010106.

(37) Reinartz, J.; Bruyns, E.; Lin, J.-Z.; Burcham, T.; Brenner, S.; Bowen, B.; Kramer, M.; Woychik, R. Massively Parallel Signature Sequencing (MPSS) as a Tool for in-Depth Quantitative Gene Expression Profiling in All Organisms. *Brief Funct Genomics* **2002**, *1* (1), 95–104. https://doi.org/10.1093/bfgp/1.1.95.

(38) Ronaghi, M.; Karamohamed, S.; Pettersson, B.; Uhlén, M.; Nyrén, P. Real-Time DNA Sequencing Using Detection of Pyrophosphate Release. *Anal Biochem* **1996**, *242* (1), 84–89. https://doi.org/10.1006/abio.1996.0432.

(39) Whitesides, G. M. The Origins and the Future of Microfluidics. *Nature* **2006**, *442* (7101), 368–373. https://doi.org/10.1038/nature05058.

(40) Shields IV, C. W.; Reyes, C. D.; López, G. P. Microfluidic Cell Sorting: A Review of the Advances in the Separation of Cells from Debulking to Rare Cell Isolation. *Lab Chip* **2015**, *15* (5), 1230–1249. https://doi.org/10.1039/C4LC01246A.

(41) Chen, Y.; Li, P.; Huang, P.-H.; Xie, Y.; Mai, J. D.; Wang, L.; Nguyen, N.-T.; Huang, T. J. Rare Cell Isolation and Analysis in Microfluidics. *Lab Chip* **2014**, *14* (4), 626. https://doi.org/10.1039/c3lc90136j.

(42) McFaul, S. M.; Lin, B. K.; Ma, H. Cell Separation Based on Size and Deformability Using Microfluidic Funnel Ratchets. *Lab Chip* **2012**, *12* (13), 2369. https://doi.org/10.1039/c2lc21045b.

(43) Inglis, D. W.; Davis, J. A.; Austin, R. H.; Sturm, J. C. Critical Particle Size for Fractionation by Deterministic Lateral Displacement. *Lab Chip* **2006**, *6* (5), 655. https://doi.org/10.1039/b515371a.

(44) Kuntaegowdanahalli, S. S.; Bhagat, A. A. S.; Kumar, G.; Papautsky, I. Inertial Microfluidics for Continuous Particle Separation in Spiral Microchannels. *Lab Chip* **2009**, *9* (20), 2973. https://doi.org/10.1039/b908271a.

(45) Di Carlo, D. Inertial Microfluidics. *Lab Chip* **2009**, *9* (21), 3038. https://doi.org/10.1039/b912547g.

(46) Di Carlo, D.; Irimia, D.; Tompkins, R. G.; Toner, M. Continuous Inertial Focusing, Ordering, and Separation of Particles in Microchannels. *Proceedings of the National Academy of Sciences* **2007**, *104* (48), 18892–18897. https://doi.org/10.1073/pnas.0704958104.

(47) Lin, E.; Rivera-Báez, L.; Fouladdel, S.; Yoon, H. J.; Guthrie, S.; Wieger, J.; Deol, Y.; Keller, E.; Sahai, V.; Simeone, D. M.; Burness, M. L.; Azizi, E.; Wicha, M. S.; Nagrath, S. High-Throughput Microfluidic Labyrinth for the Label-Free Isolation of Circulating Tumor Cells. *Cell Syst* **2017**, *5* (3), 295-304.e4. https://doi.org/10.1016/j.cels.2017.08.012.

(48) Choi, S.; Karp, J. M.; Karnik, R. Cell Sorting by Deterministic Cell Rolling. *Lab Chip* **2012**, *12* (8), 1427. https://doi.org/10.1039/c2lc21225k.

(49) Nagrath, S.; Sequist, L. V.; Maheswaran, S.; Bell, D. W.; Irimia, D.; Ulkus, L.; Smith, M. R.; Kwak, E. L.; Digumarthy, S.; Muzikansky, A.; Ryan, P.; Balis, U. J.; Tompkins, R. G.; Haber, D. A.; Toner, M. Isolation of Rare Circulating Tumour Cells in Cancer Patients by Microchip Technology. *Nature* **2007**, *450* (7173), 1235–1239. https://doi.org/10.1038/nature06385.

(50) Yoon, H. J.; Kim, T. H.; Zhang, Z.; Azizi, E.; Pham, T. M.; Paoletti, C.; Lin, J.; Ramnath, N.; Wicha, M. S.; Hayes, D. F.; Simeone, D. M.; Nagrath, S. Sensitive Capture of Circulating Tumour Cells by Functionalized Graphene Oxide Nanosheets. *Nat Nanotechnol* **2013**, *8* (10), 735–741. https://doi.org/10.1038/nnano.2013.194.

(51) Zhao, W.; Cui, C. H.; Bose, S.; Guo, D.; Shen, C.; Wong, W. P.; Halvorsen, K.; Farokhzad, O. C.; Teo, G. S. L.; Phillips, J. A.; Dorfman, D. M.; Karnik, R.; Karp, J. M. Bioinspired Multivalent DNA Network for Capture and Release of Cells. *Proceedings of the National Academy of Sciences* **2012**, *109* (48), 19626–19631. https://doi.org/10.1073/pnas.1211234109.

(52) Wang, L.; Flanagan, L. A.; Jeon, N. L.; Monuki, E.; Lee, A. P. Dielectrophoresis Switching with Vertical Sidewall Electrodes for Microfluidic Flow Cytometry. *Lab Chip* **2007**, *7* (9), 1114. https://doi.org/10.1039/b705386j.

(53) Di Trapani, M.; Manaresi, N.; Medoro, G. DEPArray™ System: An Automatic Image-based Sorter for Isolation of Pure Circulating Tumor Cells. *Cytometry Part A* **2018**, *93* (12), 1260–1266. https://doi.org/10.1002/cyto.a.23687.

(54) Cao, Z.; Chen, C.; He, B.; Tan, K.; Lu, C. A Microfluidic Device for Epigenomic Profiling Using 100 Cells. *Nat Methods* **2015**, *12* (10), 959–962. https://doi.org/10.1038/nmeth.3488.

(55) Cedillo-Alcantar, D. F.; Rodriguez-Moncayo, R.; Maravillas-Montero, J. L.; Garcia-Cordero, J. L. On-Chip Analysis of Protein Secretion from Single Cells Using Microbead Biosensors. *ACS Sens* **2023**, *8* (2), 655–664. https://doi.org/10.1021/acssensors.2c02148.

(56) Xia, N.; Hunt, T. P.; Mayers, B. T.; Alsberg, E.; Whitesides, G. M.; Westervelt, R. M.; Ingber, D. E. Combined Microfluidic-Micromagnetic Separation of Living Cells in Continuous Flow. *Biomed Microdevices* **2006**, *8* (4), 299–308. https://doi.org/10.1007/s10544-006-0033-0.

(57) Lagus, T. P.; Edd, J. F. A Review of the Theory, Methods and Recent Applications of High-Throughput Single-Cell Droplet Microfluidics. *J Phys D Appl Phys* **2013**, *46* (11), 114005. https://doi.org/10.1088/0022-3727/46/11/114005.

(58) Wang, J.; Wang, J.; Feng, L.; Lin, T. Fluid Mixing in Droplet-Based Microfluidics with a Serpentine Microchannel. *RSC Adv* **2015**, *5* (126), 104138–104144. https://doi.org/10.1039/C5RA21181F.

(59) Bringer, M. R.; Gerdts, C. J.; Song, H.; Tice, J. D.; Ismagilov, R. F. Microfluidic Systems for Chemical Kinetics That Rely on Chaotic Mixing in Droplets. *Philosophical Transactions of the Royal Society of London. Series A: Mathematical, Physical and Engineering Sciences* **2004**, *362* (1818), 1087–1104. https://doi.org/10.1098/rsta.2003.1364.

(60) Abate, A. R.; Hung, T.; Mary, P.; Agresti, J. J.; Weitz, D. A. High-Throughput Injection with Microfluidics Using Picoinjectors. *Proceedings of the National Academy of Sciences* **2010**, *107* (45), 19163–19166. https://doi.org/10.1073/pnas.1006888107.

(61) Doonan, S. R.; Bailey, R. C. K-Channel: A Multifunctional Architecture for Dynamically Reconfigurable Sample Processing in Droplet Microfluidics. *Anal Chem* **2017**, *89* (7), 4091–4099. https://doi.org/10.1021/acs.analchem.6b05041.

(62) Doonan, S. R.; Lin, M.; Bailey, R. C. Droplet CAR-Wash: Continuous Picoliter-Scale Immunocapture and Washing. *Lab Chip* **2019**, *19* (9), 1589–1598. https://doi.org/10.1039/C9LC00125E.

(63) Baret, J.-C.; Miller, O. J.; Taly, V.; Ryckelynck, M.; El-Harrak, A.; Frenz, L.; Rick, C.; Samuels, M. L.; Hutchison, J. B.; Agresti, J. J.; Link, D. R.; Weitz, D. A.; Griffiths, A. D. Fluorescence-Activated Droplet Sorting (FADS): Efficient Microfluidic Cell Sorting Based on Enzymatic Activity. *Lab Chip* **2009**, *9* (13), 1850. https://doi.org/10.1039/b902504a.

(64) Holland-Moritz, D. A.; Wismer, M. K.; Mann, B. F.; Farasat, I.; Devine, P.; Guetschow, E. D.; Mangion, I.; Welch, C. J.; Moore, J. C.; Sun, S.; Kennedy, R. T. Mass Activated Droplet Sorting (MADS) Enables High-Throughput Screening of

Enzymatic Reactions at Nanoliter Scale. *Angewandte Chemie International Edition* **2020**, *59* (11), 4470–4477. https://doi.org/10.1002/anie.201913203.

(65) Tang, F.; Barbacioru, C.; Wang, Y.; Nordman, E.; Lee, C.; Xu, N.; Wang, X.; Bodeau, J.; Tuch, B. B.; Siddiqui, A.; Lao, K.; Surani, M. A. MRNA-Seq Whole-Transcriptome Analysis of a Single Cell. *Nat Methods* **2009**, *6* (5), 377–382. https://doi.org/10.1038/nmeth.1315.

(66) Lareau, C. A.; Duarte, F. M.; Chew, J. G.; Kartha, V. K.; Burkett, Z. D.; Kohlway, A. S.; Pokholok, D.; Aryee, M. J.; Steemers, F. J.; Lebofsky, R.; Buenrostro, J. D. Droplet-Based Combinatorial Indexing for Massive-Scale Single-Cell Chromatin Accessibility. *Nat Biotechnol* **2019**, *37* (8), 916–924. https://doi.org/10.1038/s41587-019-0147-6.

(67) Macosko, E. Z.; Basu, A.; Satija, R.; Nemesh, J.; Shekhar, K.; Goldman, M.; Tirosh, I.; Bialas, A. R.; Kamitaki, N.; Martersteck, E. M.; Trombetta, J. J.; Weitz, D. A.; Sanes, J. R.; Shalek, A. K.; Regev, A.; McCarroll, S. A. Highly Parallel Genome-Wide Expression Profiling of Individual Cells Using Nanoliter Droplets. *Cell* **2015**, *161* (5), 1202–1214. https://doi.org/10.1016/j.cell.2015.05.002.

(68) Radhakrishnan, K.; Halász, Á.; Vlachos, D.; Edwards, J. S. Quantitative Understanding of Cell Signaling: The Importance of Membrane Organization. *Curr Opin Biotechnol* **2010**, *21* (5), 677–682. https://doi.org/https://doi.org/10.1016/j.copbio.2010.08.006.

(69) Armingol, E.; Officer, A.; Harismendy, O.; Lewis, N. E. Deciphering Cell–Cell Interactions and Communication from Gene Expression. *Nat Rev Genet* **2021**, *22* (2), 71–88. https://doi.org/10.1038/s41576-020-00292-x.

(70) van Niel, G.; D'Angelo, G.; Raposo, G. Shedding Light on the Cell Biology of Extracellular Vesicles. *Nat Rev Mol Cell Biol* **2018**, *19* (4), 213–228. https://doi.org/10.1038/nrm.2017.125.

(71) Doyle, L.; Wang, M. Overview of Extracellular Vesicles, Their Origin, Composition, Purpose, and Methods for Exosome Isolation and Analysis. *Cells* **2019**, *8* (7), 727. https://doi.org/10.3390/cells8070727.

(72) Hattori, K.; Goda, Y.; Yamashita, M.; Yoshioka, Y.; Kojima, R.; Ota, S. Droplet Array-Based Platform for Parallel Optical Analysis of Dynamic Extracellular Vesicle Secretion from Single Cells. *Anal Chem* **2022**, *94* (32), 11209–11215. https://doi.org/10.1021/acs.analchem.2c01609.

(73) Ji, Y.; Qi, D.; Li, L.; Su, H.; Li, X.; Luo, Y.; Sun, B.; Zhang, F.; Lin, B.; Liu, T.; Lu, Y. Multiplexed Profiling of Single-Cell Extracellular Vesicles Secretion. *Proceedings of the National Academy of Sciences* **2019**, *116* (13), 5979–5984. https://doi.org/10.1073/pnas.1814348116.

(74) Dechantsreiter, S.; Ambrose, A. R.; Worboys, J. D.; Lim, J. M. E.; Liu, S.; Shah, R.; Montero, M. A.; Quinn, A. M.; Hussell, T.; Tannahill, G. M.; Davis, D. M. Heterogeneity in Extracellular Vesicle Secretion by Single Human Macrophages Revealed by Super-Resolution Microscopy. *J Extracell Vesicles* **2022**, *11* (4), e12215. https://doi.org/https://doi.org/10.1002/jev2.12215.

(75) Zhang, M.; Jin, K.; Gao, L.; Zhang, Z.; Li, F.; Zhou, F.; Zhang, L. Methods and Technologies for Exosome Isolation and Characterization. *Small Methods* **2018**, *2* (9), 1800021. https://doi.org/10.1002/smtd.201800021.

(76) Muller, L.; Hong, C.-S.; Stolz, D. B.; Watkins, S. C.; Whiteside, T. L. Isolation of Biologically-Active Exosomes from Human Plasma. *J Immunol Methods* **2014**, *411*, 55–65. https://doi.org/10.1016/j.jim.2014.06.007.

(77) Nizamudeen, Z.; Markus, R.; Lodge, R.; Parmenter, C.; Platt, M.; Chakrabarti, L.; Sottile, V. Rapid and Accurate Analysis of Stem Cell-Derived Extracellular Vesicles with Super Resolution Microscopy and Live Imaging. *Biochimica et Biophysica Acta (BBA) - Molecular Cell Research* **2018**, *1865* (12), 1891–1900. https://doi.org/10.1016/j.bbamcr.2018.09.008.

(78) Colombo, F.; Norton, E. G.; Cocucci, E. Microscopy Approaches to Study Extracellular Vesicles. *Biochimica et Biophysica Acta (BBA) - General Subjects* **2021**, *1865* (4), 129752. https://doi.org/10.1016/j.bbagen.2020.129752.

(79) Liu, D.; Paczkowski, P.; Mackay, S.; Ng, C.; Zhou, J. Single-Cell Multiplexed Proteomics on the IsoLight Resolves Cellular Functional Heterogeneity to Reveal Clinical Responses of Cancer Patients to Immunotherapies; 2020; pp 413–431. https://doi.org/10.1007/978-1-4939-9773-2_19.

(80) Zhu, F.; Ji, Y.; Li, L.; Bai, X.; Liu, X.; Luo, Y.; Liu, T.; Lin, B.; Lu, Y. High-Throughput Single-Cell Extracellular Vesicle Secretion Analysis on a Desktop Scanner without Cell Counting. *Anal Chem* **2021**, *93* (39), 13152–13160. https://doi.org/10.1021/acs.analchem.1c01446.

(81) Li, P.; Kaslan, M.; Lee, S. H.; Yao, J.; Gao, Z. Progress in Exosome Isolation Techniques. *Theranostics* **2017**, *7* (3), 789–804. https://doi.org/10.7150/thno.18133.

(82) Vaidyanathan, R.; Naghibosadat, M.; Rauf, S.; Korbie, D.; Carrascosa, L. G.; Shiddiky, M. J. A.; Trau, M. Detecting Exosomes Specifically: A Multiplexed Device Based on Alternating Current Electrohydrodynamic Induced *Nanoshearing*. *Anal Chem* **2014**, *86* (22), 11125–11132. https://doi.org/10.1021/ac502082b.

(83) Buenrostro, J. D.; Wu, B.; Chang, H. Y.; Greenleaf, W. J. ATAC-seq: A Method for Assaying Chromatin Accessibility Genome-Wide. *Curr Protoc Mol Biol* **2015**, *109* (1). https://doi.org/10.1002/0471142727.mb2129s109.

(84) Pratt, B. M.; Won, H. Advances in Profiling Chromatin Architecture Shed Light on the Regulatory Dynamics Underlying Brain Disorders. *Semin Cell Dev Biol* **2022**, *121*, 153–160. https://doi.org/10.1016/j.semcdb.2021.08.013.

(85) Annunziato, A. T. *Chromosomes and Cytogenetics | Lead Editor: Clare O'Connor Chromosomes and Cytogenetics DNA Packaging: Nucleosomes and Chromatin*. Nature Education.

(86) Rothbart, S. B.; Strahl, B. D. Interpreting the Language of Histone and DNA Modifications. *Biochimica et Biophysica Acta (BBA) - Gene Regulatory Mechanisms* **2014**, *1839* (8), 627–643. https://doi.org/10.1016/j.bbagrm.2014.03.001.

(87) Soshnev, A. A.; Josefowicz, S. Z.; Allis, C. D. Greater Than the Sum of Parts: Complexity of the Dynamic Epigenome. *Mol Cell* **2016**, *62* (5), 681–694. https://doi.org/10.1016/j.molcel.2016.05.004.

(88) Simmons, D. *Epigenetic Influences and Disease*. Nature Education. https://www.nature.com/scitable/topicpage/epigenetic-influences-and-disease-895/ (accessed 2023-06-07).

(89) Samanta, S.; Rajasingh, S.; Cao, T.; Dawn, B.; Rajasingh, J. Epigenetic Dysfunctional Diseases and Therapy for Infection and Inflammation. *Biochimica et Biophysica Acta (BBA) - Molecular Basis of Disease* **2017**, *1863* (2), 518–528. https://doi.org/10.1016/j.bbadis.2016.11.030.

(90) Zhao, Z.; Shilatifard, A. Epigenetic Modifications of Histones in Cancer. *Genome Biol* **2019**, *20* (1), 245. https://doi.org/10.1186/s13059-019-1870-5.

(91) Loscalzo, J.; Handy, D. E. Epigenetic Modifications: Basic Mechanisms and Role in Cardiovascular Disease (2013 Grover Conference Series). *Pulm Circ* **2014**, *4* (2), 169–174. https://doi.org/10.1086/675979.

(92) Martínez-Iglesias, O.; Naidoo, V.; Cacabelos, N.; Cacabelos, R. Epigenetic Biomarkers as Diagnostic Tools for Neurodegenerative Disorders. *Int J Mol Sci* **2021**, *23* (1), 13. https://doi.org/10.3390/ijms23010013.

(93) Mazzone, R.; Zwergel, C.; Artico, M.; Taurone, S.; Ralli, M.; Greco, A.; Mai, A. The Emerging Role of Epigenetics in Human Autoimmune Disorders. *Clin Epigenetics* **2019**, *11* (1), 34. https://doi.org/10.1186/s13148-019-0632-2.

(94) Dirks, R. A. M.; Stunnenberg, H. G.; Marks, H. Genome-Wide Epigenomic Profiling for Biomarker Discovery. *Clin Epigenetics* **2016**, *8* (1), 122. https://doi.org/10.1186/s13148-016-0284-4.

(95) Shendure, J.; Ji, H. Next-Generation DNA Sequencing. *Nat Biotechnol* **2008**, *26* (10), 1135–1145. https://doi.org/10.1038/nbt1486.

(96) Mardis, E. R. Next-Generation DNA Sequencing Methods. *Annu Rev Genomics Hum Genet* **2008**, *9* (1), 387–402. https://doi.org/10.1146/annurev.genom.9.081307.164359.

(97) Meaburn, E.; Schulz, R. Next Generation Sequencing in Epigenetics: Insights and Challenges. *Semin Cell Dev Biol* **2012**, *23* (2), 192–199. https://doi.org/10.1016/j.semcdb.2011.10.010.

(98) Moore, L. D.; Le, T.; Fan, G. DNA Methylation and Its Basic Function. *Neuropsychopharmacology* **2013**, *38* (1), 23–38. https://doi.org/10.1038/npp.2012.112.

(99) Phillips, T. *The Role of Methylation in Gene Expression*. Nature Education. https://www.nature.com/scitable/topicpage/the-role-of-methylation-in-gene-expression-1070/ (accessed 2023-06-07).

(100) Kumar, S.; Chinnusamy, V.; Mohapatra, T. Epigenetics of Modified DNA Bases: 5-Methylcytosine and Beyond. *Front Genet* **2018**, *9*. https://doi.org/10.3389/fgene.2018.00640.

(101) Liyanage, V.; Jarmasz, J.; Murugeshan, N.; Del Bigio, M.; Rastegar, M.; Davie, J. DNA Modifications: Function and Applications in Normal and Disease States. *Biology (Basel)* **2014**, *3* (4), 670–723. https://doi.org/10.3390/biology3040670.

(102) Allfrey, V. G.; Faulkner, R.; Mirsky, A. E. ACETYLATION AND METHYLATION OF HISTONES AND THEIR POSSIBLE ROLE IN THE REGULATION OF RNA SYNTHESIS. *Proceedings of the National Academy of Sciences* **1964**, *51* (5), 786–794. https://doi.org/10.1073/pnas.51.5.786.

(103) Jenuwein, T.; Allis, C. D. Translating the Histone Code. *Science (1979)* **2001**, *293* (5532), 1074–1080. https://doi.org/10.1126/science.1063127.

(104) Bannister, A. J.; Kouzarides, T. Regulation of Chromatin by Histone Modifications. *Cell Res* **2011**, *21* (3), 381–395. https://doi.org/10.1038/cr.2011.22.

(105) Partridge, E. C.; Chhetri, S. B.; Prokop, J. W.; Ramaker, R. C.; Jansen, C. S.; Goh, S.-T.; Mackiewicz, M.; Newberry, K. M.; Brandsmeier, L. A.; Meadows, S. K.; Messer, C. L.; Hardigan, A. A.; Coppola, C. J.; Dean, E. C.; Jiang, S.; Savic, D.; Mortazavi, A.; Wold, B. J.; Myers, R. M.; Mendenhall, E. M. Occupancy Maps of 208 Chromatin-Associated Proteins in One Human Cell Type. *Nature* **2020**, *583* (7818), 720–728. https://doi.org/10.1038/s41586-020-2023-4.

(106) Lambert, S. A.; Jolma, A.; Campitelli, L. F.; Das, P. K.; Yin, Y.; Albu, M.; Chen, X.; Taipale, J.; Hughes, T. R.; Weirauch, M. T. The Human Transcription Factors. *Cell* **2018**, *172* (4), 650–665. https://doi.org/10.1016/j.cell.2018.01.029.

(107) Farnham, P. J. Insights from Genomic Profiling of Transcription Factors. *Nat Rev Genet* **2009**, *10* (9), 605–616. https://doi.org/10.1038/nrg2636.

(108) Cremer, T.; Cremer, C. Chromosome Territories, Nuclear Architecture and Gene Regulation in Mammalian Cells. *Nat Rev Genet* **2001**, *2* (4), 292–301. https://doi.org/10.1038/35066075.

(109) Cremer, T.; Cremer, M. Chromosome Territories. *Cold Spring Harb Perspect Biol* **2010**, *2* (3), a003889–a003889. https://doi.org/10.1101/cshperspect.a003889.

(110) Kadauke, S.; Blobel, G. A. Chromatin Loops in Gene Regulation. *Biochimica et Biophysica Acta (BBA) - Gene Regulatory Mechanisms* **2009**, *1789* (1), 17–25. https://doi.org/10.1016/j.bbagrm.2008.07.002.

(111) Sandelin, A.; Carninci, P.; Lenhard, B.; Ponjavic, J.; Hayashizaki, Y.; Hume, D. A. Mammalian RNA Polymerase II Core Promoters: Insights from Genome-Wide Studies. *Nat Rev Genet* **2007**, *8* (6), 424–436. https://doi.org/10.1038/nrg2026.

(112) Tsompana, M.; Buck, M. J. Chromatin Accessibility: A Window into the Genome. *Epigenetics Chromatin* **2014**, *7* (1), 33. https://doi.org/10.1186/1756-8935-7-33.

(113) Murakami, Y. Heterochromatin and Euchromatin. In *Encyclopedia of Systems Biology*; Springer New York: New York, NY, 2013; pp 881–884. https://doi.org/10.1007/978-1-4419-9863-7_1413.

(114) Schones, D. E.; Cui, K.; Cuddapah, S.; Roh, T.-Y.; Barski, A.; Wang, Z.; Wei, G.; Zhao, K. Dynamic Regulation of Nucleosome Positioning in the Human Genome. *Cell* **2008**, *132* (5), 887–898. https://doi.org/10.1016/j.cell.2008.02.022.

(115) Henikoff, J. G.; Belsky, J. A.; Krassovsky, K.; MacAlpine, D. M.; Henikoff, S. Epigenome Characterization at Single Base-Pair Resolution. *Proceedings of the National Academy of Sciences* **2011**, *108* (45), 18318–18323. https://doi.org/10.1073/pnas.1110731108.

(116) Furuyama, S.; Biggins, S. Centromere Identity Is Specified by a Single Centromeric Nucleosome in Budding Yeast. *Proceedings of the National Academy of Sciences* **2007**, *104* (37), 14706–14711. https://doi.org/10.1073/pnas.0706985104.

(117) NOLL, M. Subunit Structure of Chromatin. *Nature* **1974**, *251* (5472), 249–251. https://doi.org/10.1038/251249a0.

(118) Cook, A.; Mieczkowski, J.; Tolstorukov, M. Y. Single-Assay Profiling of Nucleosome Occupancy and Chromatin Accessibility. *Curr Protoc Mol Biol* **2017**, *120* (1). https://doi.org/10.1002/cpmb.45.

(119) Boyle, A. P.; Davis, S.; Shulha, H. P.; Meltzer, P.; Margulies, E. H.; Weng, Z.; Furey, T. S.; Crawford, G. E. High-Resolution Mapping and Characterization of Open Chromatin across the Genome. *Cell* **2008**, *132* (2), 311–322. https://doi.org/10.1016/j.cell.2007.12.014.

(120) Meyer, C. A.; Liu, X. S. Identifying and Mitigating Bias in Next-Generation Sequencing Methods for Chromatin Biology. *Nat Rev Genet* **2014**, *15* (11), 709–721. https://doi.org/10.1038/nrg3788.

(121) Grandi, F. C.; Modi, H.; Kampman, L.; Corces, M. R. Chromatin Accessibility Profiling by ATAC-Seq. *Nat Protoc* **2022**, *17* (6), 1518–1552. https://doi.org/10.1038/s41596-022-00692-9.

(122) Li, N.; Jin, K.; Bai, Y.; Fu, H.; Liu, L.; Liu, B. Tn5 Transposase Applied in Genomics Research. *Int J Mol Sci* **2020**, *21* (21), 8329. https://doi.org/10.3390/ijms21218329.

(123) Buenrostro, J. D.; Giresi, P. G.; Zaba, L. C.; Chang, H. Y.; Greenleaf, W. J. Transposition of Native Chromatin for Fast and Sensitive Epigenomic Profiling of Open Chromatin, DNA-Binding Proteins and Nucleosome Position. *Nat Methods* **2013**, *10* (12), 1213–1218. https://doi.org/10.1038/nmeth.2688.

(124) Barski, A.; Cuddapah, S.; Cui, K.; Roh, T.-Y.; Schones, D. E.; Wang, Z.; Wei, G.; Chepelev, I.; Zhao, K. High-Resolution Profiling of Histone Methylations in the

Human Genome. *Cell* **2007**, *129* (4), 823–837. https://doi.org/10.1016/j.cell.2007.05.009.

(125) Euskirchen, G. M.; Rozowsky, J. S.; Wei, C.-L.; Lee, W. H.; Zhang, Z. D.; Hartman, S.; Emanuelsson, O.; Stolc, V.; Weissman, S.; Gerstein, M. B.; Ruan, Y.; Snyder, M. Mapping of Transcription Factor Binding Regions in Mammalian Cells by ChIP: Comparison of Array- and Sequencing-Based Technologies. *Genome Res* **2007**, *17* (6), 898–909. https://doi.org/10.1101/gr.5583007.

(126) Deng, C.; Naler, L. B.; Lu, C. Microfluidic Epigenomic Mapping Technologies for Precision Medicine. *Lab Chip* **2019**, *19* (16), 2630–2650. https://doi.org/10.1039/C9LC00407F.

(127) Xu, Y.; Doonan, S. R.; Ordog, T.; Bailey, R. C. Translational Opportunities for Microfluidic Technologies to Enable Precision Epigenomics. *Anal Chem* **2020**, *92* (12), 7989–7997. https://doi.org/10.1021/acs.analchem.0c01288.

(128) Lion, M.; Tolstorukov, M. Y.; Oettinger, M. A. Low-Input MNase Accessibility of Chromatin (Low-Input MACC). *Curr Protoc Mol Biol* **2019**, *127* (1). https://doi.org/10.1002/cpmb.91.

(129) Kaya-Okur, H. S.; Wu, S. J.; Codomo, C. A.; Pledger, E. S.; Bryson, T. D.; Henikoff, J. G.; Ahmad, K.; Henikoff, S. CUT&Tag for Efficient Epigenomic Profiling of Small Samples and Single Cells. *Nat Commun* **2019**, *10* (1), 1930. https://doi.org/10.1038/s41467-019-09982-5.

(130) Skene, P. J.; Henikoff, S. An Efficient Targeted Nuclease Strategy for High-Resolution Mapping of DNA Binding Sites. *Elife* **2017**, *6*. https://doi.org/10.7554/eLife.21856.

(131) Buenrostro, J. D.; Wu, B.; Litzenburger, U. M.; Ruff, D.; Gonzales, M. L.; Snyder, M. P.; Chang, H. Y.; Greenleaf, W. J. Single-Cell Chromatin Accessibility Reveals Principles of Regulatory Variation. *Nature* **2015**, *523* (7561), 486–490. https://doi.org/10.1038/nature14590.

(132) Jin, W.; Tang, Q.; Wan, M.; Cui, K.; Zhang, Y.; Ren, G.; Ni, B.; Sklar, J.; Przytycka, T. M.; Childs, R.; Levens, D.; Zhao, K. Genome-Wide Detection of DNase I Hypersensitive Sites in Single Cells and FFPE Tissue Samples. *Nature* **2015**, *528* (7580), 142–146. https://doi.org/10.1038/nature15740.

(133) Lion, M.; Muhire, B.; Namiki, Y.; Tolstorukov, M. Y.; Oettinger, M. A. Alterations in Chromatin at Antigen Receptor Loci Define Lineage Progression during B Lymphopoiesis. *Proceedings of the National Academy of Sciences* **2020**, *117* (10), 5453–5462. https://doi.org/10.1073/pnas.1914923117.

(134) Xu, Y.; Lee, J.-H.; Li, Z.; Wang, L.; Ordog, T.; Bailey, R. C. A Droplet Microfluidic Platform for Efficient Enzymatic Chromatin Digestion Enables Robust Determination of Nucleosome Positioning. *Lab Chip* **2018**, *18* (17), 2583–2592. https://doi.org/10.1039/C8LC00599K.

(135) Cusanovich, D. A.; Daza, R.; Adey, A.; Pliner, H. A.; Christiansen, L.; Gunderson, K. L.; Steemers, F. J.; Trapnell, C.; Shendure, J. Multiplex Single-Cell Profiling of Chromatin Accessibility by Combinatorial Cellular Indexing. *Science (1979)* **2015**, *348* (6237), 910–914. https://doi.org/10.1126/science.aab1601.

(136) Satpathy, A. T.; Granja, J. M.; Yost, K. E.; Qi, Y.; Meschi, F.; McDermott, G. P.; Olsen, B. N.; Mumbach, M. R.; Pierce, S. E.; Corces, M. R.; Shah, P.; Bell, J. C.; Jhutty, D.; Nemec, C. M.; Wang, J.; Wang, L.; Yin, Y.; Giresi, P. G.; Chang, A. L.

S.; Zheng, G. X. Y.; Greenleaf, W. J.; Chang, H. Y. Massively Parallel Single-Cell Chromatin Landscapes of Human Immune Cell Development and Intratumoral T Cell Exhaustion. *Nat Biotechnol* **2019**, *37* (8), 925–936. https://doi.org/10.1038/s41587-019-0206-z.

(137) Ragunathan, K.; Jih, G.; Moazed, D. Epigenetic Inheritance Uncoupled from Sequence-Specific Recruitment. *Science (1979)* **2015**, *348* (6230). https://doi.org/10.1126/science.1258699.

(138) Struhl, K.; Segal, E. Determinants of Nucleosome Positioning. *Nat Struct Mol Biol* **2013**, *20* (3), 267–273. https://doi.org/10.1038/nsmb.2506.

(139) Robertson, G.; Hirst, M.; Bainbridge, M.; Bilenky, M.; Zhao, Y.; Zeng, T.; Euskirchen, G.; Bernier, B.; Varhol, R.; Delaney, A.; Thiessen, N.; Griffith, O. L.; He, A.; Marra, M.; Snyder, M.; Jones, S. Genome-Wide Profiles of STAT1 DNA Association Using Chromatin Immunoprecipitation and Massively Parallel Sequencing. *Nat Methods* **2007**, *4* (8), 651–657. https://doi.org/10.1038/nmeth1068.

(140) Kong, S.; Lu, Y.; Tan, S.; Li, R.; Gao, Y.; Li, K.; Zhang, Y. Nucleosome-Omics: A Perspective on the Epigenetic Code and 3D Genome Landscape. *Genes (Basel)* **2022**, *13* (7), 1114. https://doi.org/10.3390/genes13071114.

(141) Bonner, W. A.; Hulett, H. R.; Sweet, R. G.; Herzenberg, L. A. Fluorescence Activated Cell Sorting. *Review of Scientific Instruments* **1972**, *43* (3), 404–409. https://doi.org/10.1063/1.1685647.

(142) Lacombe, F.; Belloc, F. Flow Cytometry Study of Cell Cycle, Apoptosis and Drug Resistance in Acute Leukemia. *Hematol Cell Ther* **1996**, *38* (6), 495–504. https://doi.org/10.1007/s00282-996-0495-9.

(143) Brown, M.; Wittwer, C. Flow Cytometry: Principles and Clinical Applications in Hematology. *Clin Chem* **2000**, *46* (8), 1221–1229. https://doi.org/10.1093/clinchem/46.8.1221.

(144) Xia, Y.; Whitesides, G. M. Soft Lithography. *Angewandte Chemie International Edition* **1998**, *37* (5), 550–575. https://doi.org/https://doi.org/10.1002/(SICI)1521-3773(19980316)37:5<550::AID-ANIE550>3.0.CO;2-G.

(145) Agilent 2100 Bioanalyzer System: 2100 Expert Software User's Guide. Agilent Technologies February 2020.

(146) Becker, P. B. NEW EMBO MEMBER'S REVIEW: Nucleosome Sliding: Facts and Fiction. *EMBO J* **2002**, *21* (18), 4749–4753. https://doi.org/10.1093/emboj/cdf486.

(147) Fazzio, T. G.; Tsukiyama, T. Chromatin Remodeling In Vivo. *Mol Cell* **2003**, *12* (5), 1333–1340. https://doi.org/10.1016/S1097-2765(03)00436-2.

(148) Hancock, S. E.; Ding, E.; Johansson Beves, E.; Mitchell, T.; Turner, N. FACS-Assisted Single-Cell Lipidome Analysis of Phosphatidylcholines and Sphingomyelins in Cells of Different Lineages. *J Lipid Res* **2023**, *64* (3), 100341. https://doi.org/10.1016/j.jlr.2023.100341.

(149) Frenz, L.; Blank, K.; Brouzes, E.; Griffiths, A. D. Reliable Microfluidic On-Chip Incubation of Droplets in Delay-Lines. *Lab Chip* **2009**, *9* (10), 1344–1348. https://doi.org/10.1039/B816049J.

(150) Cao, Z.; Chen, C.; He, B.; Tan, K.; Lu, C. A Microfluidic Device for Epigenomic Profiling Using 100 Cells. *Nat Methods* **2015**, *12* (10), 959–962. https://doi.org/10.1038/nmeth.3488.

(151) Oh, K. W.; Lee, K.; Ahn, B.; Furlani, E. P. Design of Pressure-Driven Microfluidic Networks Using Electric Circuit Analogy. *Lab Chip* **2012**, *12* (3), 515–545. https://doi.org/10.1039/C2LC20799K.

(152) Pan, X.; Zeng, S.; Zhang, Q.; Lin, B.; Qin, J. Sequential Microfluidic Droplet Processing for Rapid DNA Extraction. *Electrophoresis* **2011**, *32* (23), 3399–3405. https://doi.org/10.1002/elps.201100078.

(153) Lin, J.; Yang, Z.; Wang, L.; Xing, D.; Lin, J. Global Research Trends in Extracellular Vesicles Based on Stem Cells from 1991 to 2021: A Bibliometric and Visualized Study. *Front Bioeng Biotechnol* **2022**, *10*. https://doi.org/10.3389/fbioe.2022.956058.

(154) Falany, J. L.; Macrina, N.; Falany, C. N. Regulation of MCF-7 Breast Cancer Cell Growth by β-Estradiol Sulfation. *Breast Cancer Res Treat* **2002**, *74* (2), 167–176. https://doi.org/10.1023/A:1016147004188.

(155) Rupp, B.; Owen, S.; Ball, H.; Smith, K. J.; Gunchick, V.; Keller, E. T.; Sahai, V.; Nagrath, S. Integrated Workflow for the Label-Free Isolation and Genomic Analysis of Single Circulating Tumor Cells in Pancreatic Cancer. *Int J Mol Sci* **2022**, *23* (14), 7852. https://doi.org/10.3390/ijms23147852.

(156) Owen, S.; Lo, T.-W.; Fouladdel, S.; Zeinali, M.; Keller, E.; Azizi, E.; Ramnath, N.; Nagrath, S. Simultaneous Single Cell Gene Expression and EGFR Mutation Analysis of Circulating Tumor Cells Reveals Distinct Phenotypes in NSCLC. *Adv*

Biosyst **2020**, *4* (8), 2000110. https://doi.org/https://doi.org/10.1002/adbi.202000110.

(157) Mishra, A.; Dubash, T. D.; Edd, J. F.; Jewett, M. K.; Garre, S. G.; Karabacak, N. M.; Rabe, D. C.; Mutlu, B. R.; Walsh, J. R.; Kapur, R.; Stott, S. L.; Maheswaran, S.; Haber, D. A.; Toner, M. Ultrahigh-Throughput Magnetic Sorting of Large Blood Volumes for Epitope-Agnostic Isolation of Circulating Tumor Cells. *Proceedings of the National Academy of Sciences* **2020**, *117* (29), 16839–16847. https://doi.org/10.1073/pnas.2006388117.

(158) Frenea-Robin, M.; Marchalot, J. Basic Principles and Recent Advances in Magnetic Cell Separation. *Magnetochemistry* **2022**, *8* (1), 11. https://doi.org/10.3390/magnetochemistry8010011.

(159) King, T. C. Tissue Homeostasis, Damage, and Repair. In *Elsevier's Integrated Pathology*; Elsevier, 2007; pp 59–88. https://doi.org/10.1016/B978-0-323-04328-1.50009-7.

(160) Payne, E. M.; Taraji, M.; Murray, B. E.; Holland-Moritz, D. A.; Moore, J. C.; Haddad, P. R.; Kennedy, R. T. Evaluation of Analyte Transfer between Microfluidic Droplets by Mass Spectrometry. *Anal Chem* **2023**, *95* (10), 4662–4670. https://doi.org/10.1021/acs.analchem.2c04985.

(161) Skhiri, Y.; Gruner, P.; Semin, B.; Brosseau, Q.; Pekin, D.; Mazutis, L.; Goust, V.; Kleinschmidt, F.; El Harrak, A.; Hutchison, J. B.; Mayot, E.; Bartolo, J.-F.; Griffiths, A. D.; Taly, V.; Baret, J.-C. Dynamics of Molecular Transport by Surfactants in Emulsions. *Soft Matter* **2012**, *8* (41), 10618. https://doi.org/10.1039/c2sm25934f.

(162) Courtois, F.; Olguin, L. F.; Whyte, G.; Theberge, A. B.; Huck, W. T. S.; Hollfelder, F.; Abell, C. Controlling the Retention of Small Molecules in Emulsion Microdroplets for Use in Cell-Based Assays. *Anal Chem* **2009**, *81* (8), 3008–3016. https://doi.org/10.1021/ac802658n.

(163) McNerney, M. P.; Styczynski, M. P. Small Molecule Signaling, Regulation, and Potential Applications in Cellular Therapeutics. *WIREs Systems Biology and Medicine* **2018**, *10* (2). https://doi.org/10.1002/wsbm.1405.

(164) Paul, S.; Lal, G. The Molecular Mechanism of Natural Killer Cells Function and Its Importance in Cancer Immunotherapy. *Front Immunol* **2017**, *8*. https://doi.org/10.3389/fimmu.2017.01124.

(165) Medcalf, E. J.; Gantz, M.; Kaminski, T. S.; Hollfelder, F. Ultra-High-Throughput Absorbance-Activated Droplet Sorting for Enzyme Screening at Kilohertz Frequencies. *Anal Chem* **2023**, *95* (10), 4597–4604. https://doi.org/10.1021/acs.analchem.2c04144.

(166) Lee, M.; Collins, J. W.; Aubrecht, D. M.; Sperling, R. A.; Solomon, L.; Ha, J.-W.; Yi, G.-R.; Weitz, D. A.; Manoharan, V. N. Synchronized Reinjection and Coalescence of Droplets in Microfluidics. *Lab Chip* **2014**, *14* (3), 509–513. https://doi.org/10.1039/C3LC51214B.

(167) Zheng, G. X. Y.; Terry, J. M.; Belgrader, P.; Ryvkin, P.; Bent, Z. W.; Wilson, R.; Ziraldo, S. B.; Wheeler, T. D.; McDermott, G. P.; Zhu, J.; Gregory, M. T.; Shuga, J.; Montesclaros, L.; Underwood, J. G.; Masquelier, D. A.; Nishimura, S. Y.; Schnall-Levin, M.; Wyatt, P. W.; Hindson, C. M.; Bharadwaj, R.; Wong, A.; Ness, K. D.; Beppu, L. W.; Deeg, H. J.; McFarland, C.; Loeb, K. R.; Valente, W. J.;

Ericson, N. G.; Stevens, E. A.; Radich, J. P.; Mikkelsen, T. S.; Hindson, B. J.; Bielas, J. H. Massively Parallel Digital Transcriptional Profiling of Single Cells. *Nat Commun* **2017**, *8* (1), 14049. https://doi.org/10.1038/ncomms14049.

(168) Unger, M. A.; Chou, H.-P.; Thorsen, T.; Scherer, A.; Quake, S. R. Monolithic Microfabricated Valves and Pumps by Multilayer Soft Lithography. *Science (1979)* **2000**, *288* (5463), 113–116. https://doi.org/10.1126/science.288.5463.113.

(169) Wolfien, M.; David, R.; Galow, A.-M. Single-Cell RNA Sequencing Procedures and Data Analysis. In *Bioinformatics*; Exon Publications, 2021; pp 19–35. https://doi.org/10.36255/exonpublications.bioinformatics.2021.ch2.